Haldo Lyon
4/23/68

THE SEDIMENTOLOGICAL RESEARCH LABORATORY

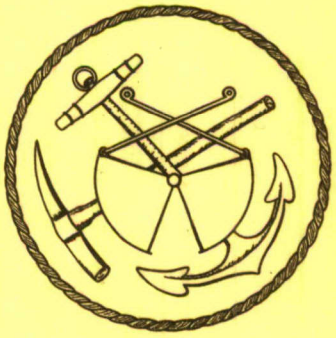

DEPARTMENT OF GEOLOGY

FLORIDA STATE UNIVERSITY

Tallahassee, Florida

DEFENSE TECHNICAL INFORMATION CENTER

Information for the Defense Community

DTIC® has determined on Month 06 Day 20 Year 2008 *that this Technical Document has the Distribution Statement checked below. The current distribution for this document can be found in the DTIC® Technical Report Database.*

☒ **DISTRIBUTION STATEMENT A.** Approved for public release; distribution is unlimited.

☐ © **COPYRIGHTED.** U.S. Government or Federal Rights License. All other rights and uses except those permitted by copyright law are reserved by the copyright owner.

☐ **DISTRIBUTION STATEMENT B.** Distribution authorized to U.S. Government agencies only. Other requests for this document shall be referred to controlling office.

☐ **DISTRIBUTION STATEMENT C.** Distribution authorized to U.S. Government Agencies and their contractors. Other requests for this document shall be referred to controlling office.

☐ **DISTRIBUTION STATEMENT D.** Distribution authorized to the Department of Defense and U.S. DoD contractors only. Other requests shall be referred to controlling office.

☐ **DISTRIBUTION STATEMENT E.** Distribution authorized to DoD Components only. Other requests shall be referred to controlling office.

☐ **DISTRIBUTION STATEMENT F.** Further dissemination only as directed by controlling office or higher DoD authority.

Distribution Statement F is also used when a document does not contain a distribution statement and no distribution statement can be determined.

☐ **DISTRIBUTION STATEMENT X.** Distribution authorized to U.S. Government Agencies and private individuals or enterprises eligible to obtain export-controlled technical data in accordance with DoDD 5230.25.

THE MINERALOGY AND GEOCHEMISTRY OF MANGANESE NODULES FROM THE SOUTHERN OCEAN

By

MAURICE A. MEYLAN

A Thesis
Submitted to the Graduate School of
The Florida State University
in partial fulfillment of the
requirements for the degree of
Master of Science

February, 1968

Contribution No. 22

ABSTRACT

X-ray diffraction studies on 228 nodules from 91 bottom trawls and 58 piston cores from the Southern Ocean collected during USNS ELTANIN cruises show that todorokite is the principal manganese oxide phase present. A correlation exists between manganese content of the gross sample and the relative amount of todorokite as expressed by the ratio of peak areas 3.34 Å (quartz) plus 3.2 Å (plagioclase-phillipsite) vs. 9.7 Å (todorokite). The areal distribution of values for this ratio roughly corresponds to the rate of delivery of detrital quartz and feldspar to a particular area, the relative proportion of todorokite being lowest near the Antarctic continent, especially in the Drake Passage and Scotia Sea.

Throughout the Southern Ocean, ferromanganese accumulations display a complex mineralogy. Birnessite and δ-MnO_2 are manganese phases of secondary importance. Minor amounts of crystalline geothite and/or maghemite were detected in many of the samples, but much of the iron present is evidently contained in an amorphous hydroxide. Authigenic and detrital silicates are contained in the ferromanganese accumulations. Quartz, plagioclase, montmorillonite, and phillipsite are almost invariably present, while clinoptilolite

and amphibole occur less frequently. Amphibole is more abundant in nodules from the Drake Passage and Scotia Sea.

Examination of nodules contained within sediment cores shows that the mineralogy and chemical composition of the concretions have remained relatively constant at any one location throughout much of the Brunhes paleomagnetic epoch. The distribution of the concretions in general has also remained unchanged.

ACKNOWLEDGMENTS

This thesis could not have been written without the efforts of many persons on behalf of the writer, and to these individuals we must at least try to express our appreciation.

Dr. H. G. Goodell has directed the thesis; in addition to his encouragement he has provided samples, equipment, data and an understanding of the elemental relationships in manganese nodules. Drs. J. K. Osmond and G. W. DeVore assisted with technical and theoretical approaches to the many problems encountered, and critically read the manuscript. Dr. M. Garstang, as the Graduate School Representative, also helped to edit and organize the thesis.

Mr. Dennis Cassidy of the Sedimentology Research Laboratory has provided invaluable assistance during the laboratory research phase of this work, many times interrupting his busy routine to locate needed equipment or to offer technical advice. He also helped to make the X-radiographic plate of manganese nodule internal structure. Dr. Mohanty of the School of Engineering Science allowed the writer access to a diffractometer having a monochromator attachment.

Mr. Ted Paster provided a sample of marine phillipsite for use as a standard, but more importantly, contributed

many ideas and much information during a number of discussions concerning ferromanganese accumulations on submarine extrusive basalt.

Numerous fellow graduate students assisted with the preparation of certain segments of this thesis. Mr. Ivar Zemmels performed a number of element tests with the X-ray fluorescence spectrograph. Mr. Dennis Edwards provided information on heavy minerals found in sediments adjacent to the Palmer Peninsula.

The Materials Laboratory of the Newport News Shipbuilding and Drydock Company performed a large number of elemental analyses; without their excellent data many possible relationships could not have been investigated.

Financial support in the form of a research assistantship was provided by the Office of Antartic Research of the National Science Foundation (Grant GA-40). NSF has also been responsible for collection of the samples and for funding the facilities used to study the manganese nodules. This support is gratefully acknowledged.

Mr. Steven Chesser drafted a number of the illustrations. The manuscript was typed by Mrs. Harriett Campbell.

TABLE OF CONTENTS

LIST OF ILLUSTRATIONS

LIST OF TABLES

INTRODUCTION

Concretions consisting primarily of manganese and iron oxides and hydroxides have been recovered from the Southern Ocean bottom during dredging and coring operations conducted aboard the USNS ELTANIN. These concretions, commonly known as manganese nodules, are not unique to the ocean surrounding Antarctica, since every large ocean basin and even some fresh water lakes contain similar concretions (Mero, 1965; Beals, 1966).

Although a large body of literature has arisen, devoted mostly to their composition, the origin of manganese nodules remains clouded by controversy, primarily because of a lack of experimental and observational data.

This study depicts the relationships between the mineralogy and the elemental chemistry of the ferromanganese nodules of the Southern Ocean, and correlates the physical, mineralogical, and chemical properties of the concretions with such environmental parameters as depth, proximity to volcanism, and distance from continental areas. Possible changes in nodule characteristics with time are also investigated, using samples found at various depths of burial in sediment cores.

The USNS ELTANIN is not the first research vessel to encounter manganese nodules on traverses across the southern polar seas. The voyage of HMS CHALLENGER (1873-1876) produced the first deep-sea manganese nodules, some of which were collected from stations in the Southern Ocean. The superb report of the CHALLENGER Expedition provides descriptions, chemical analyses, detailed drawings, and a discussion of the origin of the concretions (Murray and Renard, 1891).

Since the pioneering work of the CHALLENGER scientists, a number of oceanographic cruises in the Pacific have gathered other collections of manganese nodules for study. Murray and Lee (1909) reported dense concentrations of nodules collected aboard the ALBATROSS during several voyages in the southeastern Pacific. Hamilton (1956) described manganese nodules and manganese dioxide-encrusted rock outcrops occurring on the guyots studied during the Mid-Pacific Expedition. The Scripps Institute of Oceanography sponsored the Downwind Expedition during IGY; investigators photographed, cored, and dredged nodules primarily from the Southwest Pacific Basin (Menard and Shipek, 1958). At about the same time, scientists of the Russian ship VITIAZ conducted a similar photograph-core-dredge program in the Equatorial Pacific (Skornyakova and Zenkevitch, 1961).

During the past decade, several authors have summarized the many available observations and analyses of

ferromanganese concretions, together with the multitude of diverse opinions as to their origin. Goldberg and Arrhenius (1958) treated in some detail the chemistry of Pacific pelagic sediments, especially the elemental distributions in dissolved, sorbed, and solid phases. The distribution of iron and manganese in ferromanganese oxide minerals was interpreted on the basis of the mineral synthesizing work of Buser and Grütter (1956). Goldberg and Arrhenius also thoroughly reviewed the literature concerning genesis and decided, on the basis of their observations, that colloidal iron catalyzes the oxidation of manganous ions to insoluble manganese dioxide.

Arrhenius (1963) presented a general discussion of the mineralogy, chemistry, distribution, structure, rate of accumulation, and origin of manganese nodules. His coverage of the non-ferromanganese oxide mineralogy of the nodules is the most complete of any work. Menard's (1964) synthesis is similar to that of Arrhenius, although Menard emphasized the distributional aspects of occurrence and elemental ratios in the Pacific Ocean.

The most exhaustive treatment to date of the subject of manganese nodules has been produced by Mero (1965) for the purpose of evaluating the economic possibilities of ocean-floor ferromanganese concretions.

Manheim (1965) has assembled information on the shallow marine occurrences of manganese nodules, notably the

deposits of the Blake Plateau and the seas of northern Europe, and also presented the first comparison of X-ray diffraction data between continental and marine ferromanganese oxide minerals.

Several aspects of the Southern Ocean concretion deposits have been studied by Goodell (1964, 1965, 1967), who presented the density and distribution of the nodules at the present sediment-water interface from thousands of bottom photographs. In addition, he has determined Mn, Fe, Ni, Co, and Cu element pair relationships in the nodules, and the distributional trends of elemental ratios.

Grant (1967) utilized samples from ELTANIN Cruises 4-17 to establish the morphogenetic categories of Southern Ocean nodules, and investigated the rate of nodule accumulation. He attempted to correlate environmental factors with morphogenetic type.

Barnes (1967) compared the elemental chemistry and mineralogy of marine ferromanganese nodules, and determined that the minor element composition is controlled by the mineralogy. His data indicated to him that the formation of the manganese mineral phases is depth dependent.

Arrhenius (1967) has recently reviewed advances in the study of pelagic sedimentation, including manganese nodule deposits.

STUDY AREA

The study area encompasses the South Pacific Ocean, the Drake Passage, and the Scotia Sea, from 27°W. to 154°E. Longitude and from 33°S. to 78°S. Latitude. This segment of the Southern Ocean has been extensively sampled during USNS ELTANIN cruises as a part of the United States Antarctic Research Program.

Bathymetry

A general east to west traverse across Figure 1 shows the study area to include a complex ridge-trench system (Scotia Ridge and South Sandwich Trench) surrounding basins with moderately high relief (East and West Scotia Basins), an ill-defined rise in the Drake Passage, an abyssal plain with little relief (the Pacific-Antarctic Basin), a gentle rise in the center of the South Pacific (the East Pacific Rise), another deep abyssal plain (the Southwest Pacific Basin), and a series of rises and basins between Australia-New Zealand and the Antarctic Continent (New Zealand Plateau, Campbell Rise, Hjort Basin, and Macquarie Rise).

The relief and structure throughout this section of the Southern Ocean are primarily the result of tectonism and volcanic activity. The deposition of sediments has smoothed

the relief in some places, particularly the Pacific-Antarctic Basin, where abyssal hills are buried over wide areas. Volcanic seamounts abound in the Southwest Pacific Basin and in parts of the Pacific-Antarctic Basin (Zhivago, 1962, p. 74), as well as in the Drake Passage and Scotia Basins, where a general relief of 450 to 900 meters results (Mather, 1966, p. 14). The South Sandwich Islands and the adjacent trench to the east represent a typical oceanic island arc characterized by volcanism and associated deep and shallow earthquakes (Menard, 1965, p. 349).

The East Pacific Rise in the central South Pacific is a broad uplift supported by low density material in the mantle (Menard, 1964, p. 121). The Rise lacks a central rift comparable to that of the Mid-Atlantic Ridge, while the flanks are characterized by persistent ridge-and-trough topography probably produced by normal faulting (Menard, 1964). It is offset by a number of transverse faults, the most prominent of which is centered at approximately 135°W. Long., 55°S. Lat. An apparent extension of this offset, known provisionally as the Eltanin Fracture Zone, crosses the Pacific-Antarctic Basin toward the Drake Passage (Goodell, 1965, p. 6); it is characterized in the center of the basin by a steep (7 1/2°) scarp facing the Antarctic Continent (Meylan, 1966). Another transverse feature is the spur known as the Chile Rise, which extends northwest-southeast from the East Pacific Rise toward southern Chile. To the

southwest, the East Pacific Rise merges with the Pacific-Antarctic Ridge, which is seismically active and faulted into narrow asymmetrical ridges and troughs (Menard, 1964, p. 137).

More detailed descriptions of the bathmetry of the Drake Passage-Scotia Sea are given by Holmes (in Goodell, 1964, p. 5-6) and Mather (1966, p. 12-20). The bathmetry of the Pacific-Antarctic Ocean is discussed by Goodell (1965, p. 5-7) and Koster (1966, p. 5-12).

Sediments

Goodell (1965, p. 9-17) has assembled the most complete picture of the sediment distribution in the Southern Ocean (Fig. 2). The principal components are biologic (calcareous and siliceous tests) and terrigenous (wind-, water-, and ice-transported detritus). The sediment of the Scotia Sea-Drake Passage basically represents terrestrially-derived material, with a major diatomaceous proportion in the East Scotia Basin, and a significant formaminiferal content in the Drake Passage. The distributional pattern in the Pacific-Antarctic Ocean is less complex, showing well defined latitudinal bands. Coarse glacial marine deposits ring the Antarctic Continent (Hough, 1956). This material grades northward in the Pacific-Antarctic Ocean to clayey silt and then to silty clay. North of this sediment, and south of the Antarctic Convergence, is a wide belt of siliceous oozes. A belt of foraminiferal oozes is found to

the north of the mean Convergence position, at depths less than the carbon dioxide compensation level. This is in turn replaced to the north in the Pacific-Antarctic and Southwest Pacific Basins by dark red-brown clayey silt, the classic "red clay" of pelagic sediments.

Circulation

Deacon (1963) described the circulation of Southern Ocean waters. Its basic features are the Antarctic Convergence and the Antarctic Circumpolar Current. Cold, low salinity waters are generated in the Weddell and Ross Seas, and flow northward downslope as the Antarctic bottom water. Associated cold surface waters caught in the eastward-bound Antarctic Circumpolar Current encounter a warmer, more saline sub-Antarctic water mass at the Antarctic Convergence, and sink to become northward-flowing Antarctic intermediate water. South of the Convergence, the warm sub-Antarctic water mass is found beneath the Antarctic surface water. The northward deflection of the Antarctic Circumpolar Current is probably due to the general hemispheric thermodynamic circulation (Deacon, 1963, p. 288).

The infinite fetch of the prevailing westerlies, restricted southward of 50°S. Lat. only by the South American Continent at the Drake Passage, provides through the intermediary of frictional stress and resulting pressure gradient fields a driving force for the Antarctic Circumpolar Current. Maksimov (1962, p. 33) states that the surface current

direction and the current direction at a depth of 3000 meters are identical, and that the velocity at this depth averages 75 per cent of the surface velocity. Surface velocities in the area of the Antarctic Convergence in the South Pacific probably average less than 0.5 knot (H.O. Publ. No. 705). Bottom currents in the Drake Passage may be strong enough to move all but the coarsest detritus; Heezen and Hollister (1964, p. 166) believe that the bottom currents here may reach velocities of 50 centimeters/second, or slightly in excess of one knot. ELTANIN bottom photographs showing ripple and scour marks are good evidence for the action of bottom currents. Goodell (in press) relates ripple marks to manganese nodule occurrences (Fig. 3).

Fig. 1.--Bathymetry of Study Area (After H. O. Misc. 15, 254-9, 10, 11).

Fig. 2.--Distribution of Sediment Types in Study Area (After Goodell, in press).

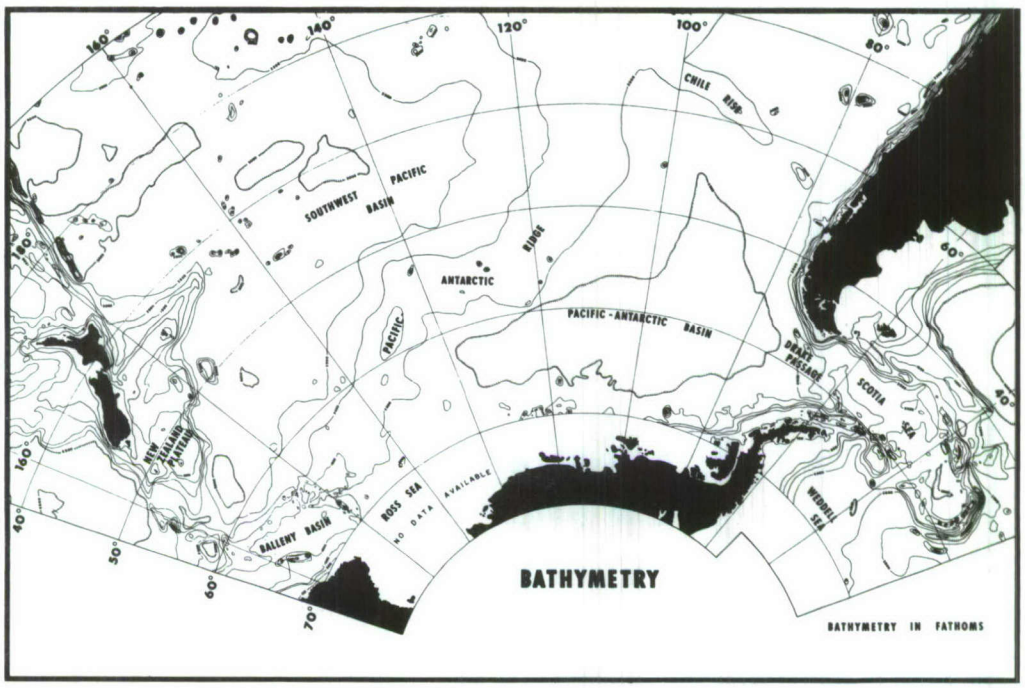
140°
120°
100°
80°
60°
40°
160°
180°
50°
60°
70°
CHILE RISE
SOUTHWEST PACIFIC BASIN
ANTARCTIC RIDGE
PACIFIC
PACIFIC-ANTARCTIC BASIN
DRAKE PASSAGE
SCOTIA SEA
NEW ZEALAND PLATEAU
BALLENY BASIN
ROSS SEA
NO DATA AVAILABLE
WEDDELL SEA
BATHYMETRY
BATHYMETRY IN FATHOMS

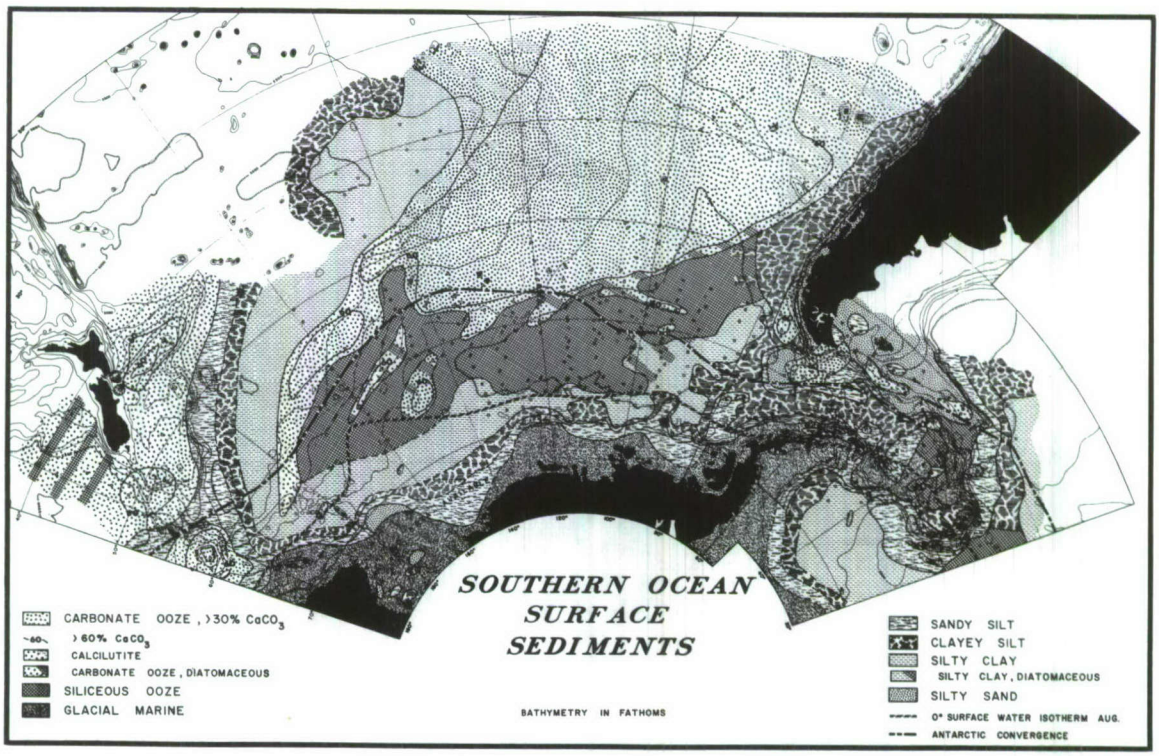
SOUTHERN OCEAN SURFACE SEDIMENTS
CARBONATE OOZE, >30% CaCO3
>60% CaCO3
CALCILUTITE
CARBONATE OOZE, DIATOMACEOUS
SILICEOUS OOZE
GLACIAL MARINE
BATHYMETRY IN FATHOMS
SANDY SILT
CLAYEY SILT
SILTY CLAY
SILTY CLAY, DIATOMACEOUS
SILTY SAND
0° SURFACE WATER ISOTHERM AUG.
ANTARCTIC CONVERGENCE

Fig. 3.--Inferred Bottom Currents of the Study Area (After Goodell, in press).

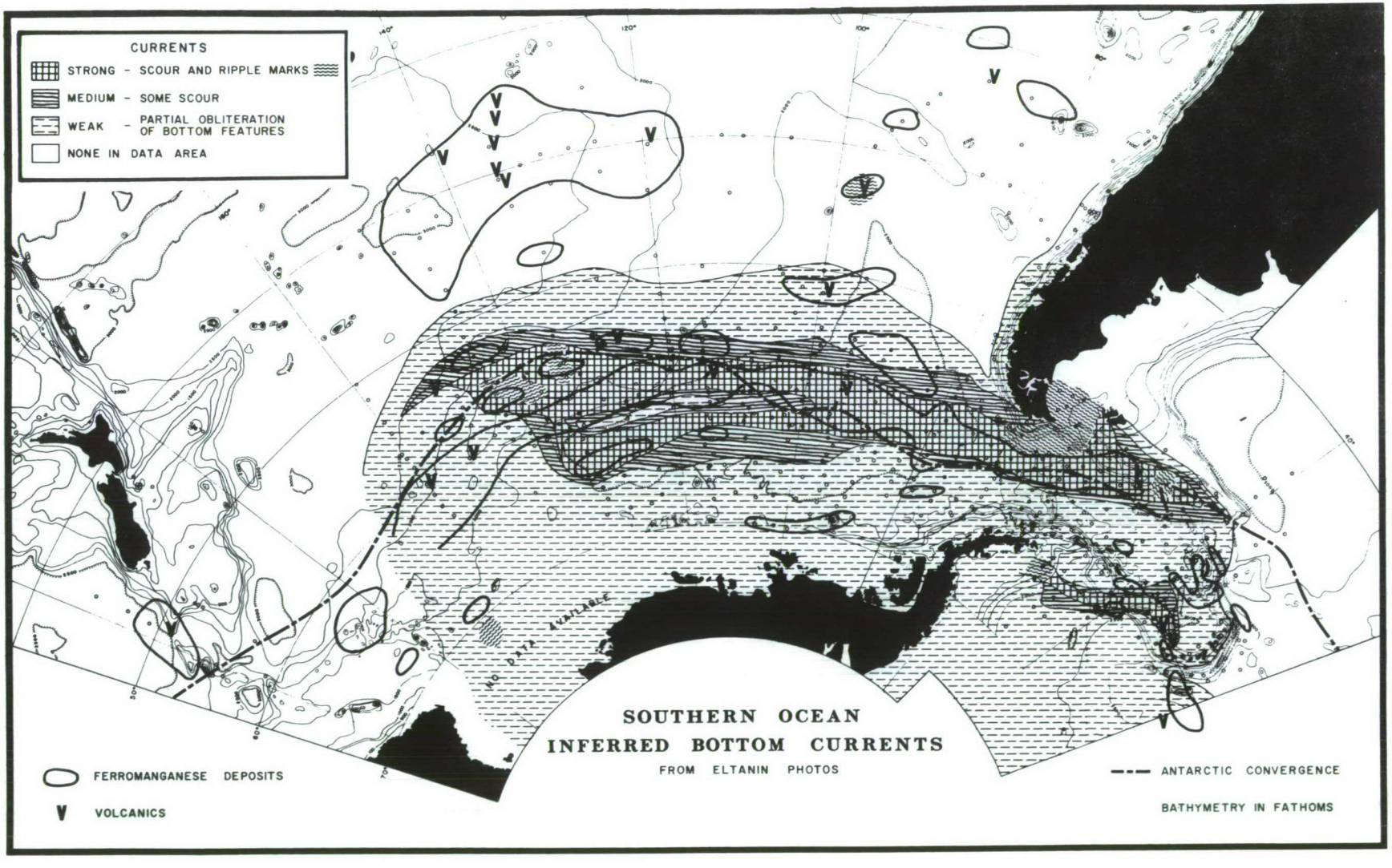
CURRENTS
STRONG - SCOUR AND RIPPLE MARKS
MEDIUM - SOME SCOUR
WEAK - PARTIAL OBLITERATION OF BOTTOM FEATURES
NONE IN DATA AREA
NO DATA AVAILABLE
SOUTHERN OCEAN
INFERRED BOTTOM CURRENTS
FROM ELTANIN PHOTOS
FERROMANGANESE DEPOSITS
VOLCANICS
ANTARCTIC CONVERGENCE
BATHYMETRY IN FATHOMS

SAMPLE COLLECTION AND DISTRIBUTION

The distribution of all ferromanganese oxide accumulations (excluding stains) collected aboard the USNS ELTANIN is given in Figure 4. Goodell (1965 and in press) has examined bottom photographs and dredge samples in order to determine the present distribution of ferromanganese nodules at the sediment-water interface (Fig. 5). Sample locations for this study are shown in Figure 6. These samples have been dredged by such trawls as the Blake, Menzies, Otter, and WHOI Epi-benthic trawls, seeking biologic specimens. A rock dredge (described by Grant, 1967, p. 18) has been used during recent cruises for sampling areas shown by bottom photographs to have outcropping rocks or a very dense concretion cover. Additional samples have been collected by piston and gravity sediment corers. Considering only those samples with sufficient ferromanganese oxide material to be called "nodules," 207 populations have been sampled in dredges and 143 in piston cores. Nodules collected by the smaller phleger corers have been generally disregarded because they do not offer enough material for convenient X-ray diffraction or chemical analyses, and because they usually duplicate the nodules recovered by other devices.

A truly representative sampling of ferromanganese concretions is not possible in the Southern Ocean. The greatest quantity of this material occurs draped on rock outcrops which do not readily yield their covering, or in the form of slabs too large to pick up in conventional bottom dredges. Therefore, our samples are limited to fragments occasionally broken off larger accumulations, together with the multitude of smaller concretions which cover the sediment surface. The smallest nodules generally are not recovered by dredging. However, piston and gravity cores collect even the most minute manganese micronodules. The Ewing piston corer and the phleger gravity corer used on the ELTANIN are limited in that they cannot collect nodules with a horizontal diameter greater than 5.6 centimeters and 3.5 centimeters, respectively.

All rock samples and sediment cores collected during ELTANIN cruises in the Southern Ocean were examined for evidence of macroscopic ferromanganese oxide accumulations. A number of observations, such as oxide thickness and nucleus type, were made for all macroscopic accumulations. Only certain nodules were selected for further study, i.e., those with ferromanganese oxide thicknesses sufficient to provide x-ray powder diffraction and chemical analysis samples.

Each of the samples selected for mineralogical and chemical analysis represents a single nodule population. A

population is here defined as a group of concretions, all of which are characterized by similar nucleic and ferromanganese oxide accumulation properties, and which were collected in a single dredge haul or sediment core horizon. ELTANIN sampling stations are spaced far enough apart so that a single deposit of identical concretions probably has not been sampled in duplicate.

Different populations can occur in an area sampled by a single dredge or in the same core interval. The physical characteristics that basically separate nodules into populations are (1) a visibly different nucleus type, (2) single vs. multiple nuclei, and (3) a markedly different oxide crust thickness.

Table 1 lists the number of populations observed in dredges, at the top of cores, and buried in sediment cores, along with the number and percentage of samples selected from each for further study. The samples are categorized into the four morphogenetic classes of Grant (1967), as well as three other categories representing ferromanganese oxide accumulations that cannot be termed nodules. An agglutination is a group of granules and/or pebbles united by a thin film of ferromanganese oxide material. A stain is a thin film of ferromanganese oxides on some solid object. Crustal material is a group of sand-size and finer particles that are coated and loosely cemented by ferromanganese oxides; crustal material does not assume any nodular form. It can

TABLE 1.--Number of concretions observed and sampled from dredge hauls and sediment cores.

Morphogenetic Categories	Dredges					At Core Tops					Buried in Cores				
	No. Populations Observed	X-ray Samples No.	% Pop.	Chemical Samples No.	% Pop.	No. Populations Observed	X-ray Samples No.	% Pop.	Chemical Samples No.	% Pop.	No. Populations Observed	X-ray Samples No.	% Pop.	Chemical Samples No.	% Pop.
Nodules	47	29	61.7	35	74.5	12	11	91.8	8	66.7	40	26	65.0	11	27.5
Crusts	103	66	64.1	65	63.1	14	10	71.5	3	21.4	29	15	51.8	2	6.9
Botryoidals	30	17	56.7	22	73.4	3	3	100	1	33.3	15	14	93.4	3	20.0
Agglomerates	27	20	74.2	14	51.8	6	1	16.7	0	0	24	12	50.0	0	0
Agglutinations	4	0	0	0	0	2	0	0	0	0	47	0	0	0	0
Stained Rocks	62	0	0	0	0	12	0	0	0	0	98	0	0	0	0
Crustal Material	0	0	0	0	0	3	2	66.7	0	0	4	2	50.0	0	0

be seen from Table 1 that a higher percentage of nodules and botryoidals were selected for further study, reflecting the greater relative ferromanganese oxide crust thicknesses of these types in comparison to crusts and agglomerates.

Fig. 4.--Distribution of Concretions Collected during ELTANIN Cruises 4-27.

Fig. 5.--Distribution of Ferromanganese Concretions in the Study Area (After Goodell, in press).

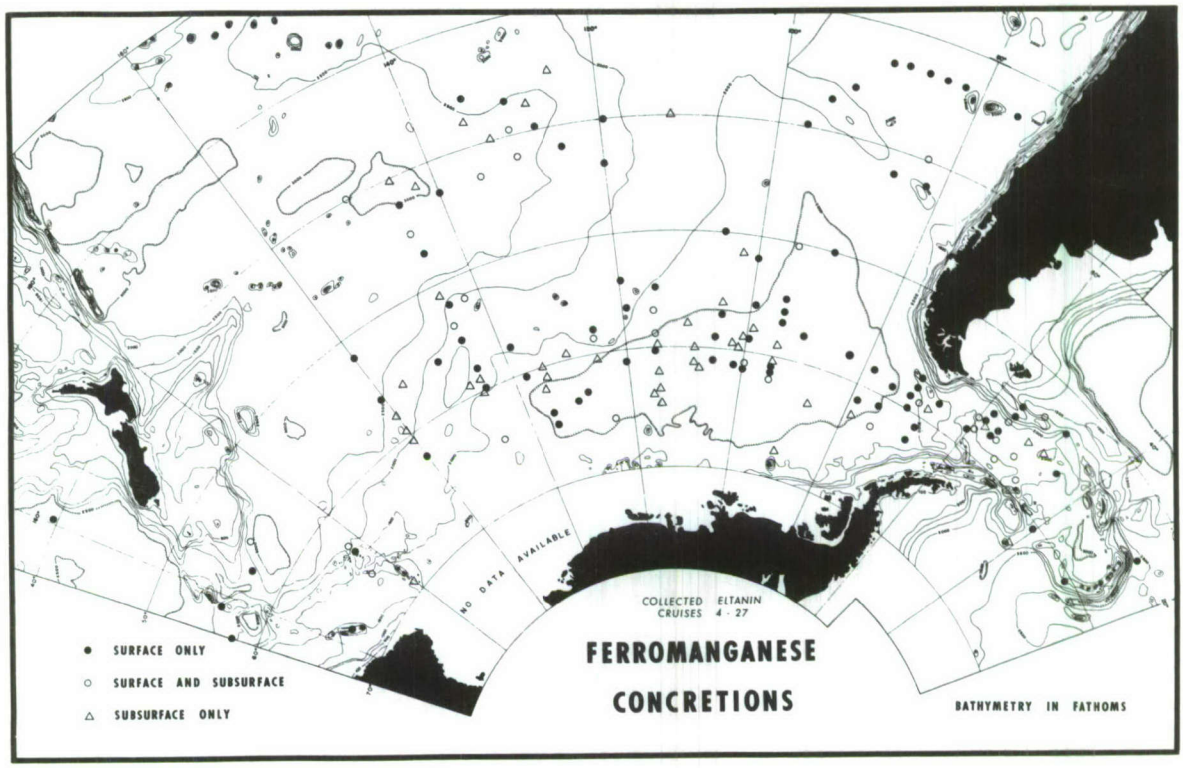
NO DATA AVAILABLE
COLLECTED ELTANIN CRUISES 4 - 27
FERROMANGANESE CONCRETIONS
SURFACE ONLY
SURFACE AND SUBSURFACE
SUBSURFACE ONLY
BATHYMETRY IN FATHOMS

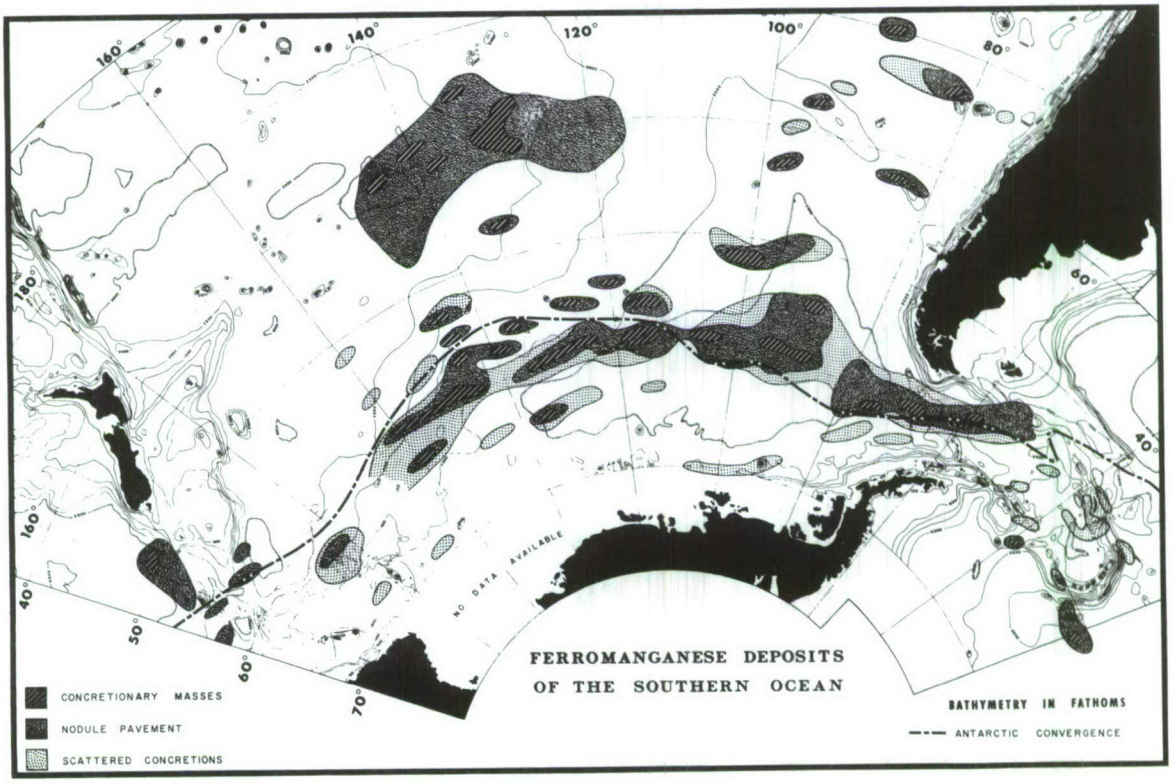
160°
140°
120°
100°
80°
60°
40°
180°
160°
40°
50°
60°
70°
NO DATA AVAILABLE
FERROMANGANESE DEPOSITS OF THE SOUTHERN OCEAN
CONCRETIONARY MASSES
NODULE PAVEMENT
SCATTERED CONCRETIONS
BATHYMETRY IN FATHOMS
ANTARCTIC CONVERGENCE

Fig. 6.--Sample Locations.

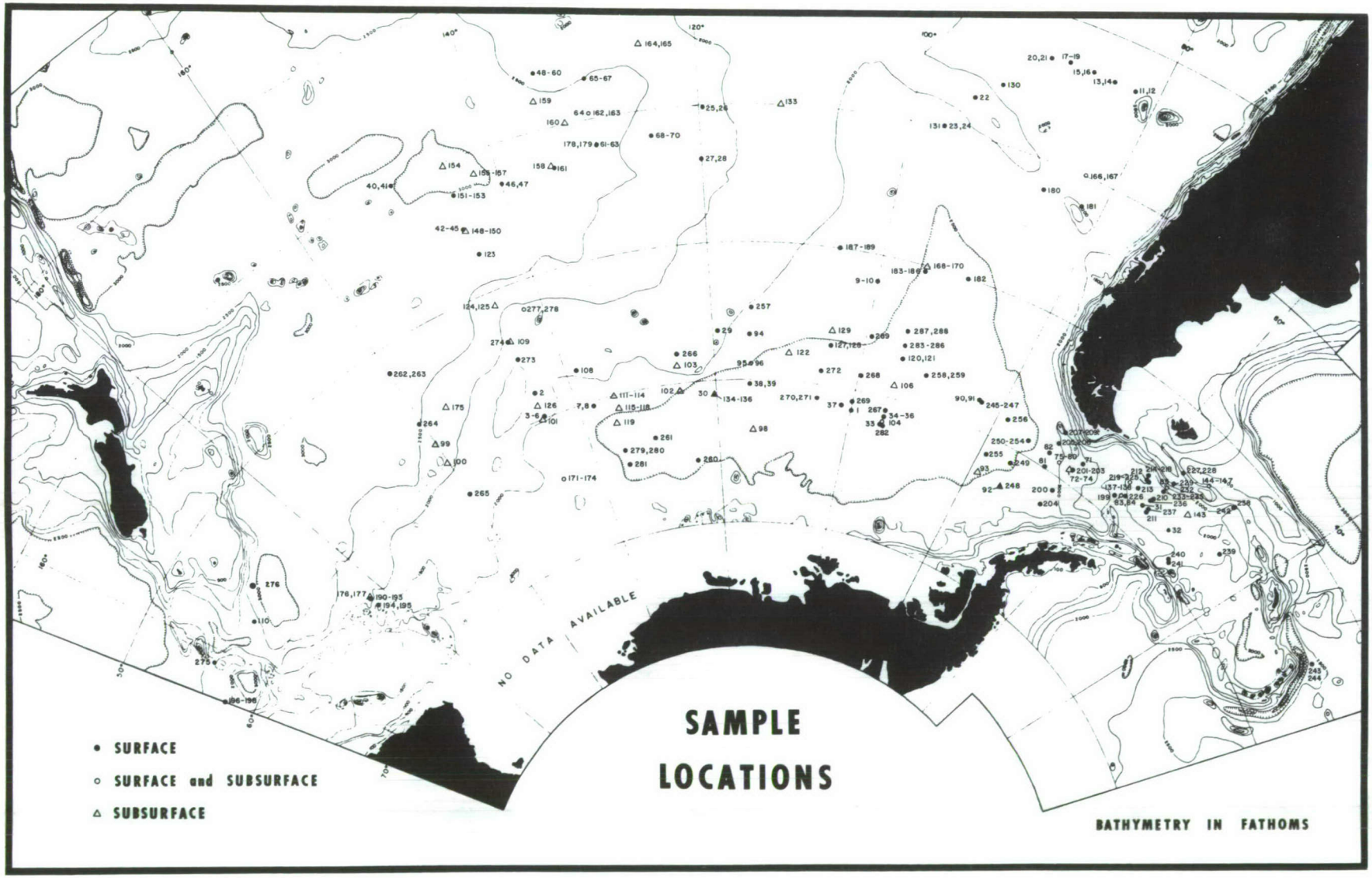
SAMPLE LOCATIONS
• SURFACE
○ SURFACE and SUBSURFACE
△ SUBSURFACE
NO DATA AVAILABLE
BATHYMETRY IN FATHOMS

NODULE SIZE, SHAPE, AND SURFACE FEATURES

The physical characteristics of each nodule selected for mineralogical and chemical analysis were determined prior to processing. Among the observations were the measurement of the maximum, intermediate, and minimum diameters; examination of the shape and surficial features; differentiation, when possible, of the internal structure into ferromanganese oxide crust, subcrust, and nucleus; measurement of the minimum and maximum thickness of the oxide crust or undifferentiated oxide crust-subcrust; and placement of the nodule into one of the morphogenetic categories of Grant (1967) according to the number of nuclei and relative ferromanganese oxide crust thickness.

Size

The size of manganese nodules varies greatly. Micronodules less than 1 mm. in diameter are very abundant in "red clay." Slabs many meters in extent can be seen in bottom photographs (Arrhenius, 1963, p. 670). However, discrete concretions greater than 1 meter across are probably very rare. According to Mero (1965, p. 135), nodules viewed in sea-floor photographs generally average between 2

and 4 cm. in diameter, and he further states that most of the nodules recovered by dredging have not exceeded about 8 cm. in diameter. Menard (1964, p. 173) reported that spherical nodules range upward in size to about 20 cm., and that larger nodules assume a flattened form.

Nodules recovered aboard the ELTANIN closely resemble in size those found in areas exclusive of the Southern Ocean. The size gap between about 1 and 5 mm. reported by Menard (1964, p. 173) apparently also exists over wide areas of the Southern Ocean. This is probably due to a lack of suitable size nucleating material. When accumulations of 1-5 mm. do occur, they are generally accreted as part of a larger multiple-nucleus agglomerate or botryoidal. The largest nodule recovered to date aboard the ELTANIN is a slab 56 x 55 x 14 cm. that was dredged from the floor of the Southwest Pacific Basin. Figures 7 and 8 are histograms of the frequency distribution of the maximum diameters, in dredges and cores, respectively, of the concretions used for chemical and/or x-ray analysis, plus about forty concretions from different populations that were measured but not sampled. Samples which consist only of fragments of larger concretions are not included in the distributions.

These frequency distributions are representative of the mean population sizes for all populations having a mean maximum diameter greater than about 2 cm., and smaller than the mouths of bottom dredges. Populations which have few

concretions about 2 cm. in size and many more members of 1/2 to 2 cm. in size are almost non-existent. Thus the chance of having selected a sample that is not representative of the mean of the smallest concretions sampled (1/2-2 cm.) is remote.

The histograms show that most concretions from the Southern Ocean have a maximum diameter between 3 and 5 centimeters. Another maximum would appear in the micronodule (<1 mm.) range if these tiny ferromanganese oxide grains had been included.

Bottom photographs generally show nodules from a very restricted area to have very nearly the same sizes and shapes, except in the vicinity of outcropping lava flows. Dredge samples cover a larger area than is viewed in bottom photographs, but similarities in size and shape between nodules of a single dredge haul are usually apparent. In order to determine the degree of concretion size similarity in typical bottom collections, two hauls were chosen at random and the maximum diameter of each nodule in both hauls measured. Figure 9 is the size frequency distribution of concretions in ELTANIN RS 20-5; Figure 10 represents ELTANIN RS 27-51. Both histograms show a leptokurtic distribution of sizes, the peakedness of the distribution of RS 27-51 concretion sizes being quite pronounced. But both histograms are more normal than the size frequency distributions evident for concretions in most bottom photographs.

Fig. 7.--Size Frequency Distribution of Concretions from Bottom Dredges.

Fig. 8.--Size Frequency Distribution of Concretions from Sediment Cores.

Fig. 9.--Size Frequency Distribution of Concretions from ELTANIN RS 27-51.

Fig. 10.--Size Frequency Distribution of Concretions from ELTANIN RS 20-5.

CONCRETIONS FROM DREDGES

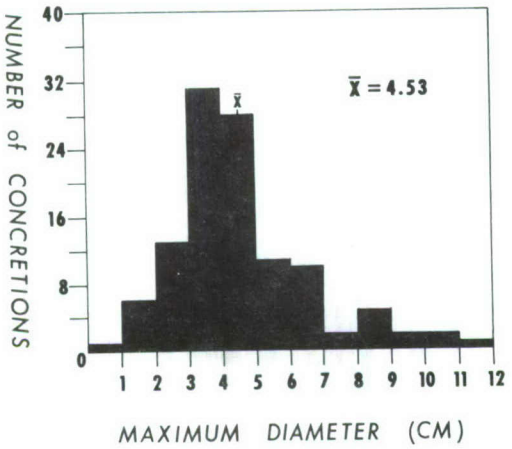

CONCRETIONS FROM CORES

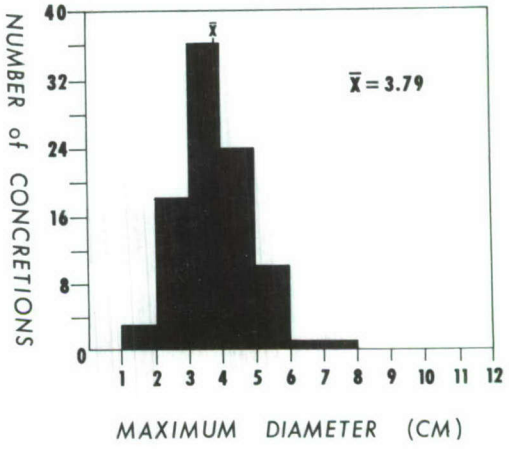

RS 27-51

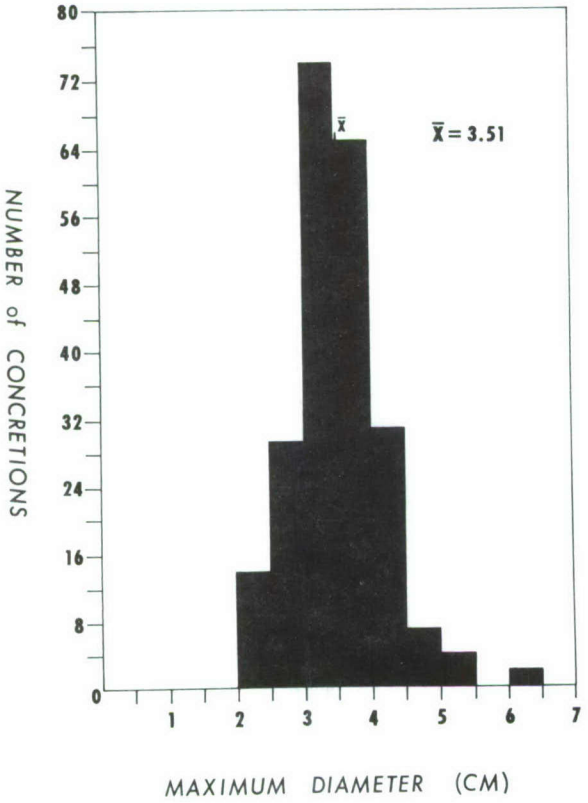

RS 20-5

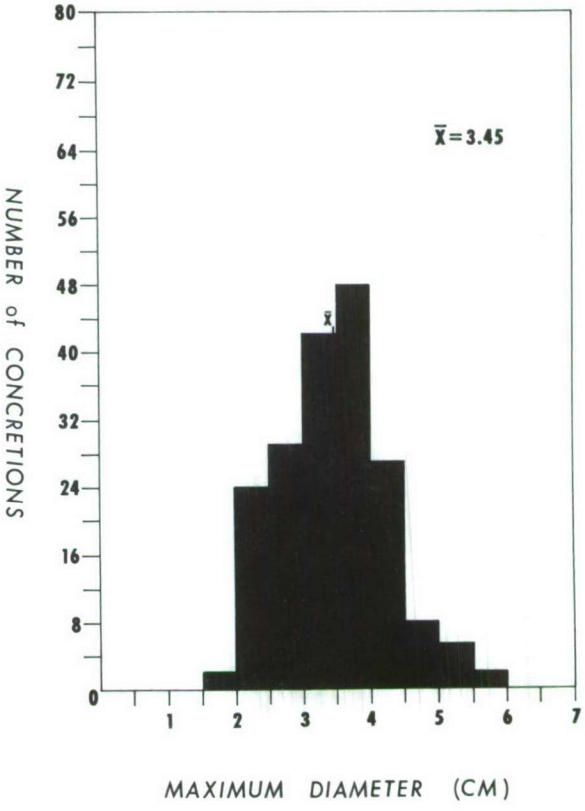

Morphology

Murray and Renard (1891, p. 344) divided manganese nodules into three groups on the basis of morphology: (1) more or less pyramidal or irregularly grape-shaped, (2) spheroidal or ellipsoidal, and (3) flattened, mammillated, and irregular. Since this early attempt at classifying the variety of manganese nodule shapes, no one has systematically approached the problem. The "morphological" categories of Grant (1967, p. 25-28) are in reality morphogenetic categories based primarily on the relative nucleus size and shape, as well as the number of nuclei present, and only secondarily on the external expression of internal characteristics.

The only reasonable approach to a classification of concretion forms is to ignore the finer details of shape and focus attention on the basic geometric form of the concretion. On this basis, the general shapes of manganese nodules are (1) spherical, (2) ellipsoidal, (3) tabular-discoidal, (4) polygonal, and (5) tubercular. Spherical and ellipsoidal shapes are characteristic of the "nodule" morphogenetic class, where only a single principal nucleus and a thick ferromanganese oxide crust is present. Many "crusts," frequently somewhat flattened, display an ellipsoidal shape. Tabular-discoidal and polygonal shapes are also typical of "crusts"; discoidal concretions usually have a volcanic nucleus, and the polygonal form is often inherited from a glacial erratic with a number of flat surfaces. "Botryoidals"

and "agglomerates" most often have a shape which resembles tubercular plant roots having two or more coalescing lobes. Table 2 lists the five basic morphologies and the number of samples of each morphogenetic type possessing a particular shape. In addition, it should be noted that 47 samples consisted only of fragments of larger ferromanganese oxide accumulations.

TABLE 2.--Comparison of concretion morphology with morphogenetic type.

	Morphogenetic Type			
Morphology	Nodules	Crusts	Botryoidals	Agglomerates
Spheroidal	14	2	4	0
Ellipsoidal	30	25	10	8
Tabular-Discoidal	2	11	2	3
Polygonal	3	4	1	1
Tubercular	4	6	16	21

Surface features

The most distinguishing feature of a manganese nodule is its mammillary surface, which is composed of closely spaced and/or coalescing mammillae, or hemispherical protrusions. The size of the mammillae relative to nodule size varies greatly, as does the "relief" of the mammillae, i.e., prominence above the general nodule surface. Usually at

least two generations of mammillae development are present on a single nodule, with tiny mammillae superimposed on larger mammillae. The mammilla shape is the result of both the habit of precipitating iron and manganese oxide-hydroxides and the irregularities introduced by coating of detrital granules which settle onto accumulating ferromanganese oxide deposits. Protrusions due to the latter often initially deviate from a hemispherical form.

Murray and Renard (1891, p. 344) were the first to note that the mammillarity of a concretion was not always uniform on every side. They found a nodule with half of the surface mammillated and with the other half smooth and bearing attached organisms, hence they postulated that the smooth surface was the upper surface. Many Southern Ocean manganese nodules show differences in mammillarity which are usually related to an asymmetrical thickness of ferromanganese oxides. The surface underlain by the thicker oxides usually has mammillae of higher relief and larger size than the surface underlain by the thinner oxides. This is interpreted to mean that the surface exposed for the greatest length of time directly to sea water tends to develop more prominent mammillae, while the mammillarity of the surface buried in sediment tends to be depressed. This interpretation does not necessarily contradict the findings of Murray and Renard (1891, p. 344). In addition, inspection of thin sections cut normal to precipitation surfaces shows

that heightened mammillarity apparently is favored by slow accumulation of fine detritus relative to oxide precipitation, rather than by more rapid accumulation of coarse detritus.

STRUCTURE AND MORPHOGENETIC TYPES

The structural components of a manganese nodule are the oxide crust, the subcrust, and the nucleus. The relative thickness of each component can vary, and one or two of the components may be absent in a particular concretion. In addition, a complete graduation between crust, subcrust, and nucleus is apparent in many nodules.

The oxide crust consists of iron and manganese hydroxides which have been precipitated in concentric shells around a nucleus and which have incorporated a minor amount of detrital crystallites. The subcrust usually consists of a zone of volcanic material that has been partially or wholly replaced by ferromanganese oxides; it often grades outward to the oxide crust, and seldom displays the type of lamination characteristic of the crust. In many instances the subcrust is slightly vesicular, and in cases of nearly complete alteration, vesicle "ghosts" may be seen. When the nucleus consists of volcanic material, subcrust and nucleus usually grade into one another. The nucleus may be composed of any solid material. The character and types of nuclei are discussed in a later section.

Several previous workers have noted zones of different texture within manganese nodules. Skornyakova, et al. (1962)

viewed microscopically a sequence of iron-manganese hydroxide bands, the thinnest characterizing the initial stage of the alteration and replacement of clastic volcanic material. Such banding may lend a laminated appearance to subcrusts composed of volcanic clastics which are not uncommonly deposited on volcanic bombs and glacial erratics. Sorem (1967), studying polished thin sections, found a nodule with distinct inner and outer zones; he suggested the textural differences may be due to differential growth rates.

Laminae of clays and other detrital minerals may alternate with the ferromanganese oxide layers. The alteration of intercalated contaminants may produce a radial dendritic form, penetrating through several layers; Riley and Sinhaseni (1958, p. 467) noted similar patterns.

Concentric shells are easily split off most nodules. In addition, a number of fractures approximately perpendicular to the colloform layering are almost always present. Menard (1964, p. 173) noted that above a certain size the concretions tend to be cracked into eight equal sections, which may be recemented by septaria. Southern Ocean nodules do not fit such a pattern. The fracture patterns are randomly oriented and branching, and are frequently avenues of influx for clays from the surrounding ocean floor. X-ray photographs (Plate 1) show the fractures as networks of lines. The fractures are probably the result of the hydration and expansion or dehydration and contraction of any one of a number of mineral phases.

Plate 1.--X-radiographs of concretion internal structure. (Left: Nodule from ELTANIN RS 24-8. Right: Botryoidals from ELTANIN RS 24-17.)

Plate 2.--Thin section of ferromanganese concretion. (Crust from ELTANIN 5-4; nucleus probably phillipsite-montmorillonite; glacial erratics incorporated in ferro-manganese oxide crust.)

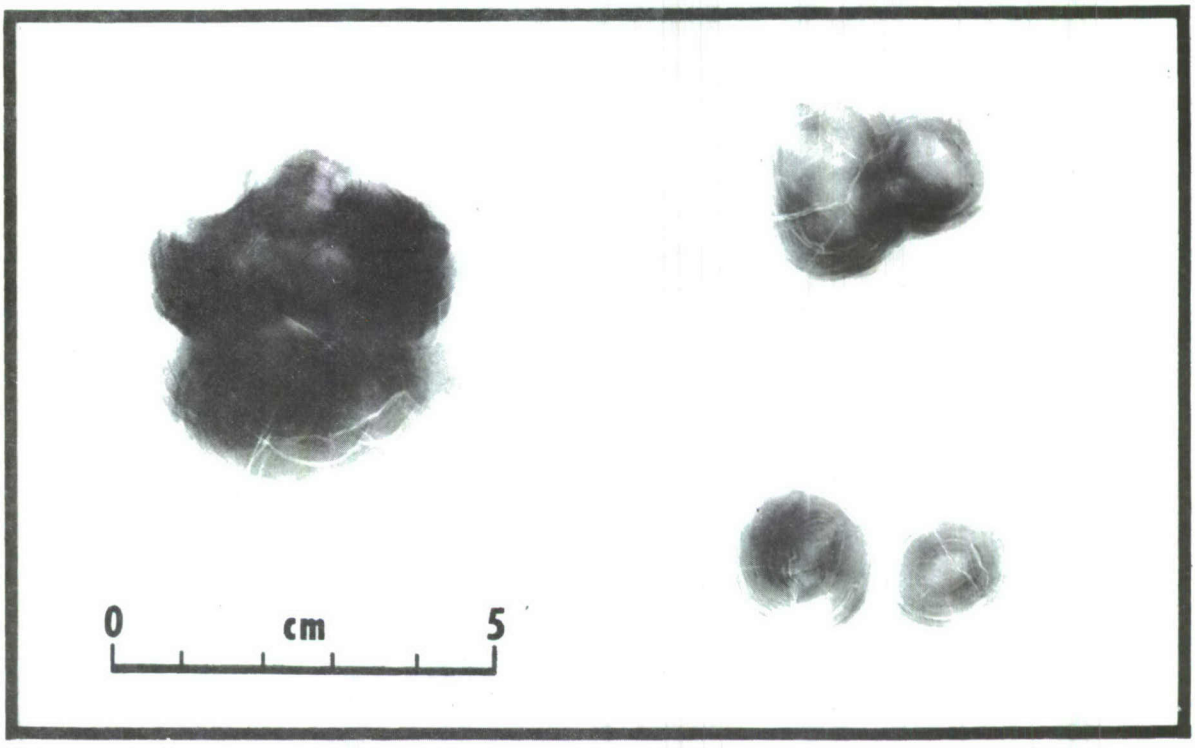
0
cm
5

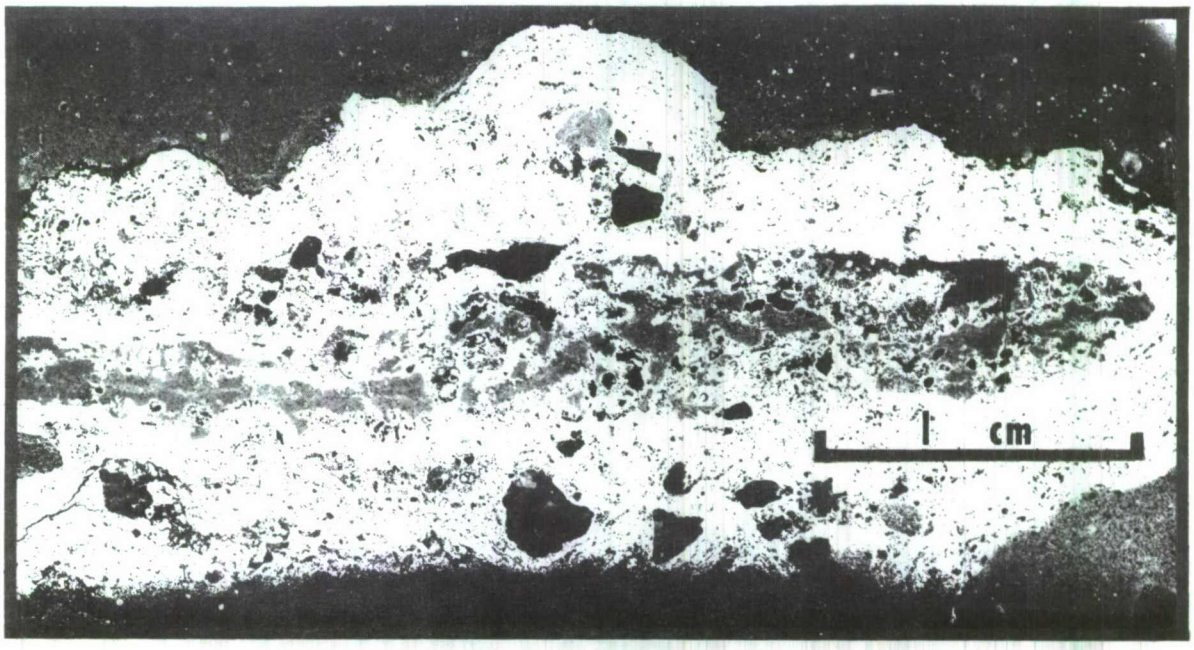
1
cm

Morphogenetic classes

The thickness of the oxide crust, the thickness of the subcrust, and the size and number of nuclei were determined for each nodule sampled whenever possible. This information served as both an objective and a subjective basis for placing a particular concretion in one of the four "morphological" classes of Grant (1967, p. 25-28). The number of nuclei can be determined objectively, but a decision as to whether there are one or more principal nuclei is often subjective. The measurement of the thickness of the oxide crust or subcrust can be objective only when the structural component in question is well differentiated from an adjacent structural component. But despite apparent difficulties, the morphogenetic class to which a concretion belongs is usually determined with ease.

The criteria used by Grant (1967, p. 25-28) to define morphogenetic classes are (1) number of nuclei, and (2) oxide crust thickness relative to nucleus size. "Nodules" and "botryoidals" have a relatively thick oxide crust; the nodule class is characterized by a single nucleus (which may be macroscopic or microscopic), while botryoidals have more than one nucleus. "Crusts" and "agglomerates" display relatively thin oxide crusts, with the former being mononucleate, and the latter possessing more than one nucleating center.

In order to determine quantitatively the relative oxide crust thickness of each concretion type, graphical plots (Fig. 11) of the absolute oxide crust thickness/concretion minimum diameter ratios for concretions belonging to each of the four morphogenetic classes were made. (The class membership was designated in advance by a relative thick-or-thin oxide crust appraisal.) These plots show that most of the concretions originally designated as crusts and agglomerates have a relative thickness of less than 0.4, i.e., ferromanganese oxide deposits make up less than 40% of the minimum thickness of the concretions. More than 40% of the minimum diameter of most nodules and botryoidals is comprised of ferromanganese oxides.

Fig. 11.--Ratio of Oxide Crust Thickness to Concretion Minimum Diameter for Crusts, Nodules, Botryoidals, and Agglomerates.

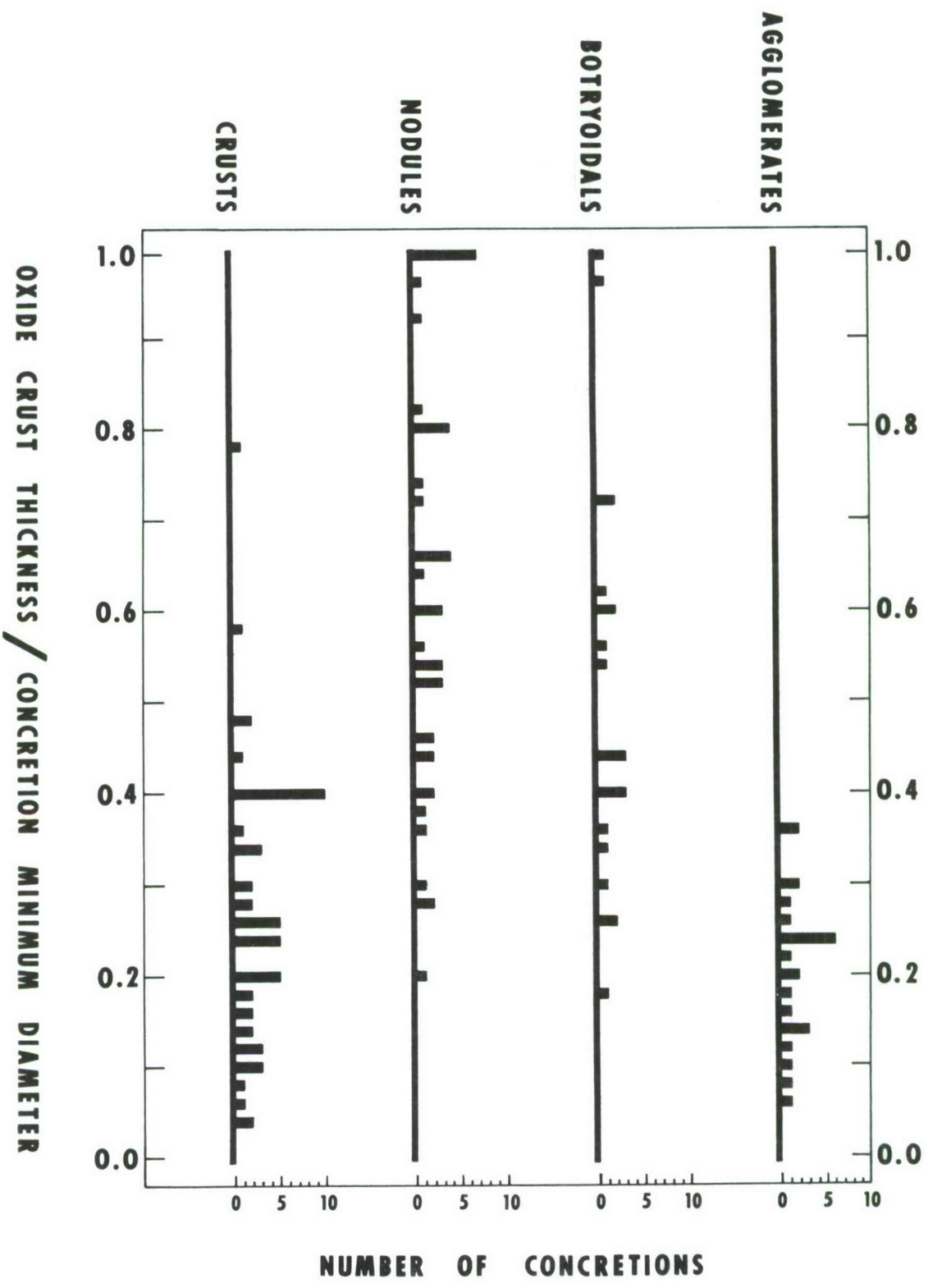
CRUSTS
NODULES
BOTRYOIDALS
AGGLOMERATES
OXIDE CRUST THICKNESS / CONCRETION MINIMUM DIAMETER
1.0
0.8
0.6
0.4
0.2
0.0
0 5 10
NUMBER OF CONCRETIONS

MORPHOGENETIC SPECIES DISTRIBUTION IN THE SOUTHERN OCEAN

Grant (1967, p. 31-38) has previously discussed the distribution of morphogenetic types, noting that there was no apparent correlation in the Southern Ocean between type and (1) longitude, (2) surface currents, (3) position of the Antarctic Convergence, or (4) associated sediment. Only a concentration of agglomerates in more southerly latitudes was noted. With the aid of many more samples and a variety of observations, these tentative conclusions have been reviewed, and possible correlations between type and (1) depth, (2) bottom currents, and (3) nucleus material have been examined.

Figure 12 depicts the areal distribution of the morphogenetic types. Only crusts and nodules have been found on the Chile Rise and its flanks, and between the Chile Rise and the Robinson Crusoe Islands. Crusts, nodules, and botryoidals are all found in the Southwest Pacific Basin. Crusts are predominant on the Pacific-Antarctic Ridge-Rise system. All four concretion types have been dredged from the Pacific-Antarctic Basin, Drake Passage, and Scotia Sea. The most significant regional trend is a concentration of agglomerates, which almost always have glacial erratic

nuclei, within about 3-4° of the 60° South parallel of latitude. No agglomerates are found north of 50°S. Lat. This suggests that concretions of this type are dependent on granule- and small pebble-size glacial erratics for nucleation centers, with some other agent (probable bottom currents, Fig. 3) to assist in coalescing adjacent or near-by centers of ferromanganese oxide accumulation. Grant (1967) noted the longitudinal dependence of agglomerate distribution.

Table 3 lists the number of populations of each morphogenetic type found in dredge hauls, at the surface of sediment cores, and buried in sediment cores, along with the percentage of all concretion populations contributed by each of the nodule classes. Mononucleate concretions outnumber multinucleate concretions by about 7:3.

TABLE 3.--Number of morphogenetic populations found in dredge hauls and sediment cores.

Morphogenetic Type	Dredges	Cores, Surface	Cores, Buried	Total No.	Percent
Nodules	47	12	40	99	28.3
Crusts	103	14	29	146	41.7
Botryoidals	30	3	15	48	13.7
Agglomerates	27	6	24	57	16.3

Nodules and botryoidals also display a wide variety of nucleus types, but most often the nuclei are volcanics

in differing stages of alteration to ferromanganese oxides. Agglomerates, as stated before, almost always have glacial erratic nuclei. Table 4 divides the concretions into those having macroscopic volcanic nuclei, those having both volcanic and glacial erratic nuclei, those having glacial erratic nuclei and those with organic or no discernible nuclei. In the concretions with both volcanic and glacial erratic nucleation centers, the volcanic material is usually the initial nucleus, with glacially-rafted granules and small pebbles added to the growing concretion (Plate 2). The nature of the nucleus was determined by visual inspection, and in the case of fine-grained nuclei, the determination was often supported by X-ray diffraction analysis. Plutonic igneous, metamorphic, and sedimentary rock centers were all assumed to be implaced by glacial rafting. Altered feldspathic material, palagonite, glass, angular basalt, zeolites, and montmorillonite were assumed to be derived from local volcanism.

TABLE 4.--Concretion nucleus types.

Morphogenetic Type	Erratic Nuclei	Erratic and Volcanic Nuclei	Volcanic Nuclei	Organic, Indiscernible Nuclei
Crusts	20	12	64	16
Nodules	13	6	34	23
Botryoidals	9	10	13	6
Agglomerates	35	17	2	1

The large number of indiscernible crust nuclei is due to the inclusion of a number of large fragments which appeared to have been broken off nucleation sites, and it was assumed that this warranted designating these fragments as representatives of the crust morphogenetic type. Nodules and botryoidals also show a large number of indiscernible nuclei, in most cases probably because the original nucleus has been replaced by ferromanganese oxides. In a few instances the "nucleus" appears to be a fragment of the oxide crust of a previously-existing concretion. The latter phenomenon was first noticed by Murray and Renard (1891, p. 346).

The areal distribution of nucleus types follows a predictable pattern (Fig. 13). Volcanic nuclei (angular aphanitic basalt, basaltic glass, palagonite, and zeolitite) are found throughout the area. This is to be expected in an area with extensive volcanic and tectonic features. Glacial erratic nuclei are found in concretions from stations within the range of berg ice drifting north and west from the Antarctic continent. No coarse sand-size or larger glacial erratics are found in concretions north of about 51°S. Lat., even in those nodules buried in sediment during times when the Antarctic ice cap was supposedly invading waters further to the north than at the present time.

The northern limit of glacial erratic nuclei occurrence is only vaguely related to either the present mean position of the Antarctic Convergence or the maximum limit

Fig. 12.--Distribution of Morphogenetic Concretion Types in the Study Area.

Fig. 13.--Distribution of Nucleus Types in the Study Area.

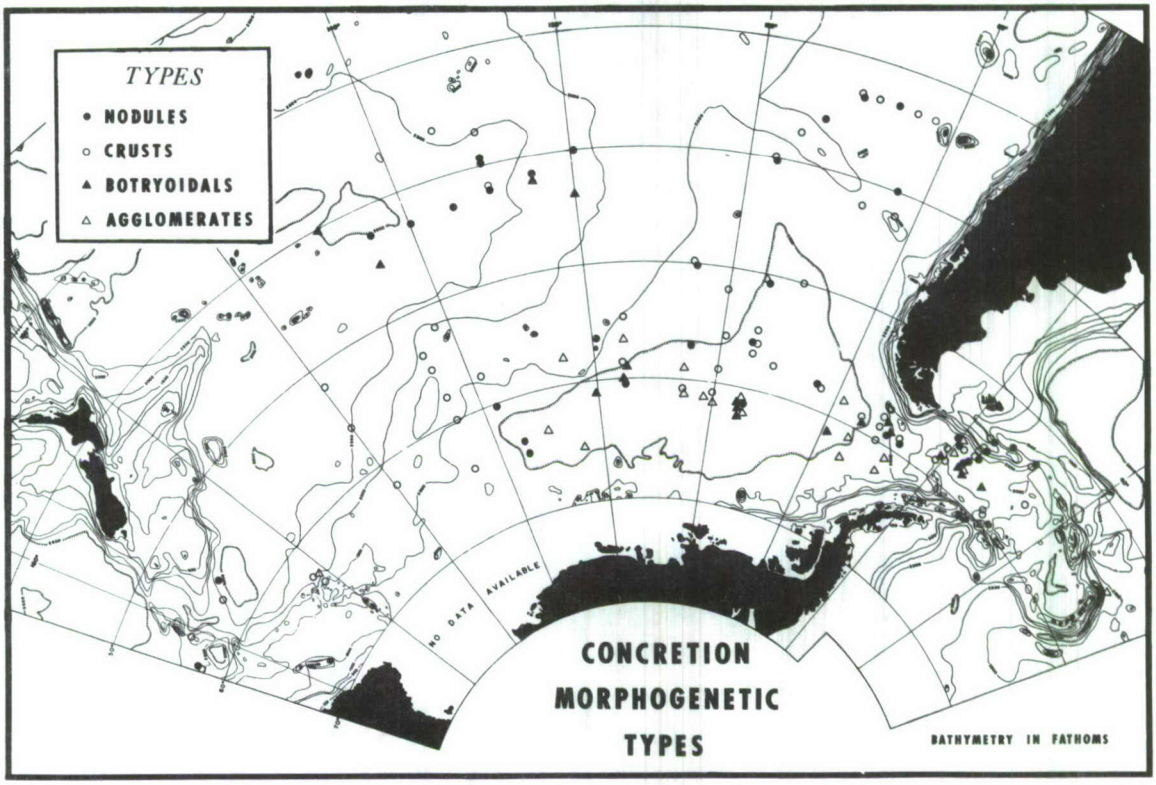
TYPES
NODULES
CRUSTS
BOTRYOIDALS
AGGLOMERATES
NO DATA AVAILABLE
CONCRETION
MORPHOGENETIC
TYPES
BATHYMETRY IN FATHOMS

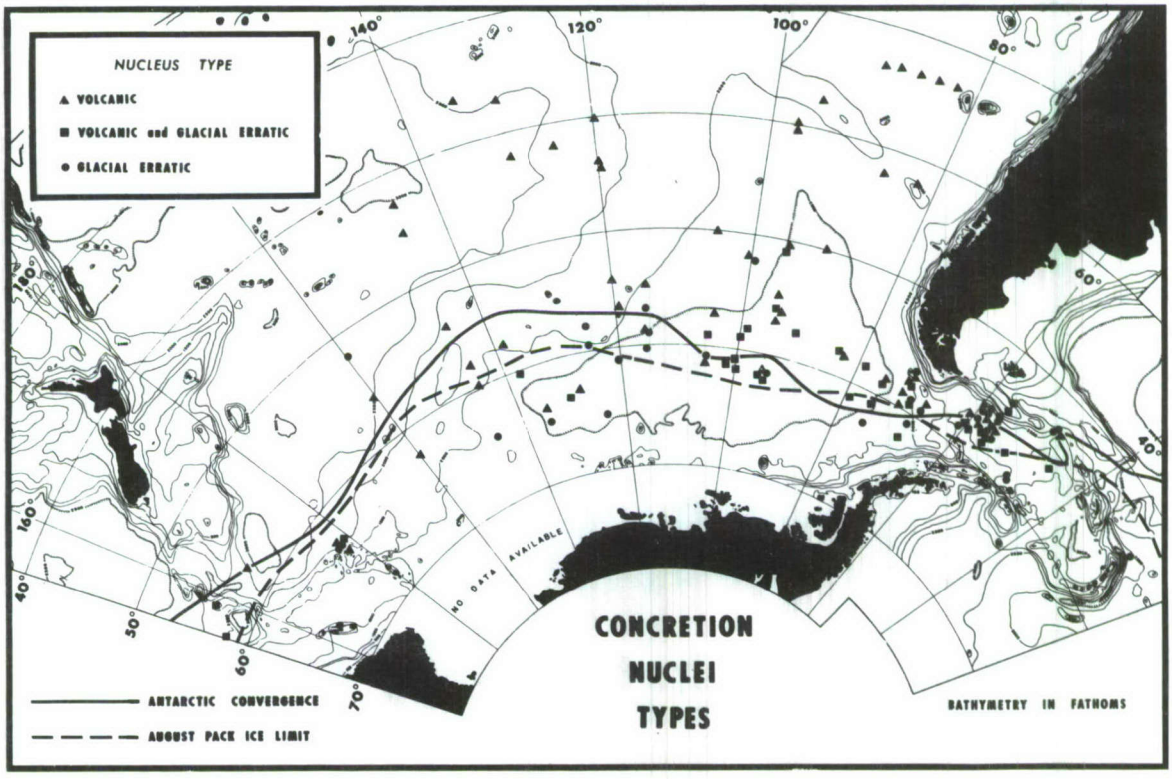
NUCLEUS TYPE
VOLCANIC
VOLCANIC and GLACIAL ERRATIC
GLACIAL ERRATIC
140°
120°
100°
80°
60°
40°
160°
180°
40°
50°
60°
70°
NO DATA AVAILABLE
CONCRETION
NUCLEI
TYPES
ANTARCTIC CONVERGENCE
AUGUST PACK ICE LIMIT
BATHYMETRY IN FATHOMS

of berg ice. In the western portion of the Pacific-Antarctic Ocean, the northern limit is uncertain because samples are too widely spaced. But the wide divergence of the glacial erratic limit and the Convergence in the Pacific-Antarctic Basin may be due to ice flows being carried unusually far to the north by the cold Humboldt Current.

An indirect correlation exists between morphogenetic type and depth. Table 5 is a listing of the percentages of each concretion type occurring in arbitrary depth zones.

TABLE 5.--Comparison of water depth with frequency of concretion occurrence.

Depth (Fm.)	Crusts	Nodules	Botryoidals	Agglomerates	Total No.
0-1699	75%	14%	0%	11%	28
1700-1899	59%	30%	0%	11%	27
1900-2099	46%	31%	11%	11%	35
2100-2299	45%	25%	20%	10%	49
2300-2499	38%	28%	19%	16%	32
2500-2699	50%	20%	12%	18%	50
2700-2899	25%	21%	29%	17%	22

Crusts show a general percentage decrease with increasing depth. (The large number of crusts between 2500-2699 fathoms is due to an abundance of volcanic crusts in the Southwest Pacific Basin and encrusted glacial erratics in

the Pacific-Antarctic Basin. Most of these two areas is characterized by abyssal hills and plains with depths of about 2500 to 2700 fathoms.) Botryoidals and agglomerates tend to comprise a larger proportion of the total concretion population as depth increases. This also reflects the general areal distribution of these two morphogenetic types--few multinucleate concretions occur on the Pacific-Antarctic Rise or in the relatively shallow depths of the Drake Passage and Antarctic continental shelf. A more reasonable correlation exists between hypothesized bottom currents (Fig. 3) or the position of the Antarctic Convergence (Fig. 13) and the occurrence of botryoidals and agglomerates, rather than strictly between water depth and morphogenetic type.

Grant concluded (1967, p. 34-35) that manganese nodules of the Southern Ocean show no preference for a particular sediment type. This contradicts Mero's (1965, p. 140) conclusion that manganese nodules are usually associated with slowly depositing red clays. Mero does not imply that the sediment itself exercises any influence, but rather that the rate of sediment accumulation or "the activity of the agency keeping the nodules at the surface" exercises some control. A comparison of the latest sediment distribution data for the Southern Ocean (Fig. 2) and the distribution of morphogenetic types (Fig. 12) shows little if any correlation between manganese nodules and their associated sediment. Since these concretions almost always display some

macroscopic nucleating material, it would seem more reasonable that a strong dependence on nucleation objects or substrata exists.

A specific manganese nodule type shows both a limited range of relative oxide crust thicknesses (Fig. 11) and a wide range of absolute oxide crust thicknesses. These values are a function of rate/time of ferromanganese oxide accumulation. The values show general distributional trends which are not related to any single known environmental factor. Figure 14 depicts the regional variation in absolute oxide crust thickness values; the values are an average of minimum and maximum thicknesses for each concretion, and where more than two values were obtained from a single station, the values were averaged (the implications of such an approach are discussed in the Appendix). The thickest ferromanganese oxide encrustations ($>$ 5 cm) occur in the Southwest Pacific Basin, northeast of the Chile Rise, in parts of the Pacific-Antarctic Basin, and in the northern parts of the Drake Passage and Scotia Sea. Intermediate thicknesses (2 1/2-5 cm) are found primarily on the Pacific-Antarctic Rise and its flanks, and in the center of the Scotia Sea. Thin deposits ($<$ 2 1/2 cm) are characteristic of areas adjacent to continents, although a limited segment of the Pacific-Antarctic Basin has concretions with thin crusts.

Fig. 14.--Distribution of Oxide Crust Thicknesses in the Study Area.

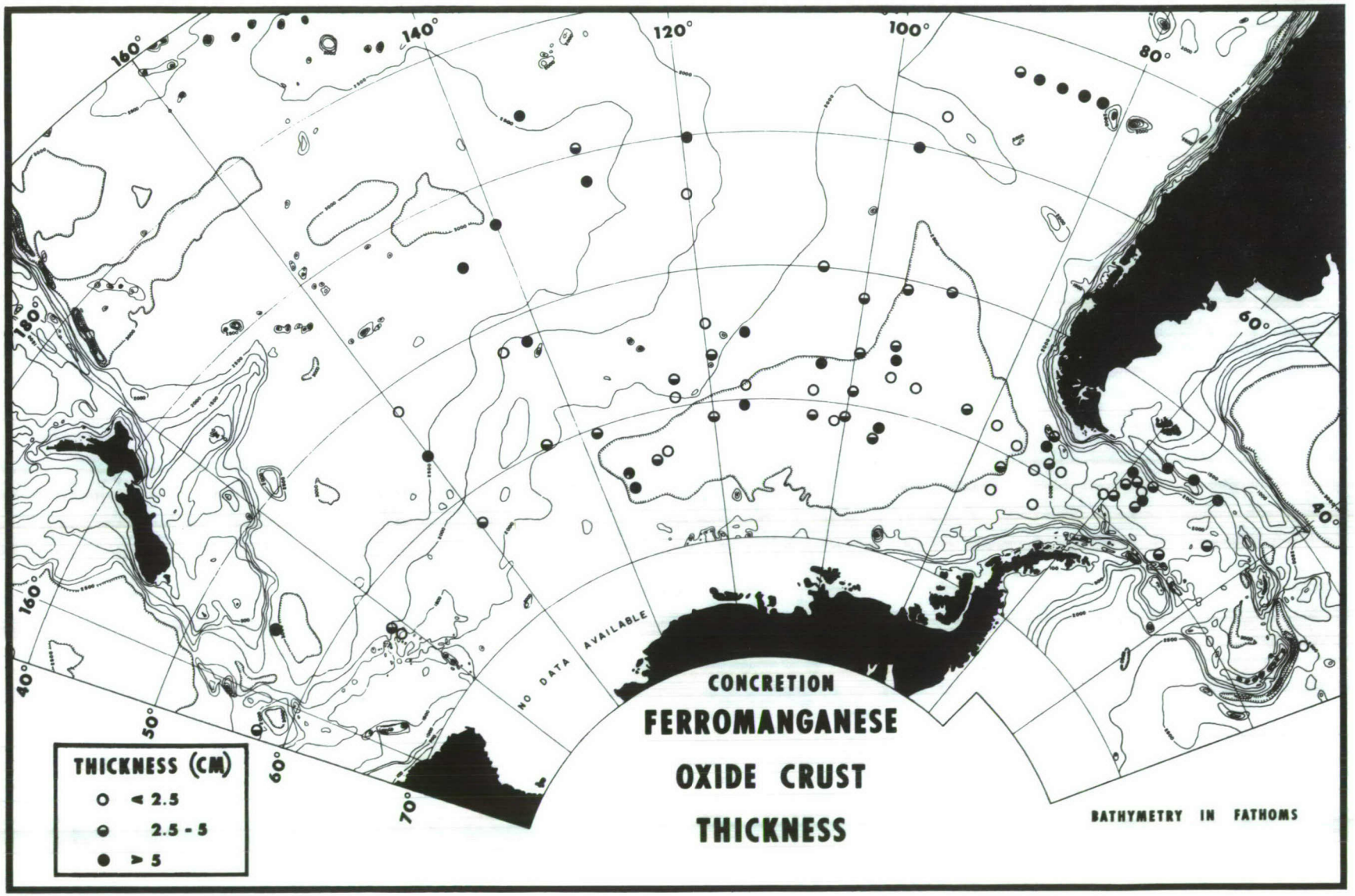
160°
140°
120°
100°
80°
180°
60°
40°
160°
40°
50°
60°
70°
NO DATA AVAILABLE
THICKNESS (CM)
< 2.5
2.5 - 5
> 5
CONCRETION
FERROMANGANESE
OXIDE CRUST
THICKNESS
BATHYMETRY IN FATHOMS

MINERALOGY

Previous work

One of the most poorly understood features of a manganese nodule is its ferromanganese mineralogy. There are good reasons for this lack of knowledge. The principal iron phase is amorphous, and the manganese mineral crystallites are so finely divided that only a few diffuse peaks appear on X-ray diffractograms; the tiny crystals cannot be studied with standard petrographic techniques. This is unfortunate, because an understanding of the genesis of manganese nodules depends upon an understanding of the thermodynamic and structural properties of the ferromanganese minerals.

Murray and Renard (1891, p. 367) stated that "the microscopic characters of the manganese concreted in the nodules do not present any peculiarities to allow of a specific determination of the mineral." On the basis of chemical analyses, they concluded (1891, p. 371) that the nodules consist of the impure variety of manganese known as wad or bog manganese ore, related to psilomelane, but being mixtures of different oxides the manganese could not be considered to belong to distinct mineral species.

Feitknecht and Marti (1945) and Buser, Graf, and Feitknecht (1954) studied synthetic manganese oxides under

laboratory control. By comparing synthetic phases with ferromanganese oxides found in manganese nodules, a model of the mineralogy has been constructed (Buser and Grütter, 1956; Grütter and Buser, 1957; and Buser, 1959). Three basic crystalline phases are recognized: δ-MnO_2, 7 Å-manganite, and 10 Å-manganite. δ-MnO_2 consists of disordered sheets of manganese (IV) dioxide that forms units as small as 50-100 Å. The manganites are double layer structures; one of the layers is an ordered manganese (IV) dioxide unit, and the alternate layer is comprised of disordered iron or manganese hydroxide in which calcium, sodium, and other ions partially substitute for iron and manganese. When iron hydroxide predominates in the disordered manganite layer, the layer is called a ferric manganite; when manganese hydroxide predominates, a manganous manganite results. A difference in thickness of the disordered manganite sheet produces different basal spacings. A 10 Å-manganite contains two discrete OH and/or H_2O layers, while the collapsed 7 Å-manganese contains only one (OH or H_2O) such layer. Buser (1959) postulates that the three crystalline structure units of manganese nodules represent three states of oxidation, with δ-MnO_2 being the most highly oxided, 7 Å-manganite being intermediate, and 10 Å-manganite showing the lowest oxidation state. The approximate empirical formulas for the manganites are $3MnO_2 \cdot Mn(OH)_2 \cdot 3H_2O$ (for 10 Å-manganites) and $4MnO_2 \cdot Mn(OH)_2 \cdot 2H_2O$ (for 7 Å-manganite) (Buser and Grütter, 1956). A possible

discrepancy between the redox relationships suggested by Buser and Grütter and the observed occurrences of the three manganese phases is reported by Barnes (1967). He finds δ-MnO_2 coexisting with 10 Å-manganite without the intermediate 7 Å-manganite.

The series of decreasing oxidation states (δ-MnO_2 to 7 Å-manganite to 10 Å-manganite) represents a series of increasing states of hydration. According to Buser, Graf, and Feitknecht (1954, p. 2333), δ-MnO_2 essentially forms "two dimensional" crystals of 2 to 3 atomic layers that display no basal reflections on X-ray diffraction patterns. 7 Å-manganites generally have a lower oxidation state, as a gradational series between the two appears to exist when the MnO_2:$Mn(OH)_2$ ratio is considered, and an added H_2O or OH layer. 10 Å-manganites have the lowest MnO_2:$MN(OH)_2$ ratio and a double OH-H_2O layer.

According to the arbitrary distinction of Buser, Graf, and Feitknecht (1954), a manganous manganite with an O:Mn ratio greater than 1.9, and having no basal spacing on its X-ray diffraction pattern, is defined as δ-MnO_2. Bricker (1965, p. 1326), taking into account surface area measurements, states that δ-MnO_2 and manganous manganite are identical except for particle size. δ-MnO_2 lacks basal X-ray reflections because of the very minute size of its crystals. If this is the case, a discussion of oxidation differences between δ-MnO_2 and manganous manganite is meaningless.

Jones and Milne (1956) reported a naturally occurring manganous manganite from a gravel pan in Scotland and give it the name birnessite. Their impure material $(Na_{0.7}Ca_{0.3})Mn_7O_{14} \cdot 2.8H_2O$, gave a 7 Å-manganite diffraction pattern. For the purposes of this study, birnessite = 7 Å-manganite = manganous manganite, and δ-MnO_2 will be the term applied to the very fine grained form of this material, i.e., lacking basal X-ray reflections. Barnes (written communication, 1967), in his study of Pacific manganese nodules, separated δ-MnO_2 and manganous manganite on the basis of the absence or presence of a 7 Å diffraction peak, respectively.

One of the most interesting aspects of the disordered half of the manganite phase is an ability to accommodate a variety of cations. Mn^{+2} and Fe^{+3} are the predominant cations, but Mg, Ni, Cu, Co, Zn, Ca, and Al ions can substitute to a limited extent for the dominant metals, especially in the formation of 10 Å-manganites (Buser, 1959, p. 962). Goodell (1965, p. 20) postulated that the change in oxygen packing necessary when polyvalent ions with a high charge density enter ferromanganese oxide structures reduces the degree of crystallinity of the oxides. This may account for the disorder in the manganite phase.

Adsorption apparently plays an even more important role. Buser and Grütter (1956) calculated the large surface areas possessed by manganese concretionary material; values ranged from 6 to 190 square meters per gram. The

highest values were reported in nodules with a large fraction of δ-MnO_2 or FeOOH. It seems possible that the rapid adsorption of Ni, Co, and Cu may force MnO_2 to grow as a finely divided mosaic of crystals rather than as a continuous structure.

Iron hydroxides are an invariable constituent of manganese nodule material. Frequently the major form is X-ray amorphous $FeOOH \cdot nH_2O$ (Grütter and Buser, 1957). Thermodynamically more stable is goethite, α-FeOOH, which is also often found in manganese nodules (Buser, 1959). Electron microprobe studies (Burns and Fuerstenau, 1966) indicate that iron hydroxide--δ-MnO_2 sheets alternate with manganite layers. Goldberg and Arrhenius (1958, p. 197) hypothesized that this alternation of layers has genetic significance, the iron hydroxides serving as a catalytic surface of accumulation for manganese oxides.

During recent years, the synthetic phases of Buser, Feitknecht, and Marti (1954) have been found as naturally-occurring minerals in both terrestrial and marine deposits, and the belief that manganese nodules consist of minerals peculiar to marine concretionary forms has been cast aside. Murata and Erd (1964, p. 647) reported psilomelane in a manganese oxide aggregate associated with sediment rich in Ba and Mn. Hewett, Fleischer, and Conklin (1963, p. 38) tentatively identified todorokite in Pacific and Indian Ocean nodules. Manheim (1965), reporting on manganese nodule

studies conducted by him and his colleagues, stated that todorokite may be a dominent Mn-bearing mineral in marine oxide concretions; Manheim also reported finding birnessite and ramsdellite (a gamma-MnO_2). Sorem (1967, p. 143) micro-sampled a Pacific Ocean concretion and found fine-grained todorokite, along with possible poorly crystallized rancieite, $(Ca, Mn^{+2})Mn_4^{+4}\ O_9 \cdot 3H_2O$, and birnessite. Groutite, Mn(OH), has been detected in a nodule from the Clipperton Fracture Zone (Grant, written communication, 1967).

A number of minerals have been reported as "contaminants" in manganese nodules. Arrhenius (1963, p. 663) described manganese nodules as being an intimate mixture of the oxides, detrital minerals, organic matter, and rutile, anatase, barite, nontronite, and opal; he lists the acid-insoluble fraction as consisting principally of quartz, feldspar, pyroxene, hornblende, micas, spinels, and apatites (1963, p. 669). Manheim (1965, p. 248) has found manganoan calcite and apatite vein fillings in Blake Plateau nodules. McFarlin (1967) described aragonite vein fillings in concretions of the same area. Sorem (1967, p. 142) discovered microfossils, quartz, and other non-opaque clastics incorporated at "unconformities" in nodule laminae.

Mineralogy of Southern Ocean ferromanganese concretions

X-ray diffraction studies of ferromanganese accumulations from the Scotia Sea, Drake Passage, and Pacific-Antarctic

Ocean reveal that todorokite, goethite, quartz, feldspar, phillipsite, and montmorillonite are almost invariably present, although the relative proportions of these constituents vary considerably. Minor amounts of birnessite, clinoptilolite and maghemite are often present, and several other detrital and authigenic minerals are occasionally detected. Because a high iron content without a significant crystalline iron mineral fraction is generally the rule, the presence of an amorphous iron hydroxide is inferred in most of the concretions.

Todorokite was first reported in manganese nodules by Hewett, et al. (1963), although many earlier workers found this phase and called it 10 Å-manganite because it appeared to be analogous to a synthetic manganite generated by Buser and his colleagues. Manheim (1965, p. 248) identified todorokite in nodules from the Pacific Ocean, Blake Plateau, Gulf of Maine, and Baltic Sea. Sorem (1967, p. 143) reported fine-grained todorokite in a nodule from the Horizon Guyot, western Pacific Ocean.

Todorokite is a complex hydrated manganese oxide, $(Mn,Mg,Ca,Ba,Na,K)_2Mn_5O_{12} \cdot 3H_2O$, characterized by a very strong peak (001) at 9.7 Å, a medium strong peak (002) at 4.8 Å, and a series of medium strength peaks around 2.4 Å (210, 012, 004, and 211) (Frondel, Marvin, and Ito, 1960). These peaks are readily identifiable on most diffractograms of Southern Ocean ferromanganese oxides, but peaks of lesser intensity are usually not well defined.

The fact that todorokite is the principal manganese oxide phase in the nodules is substantiated by a linear relationship (on a log scale) between the relative proportion of todorokite in a sample (3.34 Å quartz + 3.2 Å plagioclase-phillipsite/9.7 Å todorokite peak areas) and the weight percent manganese in the sample (Fig. 15). Todorokite is definitely present in 224 of 228 ferromanganese oxide nodules, and in the other four may be obscured by illite or muscovite.

Birnessite is a 7 Å-manganous manganite. Manheim (1965, p. 248) identified birnessite in a concretion from the Baltic Sea. Sorem (1967, p. 143) tentatively identified birnessite in a Horizon Buyot nodule. Earlier work by Grütter and Buser (1957) showed a 7 Å-manganite to be present in an Atlantic and several Pacific Ocean nodules. Barnes (1967) found 7 Å-manganites widely scattered across the eastern Pacific Ocean. Birnessite is not the major manganese oxide phase in any of the Southern Ocean concretions. It may be present in most of the nodules, but only occasionally exceeds trace amounts; when present in minute quantities it may be obscured by phillipsite or chlorite. In 36 samples, mainly from the central Pacific-Antarctic Ocean, birnessite is present in moderate amounts. A fragile fracture filling in one nodule was found to be composed of nearly pure birnessite.

Delta-MnO_2 is considered to be the ultra-cryptocrystalline analogue of birnessite, lacking basal X-ray reflections and

Fig. 15.--Weight Percent Manganese in Concretion vs. Ratio of Peak Areas 3.34 Å Quartz + 3.2 Å Plagioclase-Phillipsite / 9.7 Å Todorokite.

RATIO : 3.2Å PLAGIOCLASE, PHILLIPSITE + 3.34Å QUARTZ / 9.7Å TODOROKITE
PEAK AREAS
LOG SCALE
100
10
1
0.1
2
4
6
8
10
12
14
16
18
20
22
24
26
28
WEIGHT PERCENT MANGANESE

the crystallographically-associated disordered manganite layer of birnessite. Such material is undoubtedly common in manganese nodules, but only occasionally does an exaggerated 2.4 Å diffraction peak present itself as evidence for the presence of δ-MnO_2

Goethite, α-FeOOH, has appeared in most of the marine ferromanganese accumulations studied by previous workers (Buser and Grütter, 1956; Grütter and Buser, 1957; Manheim, 1965; and Bonatti and Joensuu, 1966). Goethite appears to be the stable deep-sea iron hydroxide phase, formed by aging of excess $FeOOH \cdot nH_2O$ that is not incorporated into ferric manganite layers (Goldberg and Arrhenius, 1958, p. 194). Goethite is probably present in all of the studied Southern Ocean nodules, but due to its cryptocrystalline nature and Fe- and Mn-produced fluorescence, it was definitely identified in only a minority of the samples.

Maghemite, γ-Fe_2O_3, has not been previously identified in ferromanganese oxide accumulations. However, Machek (1965) and Mather (1967) have found maghemite in Antarctic Ocean sediment samples. Harrison and Peterson (1965) described an authigenic mineral intermediate between magnetite and maghemite from the Indian Ocean. Maghemite may be produced artifically by dehydration of lepidocrocite, γ-FeOOH, or by the low temperature oxidation of magnetite (Hagg, 1935, cited in Deer, Howie, and Zussman, 1962, p. 73). Since magnetite is common in the volcanic sediments of the

study area, oxidation of magnetite incorporated into concretions probably produces maghemite. Maghemite is tentatively identified in many Southern Ocean nodules, but only in a few samples is its presence well established.

Montmorillonite is commonly found in sediments of the South Pacific. Griffin and Goldberg (1963) reviewed earlier work on Pacific montmorillonoids, and point out that montmorillonite is the most abundant clay mineral in the South Pacific. They observed no variation in the montmorillonite/illite ratio with either latitude or longitude. Adjacent to the Antarctic continent (except near the Ross Sea) montmorillonite is the least important clay mineral (Goodell, 1965, p. 16). Arrhenius (1963, p. 703) stated that the iron-rich variety nontronite is abundant around centers of volcanic activity.

Montmorillonite is an almost invariable constituent of Southern Ocean manganese nodules; the cation content and relative crystallinity probably vary considerably. It seldom comprises a large part of the silicate fraction in nodules, except in nuclei. Montmorillonite is generally assumed to have formed <u>in situ</u> by the alteration of volcanic glass (Arrhenius, 1963; and Bonatti and Nayudu, 1965; among others).

Zeolites of the phillipsite-harmotome series have been reported many times in Pacific pelagic sediments and manganese nodules. Bonatti (1963) discussed the distribution

in the Pacific of phillipsite and associated minerals, as well as the formation of this mineral. He suggested (1963, p. 946) that phillipsite is formed by the gradual alteration of palagonite. Arrhenius and Bonatti (1965, p. 16) stated that the formation of harmotome appears to be limited to the earlier stages of glass-sea water interaction, with phillipsite engulfing harmotome nuclei and apparently replacing montmorillonite. Morgenstein (1967) reported the barium-rich variety harmotome from near the Society Islands, but this identification is not supported by chemical analysis. Rex (1967) found that phillipsite is metastable in sea water, since long-term exposure produces etching of the crystal faces.

Grant (1967, p. 65) found phillipsite in 13 of 28 samples of non-glacial erratic nucleus materials (while at the same time detecting montmorillonite in 24 of the 28 samples). In this study, phillipsite was found in 73 of 91 nucleus samples, and montmorillonite in 88 of 91. Zemmels (verbal communication, 1967) could not detect barium in a nearly pure phillipsite sample, so it is concluded that harmotome is relatively unimportant. In addition, barite and celestobarite do not occur in detectable quantities, although their importance was noted by Arrhenius (1963, 1967). Possibly the available barium is incorporated into the todorokite structure.

Clinoptilolite is reported in pelagic sediments by Biscaye (1965) and Goodell (1965). Goodell (1965, Fig. 12) depicted clinoptilolite distribution as patches scattered throughout the Scotia Sea, Drake Passage, and Pacific-Antarctic Ocean; the clinoptilolite occurs in the clay-size sediment fraction. He postulated (1965, p. 16-17) that this zeolite is a stable phase where excess silica is provided by soluble opaline diatom and radiolarian frustules. Clinoptilolite appears to be a common trace constituent in Southern Ocean manganese nodules. It is not abundant in a single sample, but it is tentatively identified in many concretions, and definitely in several others.

Quartz and feldspar are the most important silicates found in the vast majority of marine ferromanganese oxide deposits. They probably represent current-, wind-, and ice-rafted detritus, but submarine volcanism could supply a sizeable proportion of feldspar. Rex and Goldberg (1958) studied quartz in Pacific pelagic sediments, and noted the latitudinal dependence in the eastern Pacific of quartz content, with a concentration at 30°N. Lat. They found no evidence for either volcanic or authigenic quartz. It was concluded that the quartz (being mainly 1-20 microns in size and lacking volcanic features) was supplied by aeolian transport from continental deserts. They also found the South Pacific to be essentially devoid of quartz, abundances decreasing away from continents toward mid-oceanic areas,

where rarely more than 6% quartz was found. Peterson and Goldberg (1962) disagreed with earlier work, pointing out an abundance, particularly over the crest of the East Pacific Rise, of quartz of typical volcanic morphology. Goodell (1965) reported an increase in terrigenous material, much of it quartz, toward the Antarctic Continent. Quartz is intermixed with 223 of the 228 ferromanganese oxide accumulations studied, occurring in greatest abundance in the Scotia Sea, Drake Passage and central Pacific-Antarctic Basin, and in general, in all concretions found in areas where ice-rafted detritus is found.

The most intensive study of feldspars in the southeastern Pacific Ocean has been made by Peterson and Goldberg (1962). In the coarse (greater than 32 microns) fraction they found abundant anorthoclase and a lesser amount of sanidine on the crest of the East Pacific Rise, and plagioclase (oligoclase-labradorite) on the Rise flanks. In the fine (4-8 microns) fraction they noted anorthoclase and plagioclase both on the Rise crest and on the flanks. From their data they were able to delineate a province of acidic volcanism associated with the East Pacific Rise and concluded that most feldspars in the pelagic sediments of the southeastern Pacific have been derived from the basin itself.

Plagioclase and possible trace amounts of sanidine are the only feldspars detected thus far in manganese nodules of the Southern Ocean. Plagioclase is definitely present in

226 of 228 samples of manganese and iron oxides. A composition estimation based on diffractograms places most of the plagioclase in the oligoclase-anorthite range.

Amphibole is another common constituent of Antarctic Ocean sediments and concretions. Goodell (1965) mapped the distribution of amphibole in the less-than-two micron size fraction, and finding it mostly restricted to the deeper portions of the Scotia Sea and Pacific-Antarctic Ocean, concluded that most of it is derived from submarine basalts or even by authigenesis. Edwards (verbal communication, 1967) found abundant sand-size amphibole in sediments adjacent to the Palmer Peninsula. Amphibole was only occasionally identified in Pacific-Antarctic Ocean manganese nodules, but was usually found in nodules from the Drake Passage-Scotia Sea area.

Illite-muscovite and chlorite are the most common detrital phyllosilicates of the study area. The areal distribution of these minerals in the Pacific has been discussed by Griffin and Goldberg (1963) and Goodell (1965); the former utilized samples mainly from the North Pacific, while the latter has studied the South Pacific Ocean and Scotia Sea sediments. Goodell (1965, p. 15) believes that most of the chlorite is terrigenously derived, while some of the illite may be in part hydrothermally produced by sea water-extruded basalt reactions. A small percentage of illite seems to be incorporated in Scotia Sea-Drake Passage manganese

nodules, but chlorite is rarely identifiable because its principal diffraction peak coincides with that of phillipsite.

A number of other minerals were found, none definitely present in more than a few samples. Pyroxene, olivine, magnetite, and ilmenite(?) probably represent volcanic derivatives. The same is true of glass, which may be fairly ubiquitous, but impossible to detect except when present in large quantities. Prehnite and analcime(?) probably formed during the latter stages of cooling of submarine lava flows. Apatite, calcite and cristobalite(?) can be attributed to incorporated bones, foraminiferal tests, and siliceous volcanic material, respectively. Talc/pyrophyllite and serpentine(?) may be contributed either by techtonically-associated submarine metamorphic processes or by transportation from continental metamorphic terranes.

The large number of minute but well-defined diffractogram peaks between 5 and 8 Å suggests the presence of zeolites or other hydrated minerals. In several instances sets of peaks displayed by mordenite and erionite were recognized and several hintings of epistilbite could be seen. However, it cannot be definitely stated that these zeolites are present because of the nature of the material sampled. Some of the minute peaks suggest sparse hydrated oxides of manganese and iron, such as psilomelane and β-FeOOH. And several reoccurring peaks do not seem to belong to any known substance.

A possible trace of barite and a single sample apparently consisting of a mixture of α and β quartz were also recorded. Since manganese nodules are basically "garbage collectors," almost any detrital or authigenic mineral could conceivably be found intermixed with accumulating iron and manganese oxides.

Appendix F lists the number of samples in which each mineral was definitely or possibly present. The table does not effectively show the relative importance of the minerals in oxide crust, subscrust, and nucleus sections of the concretions. Generally speaking, the proportion and variety of the silicates increases toward the center of the nodule. This is not really evident on a presence-or-absence basis.

The areal distribution of the minerals is discussed in the following section. Appendix E lists the mineralogy of each individual sample.

Areal distribution of concretion minerals

Nodules are formed by precipitated oxides that incorporate available detritus, along with some unstable minerals and glass that may be converted to more stable phases within the nodules. The proportions of minerals within the ferromanganese encrustations should reflect the associated sediment mineralogy, the surrounding sea-water chemistry, and the length of time that unstable phases are subjected to processes striving for equilibrium. The latter two effects

on mineral proportions are difficult to evaluate. Regional trends dictated by associated sediment mineralogy are evident, however.

The relative proportion of todorokite in a manganese encrustation in the Southern Ocean appears to be most dependent upon its dilution by other minerals. Dilution by the amorphous iron hydroxide phase, though quantitatively important, does not significantly alter peak area ratios, so its effect can be ignored. Thus the rates of incorporation of quartz and feldspar, and to a lesser degree, phillipsite and montmorillonite, dictate the amount of todorokite present.

Since the crystalline fraction of nodule depositions in the Southern Ocean consists essentially of todorokite, quartz, and feldspar, the relative importance of todorokite is given by the ratio of peak areas 3.34 Å quartz + 3.2 Å plagioclase (plus phillipsite) vs. 9.7 Å todorokite. The values for this ratio across the Pacific-Antarctic Ocean and Scotia Sea are contoured in Figure 16. At stations where more than one type of nodule was sampled, the values obtained were averaged. The effects of averaging and the statistical reliability of the values are discussed in the Appendix. It must be kept in mind that a great number of factors can influence the values for peak area ratios, and only broad regional trends have been sought.

The greatest concentrations of todorokite occur in more northerly latitudes, generally north of 56-60°S. Lat.,

and at distances of at least several hundred miles from the nearest continental land masses. Low and intermediate values for the ratio 3.34 Å Quartz + 3.2 Å Plagioclase - Phillipsite/ 9.7 Å Todorokite, indicating an appreciable todorokite content, are characteristic of ferromanganese accumulations from the Southwest Pacific Basin, the Pacific-Antarctic Rise, the Chile Rise-Robinson Crusoe Is. vicinity, the area between the Chile Rise and the Eltanin Fracture Zone, and the north-central segment of the Scotia Arc. The lowest proportions of todorokite are found in nodules from the southern and eastern portions of the Pacific-Antarctic Basin, the Drake Passage and the West Scotia Basin. Concretions low in todorokite are also found adjacent to the South Sandwich Trench, and on some parts of the Pacific-Antarctic Rise and its flanks.

Relative quartz and plagioclase contents are presented in Figures 17 and 18, respectively. Higher proportions of both quartz and feldspar are found in southerly latitudes where the todorokite proportion is lowest. Such a distribution of covariances undoubtedly reflects an influx of ice-rafted quartz and feldspar into waters north of the Antarctic continent.

North of the area influenced by glacial detritus, quartz and feldspar lose their latitudinal dependence. In the Southwest Pacific Basin nodule deposit, relative quartz content decreases from southwest to northeast. Concretions

very low in quartz are found in the Chile Rise sector. Assuming that quartz content does measure deposition of detrital quartz, then presumably nodules from the North Pacific in the area studied by Rex and Goldberg (1958) would show increased proportions of quartz.

Feldspar is the most constant of the three major crystalline constituents of ferromanganese accumulations, the extreme values for the 3.34 Å Quartz + 9.7 Å Todorokite/ 3.2 Å Plagioclase - Phillipsite ratio differing by only 20 orders of magnitude (while the extreme todorokite ratios differ by a factor of 225, and the maximum quartz value is 40 times the minimum). Nodules from the Pacific-Antarctic Rise, from the center of the Southwest Pacific Basin, and from the north-central Scotia Arc show the lowest relative feldspar content. Apparently the importance of the detrital contribution outweighs the volcanic contribution of feldspar, since areas of the Pacific-Antarctic Rise which might be expected to produce significant feldspar (based on the work of Peterson and Goldberg, 1962) are contributing little feldspar that is being incorporated into the accreting oxides.

Amphiboles, mainly hornblende, also appear to show a distribution consistent with deposition from melting ice (Fig. 19). Thirty of 34 stations in the West Scotia Basin and Drake Passage yielded nodules with appreciable amphibole, and three of the four remaining stations show nodules with a probable amphibole content. Several concretions from

the Pacific-Antarctic Basin also contain identifiable amphibole; only two samples north of the limit of glacial erratics definitely contain amphibole, one being from south of the New Zealand Plateau and the other from the Chile Rise. In almost every case the amphibole is contained in the oxide crust portion of the concretion, and not the nucleus.

Birnessite is a secondary manganese oxide in Southern Ocean nodules. Its distribution is shown in Figure 20. Significant birnessite content is more prevalent in the center of the Pacific-Antarctic Ocean and northeast of the Chile Rise, but no definite pattern is evident. Based on the work of Arrhenius, Mero, and Korkisch (1964), birnessite is probably more slowly crystallized than todorokite.

Montmorillonite, chlorite, maghemite, goethite, pyroxene, clinoptilolite, and analcime(?) show no discernible regional concentrations, being present in small amounts in nodules from every part of the study area. The few definite illite occurrences are in nodules closest to the Antarctic continent, south of about 60°S. Lat.

From the distribution patterns of todorokite, quartz, feldspar, amphibole and illite it is concluded that ferromanganese accumulations incorporate detritus settling from suspension in seawater (and in the case of nodules that may have rolled, from the sediment surface) in proportions relative to rates of supply of the detrital constituents to

a particular area; and further, that probable differing rates of accumulation of the manganese and iron hydroxides are not different enough to obscure regional trends of detrital deposition.

Fig. 16.--Distribution of Values for the Ratio of Peak Areas 3.34 Å Quartz + 3.2 Å Plagioclase-Phillipsite / 9.7 Å Todorokite in Concretions from the Study Area.

Fig. 17.--Distribution of Values for the Ratio of Peak Areas 3.2 Å Plagioclase-Phillipsite + 9.7 Å Todorokite / 3.34 Å Quartz in Concretions from the Study Area.

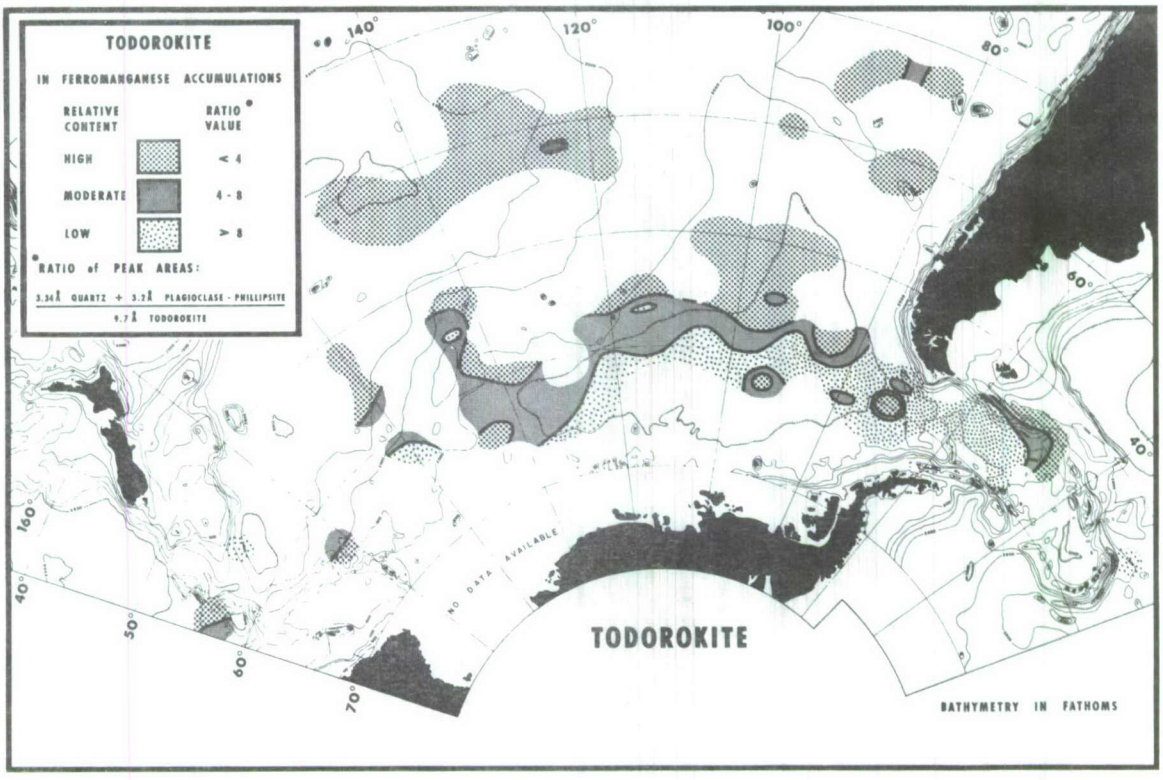
TODOROKITE
IN FERROMANGANESE ACCUMULATIONS
RELATIVE CONTENT
RATIO VALUE*
HIGH
< 4
MODERATE
4 - 8
LOW
> 8
*RATIO of PEAK AREAS:
3.34Å QUARTZ + 3.2Å PLAGIOCLASE - PHILLIPSITE
9.7Å TODOROKITE
140°
120°
100°
80°
60°
40°
160°
40°
50°
60°
70°
NO DATA AVAILABLE
TODOROKITE
BATHYMETRY IN FATHOMS

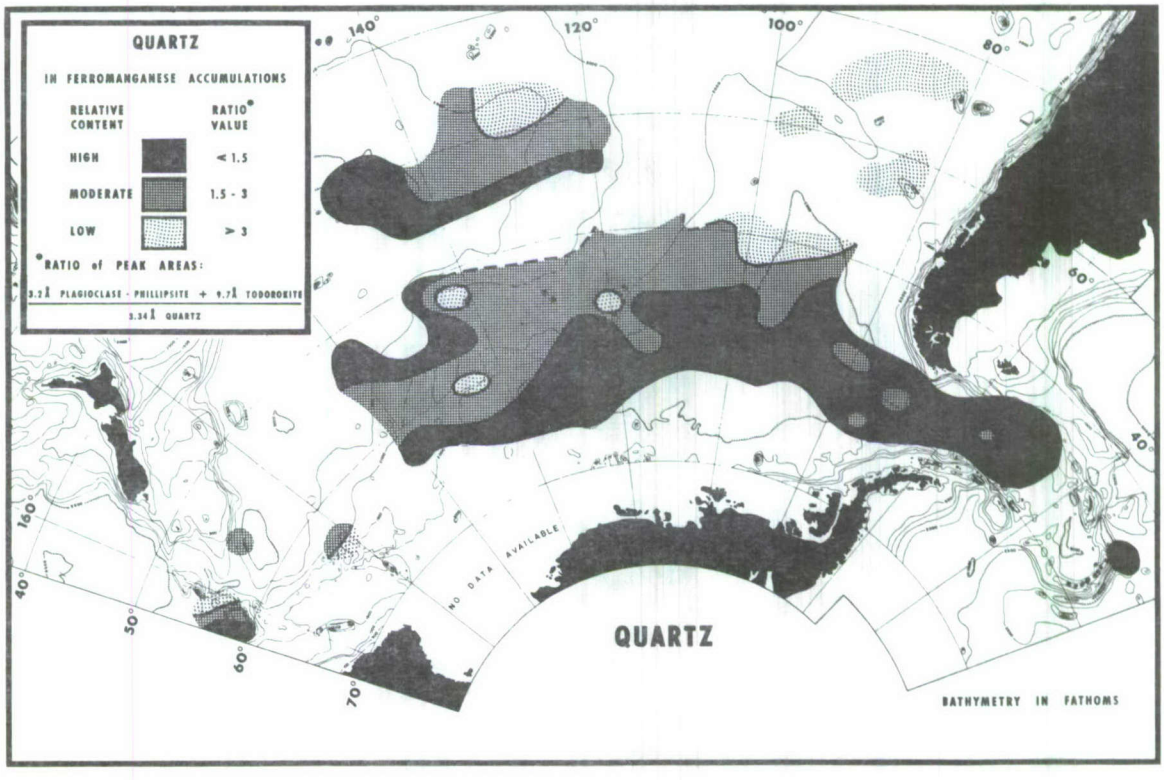
QUARTZ
IN FERROMANGANESE ACCUMULATIONS
RELATIVE CONTENT
RATIO VALUE*
HIGH
< 1.5
MODERATE
1.5 - 3
LOW
> 3
*RATIO of PEAK AREAS:
3.2Å PLAGIOCLASE - PHILLIPSITE + 9.7Å TODOROKITE
3.34Å QUARTZ
140°
120°
100°
80°
60°
40°
160°
40°
50°
60°
70°
NO DATA AVAILABLE
QUARTZ
BATHYMETRY IN FATHOMS

Fig. 18.--Distribution of Values for the Ratio of Peak Areas 3.34 Å Quartz + 9.7 Å Todorokite / 3.2 Å Plagioclase-Phillipsite in Concretions from the Study Area.

Fig. 19.--Distribution of Amphibole in Concretions from the Study Area.

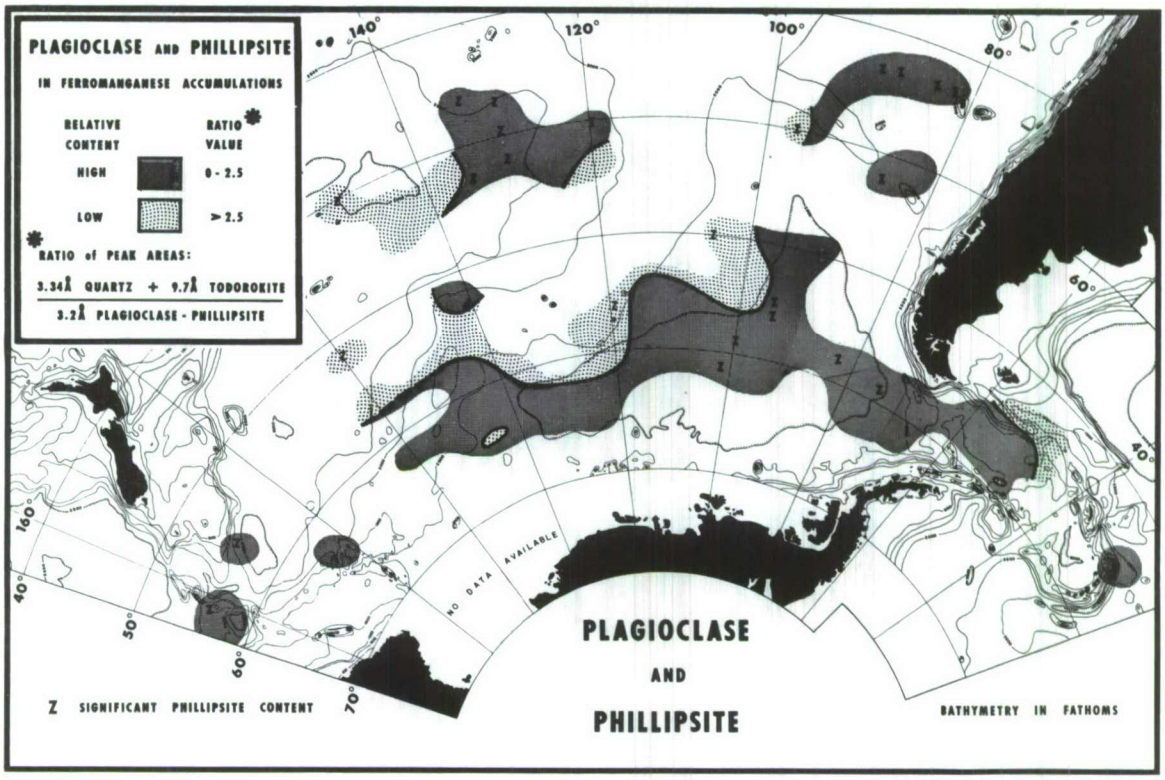
PLAGIOCLASE AND PHILLIPSITE
IN FERROMANGANESE ACCUMULATIONS
RELATIVE CONTENT
RATIO VALUE
HIGH
0 - 2.5
LOW
> 2.5
RATIO of PEAK AREAS:
3.34Å QUARTZ + 9.7Å TODOROKITE
3.2Å PLAGIOCLASE - PHILLIPSITE
140°
120°
100°
80°
60°
40°
160°
40°
50°
60°
70°
NO DATA AVAILABLE
Z SIGNIFICANT PHILLIPSITE CONTENT
PLAGIOCLASE
AND
PHILLIPSITE
BATHYMETRY IN FATHOMS

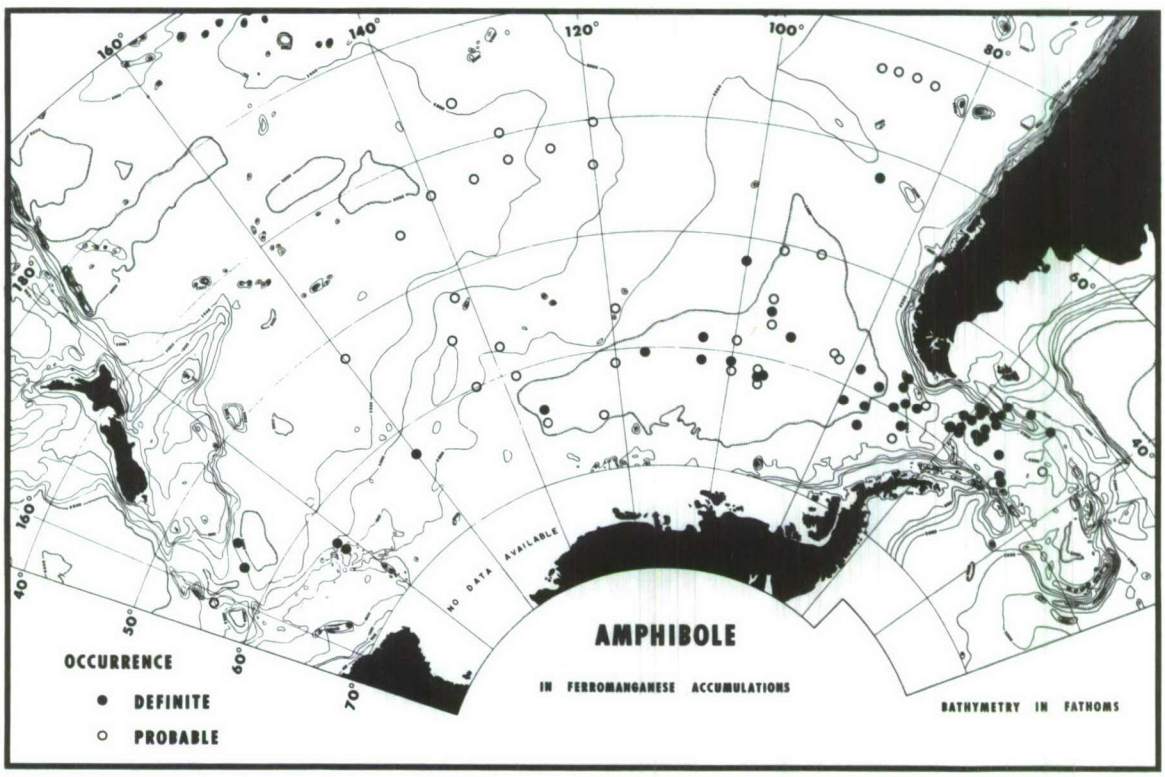
160°
140°
120°
100°
80°
180°
60°
40°
160°
40°
50°
60°
70°
NO DATA AVAILABLE
OCCURRENCE
DEFINITE
PROBABLE
AMPHIBOLE
IN FERROMANGANESE ACCUMULATIONS
BATHYMETRY IN FATHOMS

Fig. 20.--Distribution of Birnessite in Concretions from the Study Area.

Fig. 21.--Distribution of Values for Ratio Mn / Fe in Concretions from the Study Area.

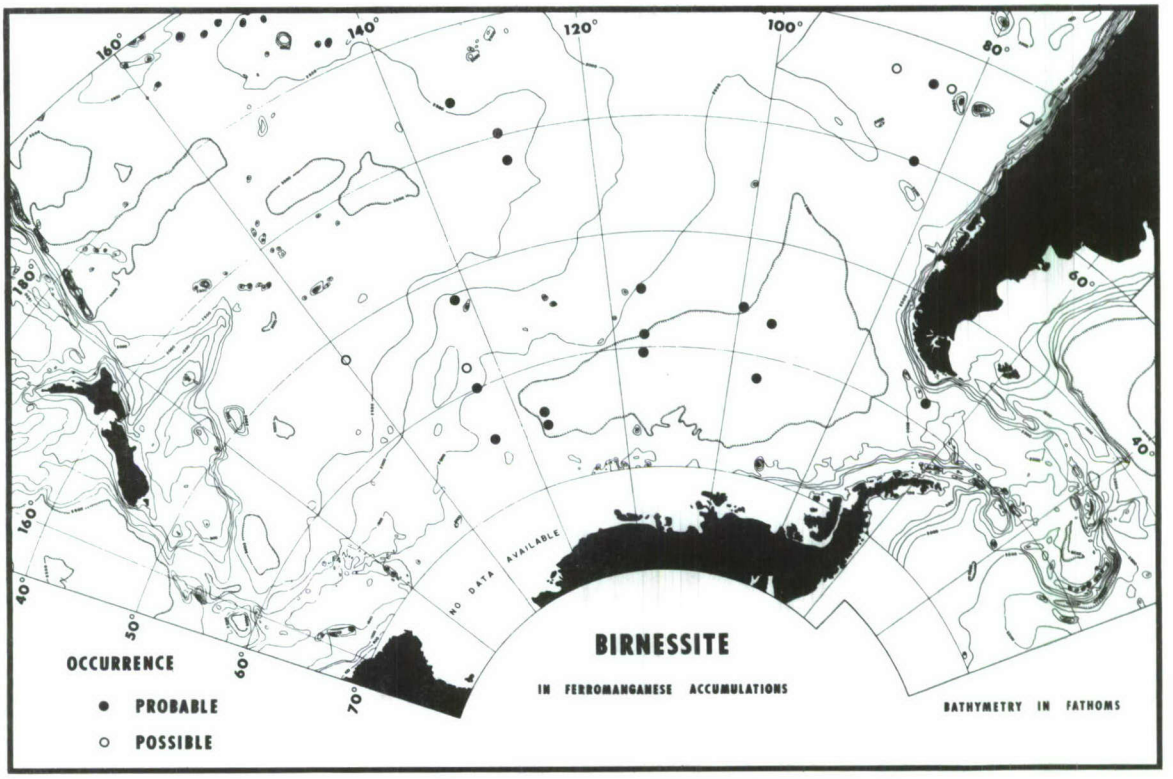
160°
140°
120°
100°
80°
60°
40°
180°
160°
40°
50°
60°
70°
NO DATA AVAILABLE
OCCURRENCE
PROBABLE
POSSIBLE
BIRNESSITE
IN FERROMANGANESE ACCUMULATIONS
BATHYMETRY IN FATHOMS

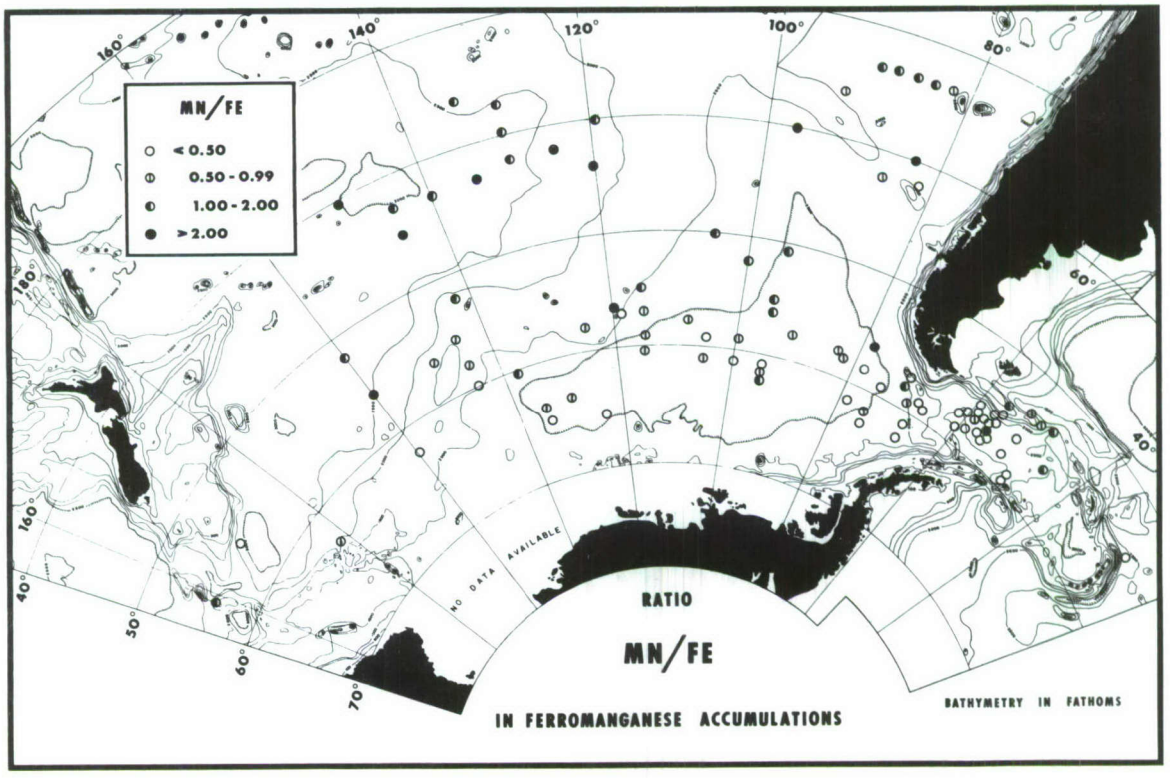
MN/FE
< 0.50
0.50 - 0.99
1.00 - 2.00
> 2.00
160°
140°
120°
100°
80°
60°
40°
180°
160°
40°
50°
60°
70°
NO DATA AVAILABLE
RATIO
MN/FE
IN FERROMANGANESE ACCUMULATIONS
BATHYMETRY IN FATHOMS

GEOCHEMISTRY

Manganese nodules are geochemically unique concentrations of Mn, Fe, Ni, Co, and Cu. Also present in significant amounts in the iron-manganese concretions are Na, Mg, Al, Si, K, Ca, Ti, and Ba (Mero, 1965, p. 180). The basic problem encountered in a study of manganese nodules is an explanation for the association and relative proportions of these elements in the nodules. The problem involves weighing continental vs. submarine volcanic elemental contributions, as well as pin-pointing one or more mechanisms for the simultaneous collection of Mn, Fe, Ni, Co, and Cu in concretionary form.

Factors pertinent to the marine geochemistry of the five important metals in manganese nodules are summarized in Table 6. These factors include the percentage of the metal in certain rocks, water, and sediment types, the transfer percentage (quantity present in sea water vs. quantity supplied to oceans during geologic time), the forms of occurrence in sea water, the degree of enrichment in marine organisms, the efficiency of cation adsorption by substances found in the ocean, ionic sizes, lattice energy coefficients (or relative cation-field intensities), and the phases in which Mn, Fe, Ni, Co, and Cu are present in manganese-nodules.

Table 6.--Factors relevant to the geochemistry of Mn, Fe, Ni, Co, and Cu in ferromanganese concretions.

Metal	Weight percent in: Crustal rocks (1)	Granite (10)	Alkali basalt (2)	Fresh water (11)	Sea water (3)	Carbonate ooze (10)	Red clay (10)	Pacific nodules(4)	Transfer Percentage (12)	Forms of occurrence in sea water: Solution	Colloidal	Particulate (5)	Enrichment factor in marine organisms (17) (content organisms/ content sea water)	Percentage removal by adsorption on colloids (18): $MnO_2.nH_2O$	$Fe_2O_3.nH_2O$	Montmorillonite	Plankton	Valence state/ relative ionic size (6 coordination) (19)	Lattice energy coefficient (12)	Phases in which metal is present in manganese nodules (9, 20, 21, this study)
Manganese	0.1	0.046	0.12	7×10^{-6}	0.002	0.1	0.67	18.5	0.00033	Mn^{+2} negligible (13) Chloro-complexes?(9) $Mn(OH)_2$? (14)	$Mn(OH)_3$ or $MnO_2.nH_2O$ (15) Organic complexes? (13)	Diadochic substitution in rock-forming minerals	?	--	--	--	--	Mn^{+2}/0.80 Mn^{+4}/0.60	Mn^{+2}/560 Mn^{+4}/2680	Mn^{+4} in δ-MnO_2 Mn^{+2} in disordered layer(s) of manganites, especially manganous manganites
Iron	5.0	2.19	7.55	7×10^{-5}	0.01	0.9	6.5	10.8	0.000036	$Fe^{+2} < 10^{-9}$ ppm (6) Chloro-complexes?	$Fe(OH)_3$ (16)	Mainly in olivine, pyroxene, amphibole, femag micas	?	--	--	--	-	Fe^{+2}/0.74 Fe^{+3}/0.64	Fe^{+2}/580 Fe^{+3}/1280	Fe^{+3} in disordered layer(s) of manganites, especially ferric manganite. $FeOOH.nH_2O$ (amorphous). Goethite, maghemite
Nickel	0.0080	0.001	0.0051	2×10^{-7}	0.002	0.003	0.022	0.65	0.00083	Ni^{+2}? $NiCl^{+}$? (8) $Ni(OH)^{+}$?	Adsorbed on colloids	Diadochic substitution in silicates, especially of ultrabasic rocks	5000	99	33	10	8	Ni^{+2}/0.69	Ni^{+2}/620	Ni^{+2} in disordered layer(s) of manganites
Cobalt	0.0045	0.0004	0.0025	4×10^{-8}	0.0001	0.0007	0.0074	0.30	0.0046	Co^{+} $CoCl^{+}$ (8) $Co(OH)^{+}$?	Adsorbed on colloids	Diadochic substitution in silicates, especially of silicic rocks	7000	93	35	18	8	Co^{+2}/0.72 Co^{+3}/0.63	Co^{+2}/620 Co^{+3}/1320	Co^{+3} substituting for Fe^{+3} in amorphous $FeOOH.nH_2O$ Co^{+2} in disordered layer(s) of manganites
Copper	0.0023	0.002	0.0036	---	0.003	0.003	0.025	0.43	0.0071	Cu^{++} $CuCl^{+}$ (7) $CuCl_2$	Adsorbed on colloids	Mainly in sulfides and sulfo-salts	2600	96	96	94	54	Cu^{+2}/630	Cu^{+2}/630	Cu^{+2} in disordered layer(s) of manganites

(1) Mason, 1958.
(2) Engel, Engel, and Havens, 1965.
(3) Goldberg, 1965.
(4) Compiled from literature.
(5) Rankama and Sahama, 1950.
(6) Sverdrup, Johnson, and Fleming, 1942.
(7) Bjerrum, 1950, cited in Krauskopf, 1956.
(8) Kurbatov, Wood, and Kurbatov, 1951, cited in Krauskopf, 1956.
(9) Goldberg and Arrhenius, 1958.
(10) Turekian and Wedepohl, 1961.
(11) Compiled in Manheim, 1965.
(12) Green, 1959.
(13) Rona, Hood, Muse, and Buglio, 1962.
(14) Harvey, 1955; and Latimer, 1952; cited in Rona et al., 1962.
(15) Krauskopf, 1957
(16) Goldberg, 1954
(17) Black and Mitchell, 1952, cited in Krauskopf, 1956.
(18) Krauskopf, 1956.
(19) Ahrens, 1952.
(20) Buser, Graf, and Feitknecht, 1954; Buser and Grütter, 1956; Grütter and Buser, 1957; Buser, 1959.
(21) Burns, 1965.

The average Mn:Fe:Ni:Co:Cu ratios in crustal rocks (Mason, 1958, p. 44), alkali basalts (Engel, Engel, and Havens, 1965, p. 721), sea water (Goldberg, 1965), and Pacific Ocean manganese nodules (data compiled from literature) are given in Table 7. The two high values and the two low values in each ratio bracket the middle value, which is given an arbitrary value of 1 for the purpose of comparison. Mn, Fe, Ni, Co, and Cu are all normally undersaturated in sea water, and, except for Fe, usually are trace constituents in rocks.

TABLE 7.--Average Mn:Fe:Ni:Co:Cu ratio in crustal rocks, alkali basalts, sea water, and Pacific Ocean manganese nodules.

	Mn:	Fe:	Ni:	Co:	Cu
Crustal Rocks	12.5	625	1	0.29	0.56
Alkali Basalt	23.5	1480	1	0.49	0.71
Sea Water	1	5	1	0.05	1.5
Manganese Nodules	28.5	16.6	1	0.46	0.67

It can be readily seen from the table that in crustal rocks, alkali basalts and sea water, iron is at least five times as abundant as manganese, while in manganese nodules, manganese is almost twice as abundant as iron. The relative proportions of Ni, Co, and Cu are comparable in rocks and manganese nodules, while sea water does not reflect the

proportions of these metals in solid phases. Evidently cobalt is accumulated in preference to copper in the nodules. This is supported by the calculation by Willis and Ahrens (1962, p. 761) of enrichment factors of Mn, Fe, Co, Ni, Co, Mo, V, Ti, and Tl in manganese nodules over percentages in sea water, igneous rocks, and deep-sea clays.

A determination of continental vs. submarine volcanic origin for the constituent elements may inculpate some diagnostic element or ratio of elements. Arrhenius, Mero, and Korkisch (1964) suggested a criterion for differentiating between ferromanganese oxide minerals derived from submarine vulcanism and those slowly formed from dilute solution, largely of continental origin. Their criterion is the Mn:Co ratio, which if greater than 300 is indicative of rapid deposition from volcanic exhalation-sea water solutions. They also note the concentration of thorium (and uranium) in those ferromanganese concretions believed to be of volcanic origin. The Mn:Co ratio criterion, when applied to nodules dredged from the Southern Ocean, appears to have little utility. All samples but one have a Mn:Co ratio less than 300, and the lowest ratios are often found in the Drake Passage and Scotia Sea, where continental influence would be greatest in the study area. The one sample having a Mn:Co ratio greater than 300 (being 740) is as likely as any of the concretions studied to be volcanically derived, having a volcanic nucleus and an East Pacific Rise locus of origin.

Barnes (1967) pointed out that the assumption made by Arrhenius, Mero, and Korkisch (1964) that Co enters the disordered (primarily 10 Å) manganite phase probably is invalid. Barnes demonstrated that Co (and Pb) are relatively more concentrated in the δ-MnO_2 phase, and since depth controls the mineralogy, Co content decreases with depth because shallow depths favor the formation of δ-MnO_2. His finding of a decrease in cobalt content with increased depth agrees with the data of Menard (1964, p. 188). Burns and Fuerstenau (1966) found that nodules containing both 7 Å-manganite and δ-MnO_2 phases are enriched in cobalt, while in concretions consisting of 10 Å-manganites, cobalt is enriched in the layers in which iron is enriched.

Bonatti and Nayudu (1965) argued for the rapid precipitation of nodules adjacent to a volcanic source, and pointed out the wealth of circumstantial evidence available to support such a conclusion. Most of the nodules that Bonatti and Nayudu studied displayed palagonite, sideromelane, phillipsite or hyaloclastite nuclei, all undoubtedly of volcanic origin. They explained (1965, p. 29-30) the accumulation of ferromanganese oxides by the oxidation of iron and manganese leached from erupting submarine lavas by the acid-reducing conditions prevalent during the eruption. The less soluble iron is precipitated first, and most of the manganese is carried farther from the lava before oxidation. Hence the Mn/Fe ratio would increase with distance from the

volcanic source. As a possible test of the hypothesis of Bonatti and Nayudu, data from bottom photographs and chemical analyses have been correlated. Iron and manganese oxide encrustations have been divided into five types of occurrences: (1) those of blanket and nodular form found where submarine outcrops were visible, (2) very dense concentrations of concretions (75-100% covering over subjacent sediment), (3) moderate to dense concentrations of concretions (10-75% cover), (4) scattered nodules (less than 10% cover), and (5) nodules dredged from stations where none could be seen in bottom photographs. Ideally such a division would indicate increasing distance from a known site of volcanism. However, the nodules used cover such as extensive area that many possible loci of eruptions are involved; variable rates of deposition cannot be taken into account; and the supposed most-distant nodule deposits (none visible in photographs) may have been buried by a few centimeters of sediment. It should also be recognized that manganese and iron may be co-precipitated rather than separated. Zelenov (1964) observed suspensions of iron and manganese hydroxides separating out of the cooling water expelled by a submarine volcanic fumerole. Hem (1964a, p. 61) conducted experiments in an aqueous solution having a pH near that of sea water, and found manganese and iron in a precipitated hydroxide.

The results of the test are presented in tabular form (Table 8). It is very apparent that the data available

concerning Mn/Fe ratio vs. inferred increased distance from a volcanic source do not support the hypothesis of Bonatti and Nayudu, but because of possible limitations, the data do not definitely refute the hypothesis, either.

TABLE 8.--Comparison of Mn:Fe ratios in concretion oxide crusts with inferred distance from volcanic source of elements.

Type of Deposit	Mn/Fe Mean	No. Stations	Range of Mn/Fe Values
(1) Submarine lava flow, associated nodules	1.06	21	0.17-2.07
(2) Dense cover of nodules (75-100%)	0.91	11	0.20-1.97
(3) Thin to moderate nodule cover (10-75%)	1.06	11	0.12-2.30
(4) Widely scattered nodules (<10% cover)	0.89	6	0.10-2.78
(5) Nodules dredged, not photographed	2.23	8	0.17-8.67

Three other approaches utilizing the Mn/Fe ratio may have some validity. Most bottom photographs show that submarine lava flows have discrete slabs or nodular concretions associated with the more extensive encrustations on outcropping rock. The discrete concretions usually lie on sediment deposited in crevasses and around the lava flow, and are presumably younger than the flow itself. If this is

the case, nodules associated with submarine lavas should show a higher Mn/Fe ratio than ferromanganese oxide accumulations deposited on the outcrops at the time of eruption. At the only two stations where samples of both material encrusting an outcrop and the associated discrete concretions are available the latter show a higher Mn/Fe ratio, lending token support to the idea of an increased Mn/Fe ratio with distance (or, in these two cases, time) from a volcanic source of elements. (ELTANIN Cruise 27, Ship Station 2: A crust fragment shows a Mn/Fe ratio of 0.53; an agglomerate with glacial erratic nuclei has an Mn/Fe ratio of 1.19. ELTANIN Cruise 5, Rock Dredge 5-16: a crust fragment with basaltic nucleus has a Mn/Fe ratio of 1.11; the associated botryoidal with primary glass nuclei and secondary erratic nuclei has a Mn/Fe ratio of 1.30.)

A third approach is based on the assumption that fragments ejected during an eruption will show a decrease in size away from the eruption site. These volcanic fragments subsequently serve as nuclei for accumulating ferromanganese oxides. If the oxides precipitate rapidly around the nuclei from a sea water solution injected with elemental volcanic material, the Mn/Fe ratio should show an increase with decreasing nucleus size. Available data are insufficient, but it is apparent from Figure 22 that if the hypothesis of Bonatti and Nayudu is correct, no simple Mn/Fe ratio vs. nucleus size relationship exists.

Fig. 22.--Mn/Fe Ratio vs. Relative Oxide Crust Thickness for Concretions from the Study Area.

Fig. 23.--Mn/Fe Ratio vs. Absolute Oxide Crust Thickness for Concretions from the Study Area.

Fig. 24.--Mn/Fe Ratio vs. Nucleus Size for Concretions from the Study Area.

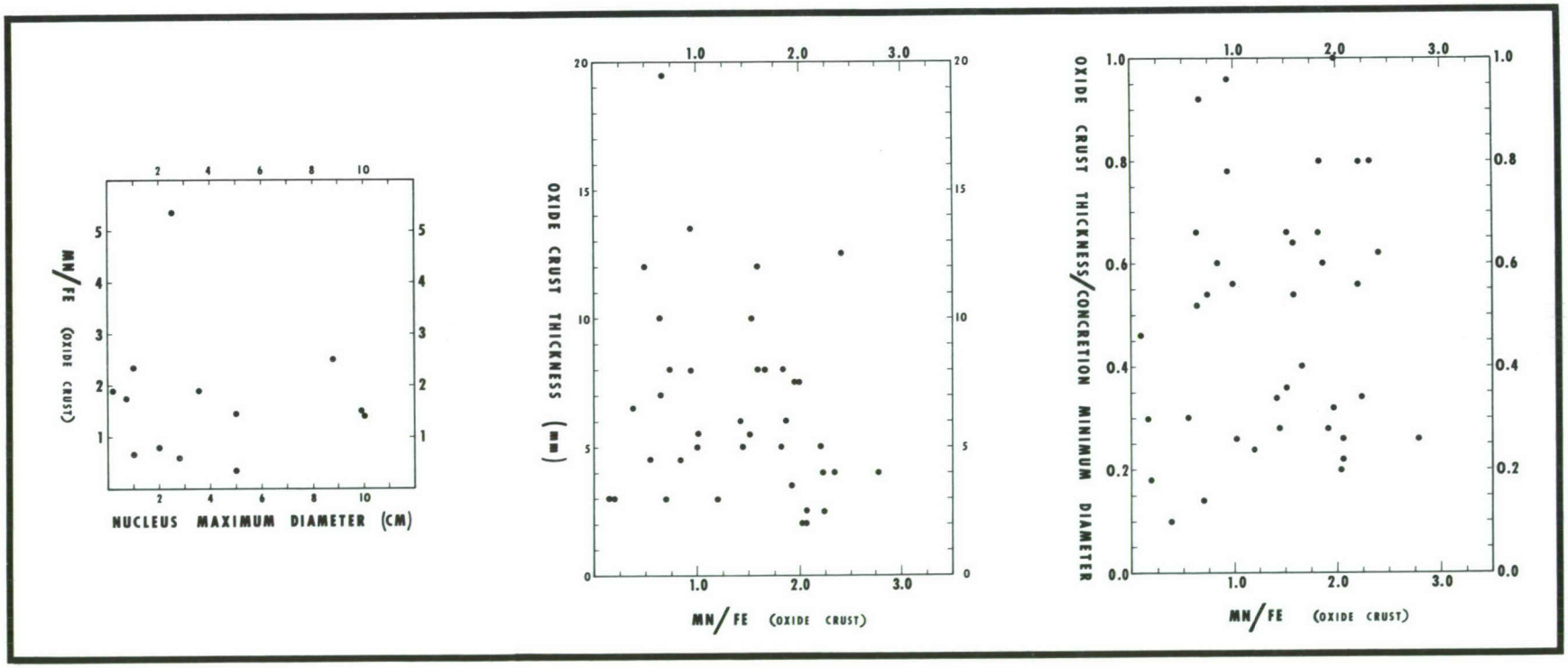
MN/FE (OXIDE CRUST)
NUCLEUS MAXIMUM DIAMETER (CM)
OXIDE CRUST THICKNESS (mm)
MN/FE (OXIDE CRUST)
OXIDE CRUST THICKNESS/CONCRETION MINIMUM DIAMETER
MN/FE (OXIDE CRUST)

The thickest ferromanganese oxide deposits in the Southern Ocean are found draped on outcropping lava flows and sea-mounts. Figure 23 is a plot of the Mn/Fe ratio vs. absolute thickness of accumulated oxides, and Figure 24 is a plot of the Mn/Fe ratio vs. relative thickness. No trend can be seen on either diagram. Assuming average oxide thicknesses decrease away from outcropping volcanics, no concomitant increase in the Mn/Fe ratio occurs. However, of 36 accumulations having an average ferromanganese oxide crust at least 10 mm. thick, 25 have a Mn/Fe ratio less than 1.0. This is not indicated in Figure 23, which includes data only on discrete concretions, and not fragments possibly torn from outcrops.

Despite efforts to delineate a volcanic origin for manganese nodules of the Southern Ocean (i.e., rapid precipitation of iron and manganese derived from volcanic eruptions), it must be concluded that either the data are not amenable to such interpretations, or else volcanic processes do not play an unsupported role in the formation of manganese nodules. Other lines of evidence, especially mineralogical compositions, support the latter conclusion. But Arrhenius and Bonatti (1965) believe that such approaches as the Hf/Zr ratio, lanthanide content, and the actinides-thorides may yet help to determine relative volcanic and continental influences on nodule composition.

Concentrations of Co, Cu, and Ni, as well as several other elements, are characteristic of deep-sea manganese nodules. A number of workers have investigated the associations of these metals with each other and with iron and manganese in the concretions. It is usually assumed that all five of these transition metals are found in the authigenic iron and manganese hydroxides of the concretions, with only insignificant amounts present in the associated detrital minerals. This assumption is not entirely valid when Southern Ocean nodules are considered. Hem (1964b) discovered that, when a feldspathic sand was introduced into a dilute manganese solution, manganese was lost to the feldspar both through ion exchange and adsorption. Manganese nodules of the study area contain plentiful feldspar. Chester and Hughes (1966) noted abundant iron and nickel, and several percent of manganese, in clays associated with manganese micronodules. Montmorillonite, if present as the nontronite variety, would contain appreciable iron; these smectite minerals might also adsorb appreciable copper (Krauskopf, 1956, p. 19). Maghemite would also contribute to the iron content.

Goodell (1967) has examined inter-element relationships in Southern Ocean manganese nodules. He found strong Mn-Ni and Fe-Co correlations, and less distinct Mn-Co, Mn-Cu, and Ni-Cu correlations. These relationships generally support those found by previous workers (Goldberg, 1954;

Goldberg and Arrhenius, 1958; Riley and Sinhaseni, 1958; Willis and Ahrens, 1962; and Burns and Fuerstenau, 1966). The degree of manganese-copper correlation was somewhat in doubt until the work of Burns and Fuerstenau, 1966, and Goodell, 1967. Table 9 presents the element-pair correlation coefficients found by Goodell (1967).

TABLE 9.--Mn, Fe, Ni, Co, and Cu element-pair correlation coefficients (after Goodell, 1967).

	Mn	Fe	Ni	Co	Cu
Mn		0.328	0.762	0.480	0.409
Fe	0.328		NS	0.526	-0.378
Ni	0.762	NS		NS	0.734
Co	0.480	0.526	NS		-0.267
Cu	0.409	-0.378	0.734	-0.267	

(for 100 Southern Ocean nodules)
(NS = Not significant at 95% confidence level)

The correlation coefficients can be rationalized on the basis of the types of phases in which Mn, Fe, Ni, Co, and Cu appear in manganese nodules. In Southern Ocean nodules todorokite (10 Å-manganite) is almost always the most important manganese phase, but variable proportions of birnessite (7 Å-manganite) and δ-MnO_2 are also present. Significant

quantities of both disordered $FeOOH \cdot nH_2O$ and ordered α-FeOOH (goethite) are found, as well. Associated with the three basic manganese phases and two iron phases are a number of cations either adsorbed on the extensive surface areas present, or contained within some disordered phase having less-than-stringent substitutional requirements. Ideally, certain proportions of the trace metals would be coexistently associated with certain phases, and if the relative importance of the various phases was known, the quantity of trace metal present could be predicted (assuming, of course, that the rate of supply of constituent elements was also known, and did not vary).

The most consistent correlation is between manganese and nickel. It necessarily follows that little iron and nickel are associated. Divalent nickel has too great an ionic radius to substitute for trivalent iron in iron phases, and nickel does not form trivalent ions. Results of the experiments of Krauskopf (1956) extrapolated to sea-water concentrations of nickel indicate that colloidal iron is a poor adsorbent for Ni^{+2}. Hence by default nickel is largely restricted to manganese phases. The study of Barnes (1967) showed that all three Mn phases, but particularly the 7 Å- and 10 Å-manganites, contain nickel; δ-MnO_2 shows a slightly lower but more consistent Ni content. Since Ni^{+2} would not likely proxy for Mn^{+4}, it appears that the nickel is mostly adsorbed on the surface of the finely-divided δ-MnO_2, which

besides being a mineral entity is also a structural component of 7 Å- and 10 Å-manganites.

Manganese-cobalt and manganese-copper correlations are distinct but not strong in Southern Ocean nodules. An iron-cobalt correlation is also distinct. Cobalt is evidently partitioned between manganese and iron phases. Burns (1965) gives evidence for the substitution of Co^{+3} for Fe^{+3} in amorphous $FeOOH \cdot nH_2O$. Divalent cobalt is most likely associated with manganese phases. Barnes (1967) shows δ-MnO_2 to be the important carrier of cobalt in Pacific manganese nodules. However, his study shows that the manganites contain much more of the manganese-associated copper than does δ-MnO_2.

Copper is negatively correlated with both iron and cobalt. Since manganese and iron are also negatively correlated, this appears to mean that copper is found only in the manganese phases. In that case, it is puzzling that manganese and copper are not more strongly correlated. It may be that significant amounts of copper are indeed bound up in montmorillonite or some undetermined organic phase.

Goodell (1967) has noted an approximately three-fold increase in the Fe/Mn ratio eastward in the Southern Ocean ferromanganese nodule deposit. Figure 21 illustrates the areal trends of the Mn/Fe ratio in the study area. The principal trend is a north to south decrease in manganese content in relation to iron. This north-south variation does

not appear to be directly related to hypothesized bottom currents (Fig. 3) nor to depositional rates inferred from a map of the Brunhes isopachs (Fig. 25). Instead, the north-south decrease in Mn/Fe ratio seems to be related to the amount of detritus incorporated into the concretions bearing iron and manganese hydroxides, hence this relationship in turn is dependent upon the proximity of the Antarctic continental source of detritus. Manheim (1965, p. 228) observed a general increase in the Fe/Mn ratio with increasing continental influence. Evidently either iron hydroxides and detrital minerals are deposited together at corresponding rates throughout much of the study area, or else the Antarctic Continent itself is serving as a source of iron. More rapid deposition of concretions in the Drake Passage and Scotia Sea may not allow extensive manganese oxide replacement of unstable phases, in addition.

The band of thick ferromanganese deposits shown in Figure 5 still must be accounted for, and the probable solution to this is the combined action of currents that sweep away detritus along with the slow incrementation of hydroxides with their associated trace metals. The ferromanganese deposits have collected on a known volcanic structural lineation that probably serves two purposes: one, as a source (but not the sole source) of elements, and two, as a contributor of outcrop and ejecta surfaces on which the oxides are found.

NODULES BURIED IN SEDIMENT

A large number of piston and gravity cores obtained from the Southern Ocean during USNS ELTANIN cruises contain fragmented or whole manganese nodules. The concretions are found both at the top of the sediment column and buried at variable depths within the sediment. Buried nodules have been noted many times in the past, but few studies have been made of them. Menard and Shipek (1958) and Menard (1964, p. 180-182) reported numerous buried nodules in Pacific sediment cores. Goodell (1965, p. 23) noted 45 Antarctic sediment cores containing nodules (through ELTANIN Cruise 15), and the usual areal coincidence of the nodules with surface ferromanganese deposits. Holmes, Goodell, and Osmond (1967) determined the increasing ages of nodules distributed down the length of a sediment core.

Table 10 lists the number of cores that contain nodules (1) only at the core top, (2) only at depth, and (3) both at the core top and within the sediment. The table contains data on all nodules larger than about 0.5 cm. that were exposed during the process of cutting the cores lengthwise into halves.

TABLE 10.--Number of cores containing concretions at the top, buried in the sediment, and both at the top and at depth.

No. of Cores having nodules at TOP ONLY	No. of Cores having nodules at DEPTH ONLY	No. of Cores having nodules at TOP and at DEPTH
14	48	15

It is easily seen from Table 10 that manganese nodules are by no means phenomena restricted to the present. On the basis of the paleomagnetic stratigraphy of Goodell and Watkins (1967), an age of more than 3.4 million years can be assigned to two nodules from a core taken on the Pacific-Antarctic Ridge (ELTANIN 14-8, depths in sediment 1600 and 1700 cm., respectively). The temporal distribution of concretions can be assessed more fully from Figures 27-29, a series of cross-sections of Southern Ocean sediments. The locations of the traverses from which the cross-sections were constructed are presented in Figure 26. The cores are correlated according to the geomagnetic polarity as interpreted by Goodell and Watkins (in press), for the most part, but data on additional cores collected since their study have also been incorporated. Watkins (verbal communication, 1967) has determined the depth to the most recent reversal in ELTANIN cores 27-1, 27-2, 27-3, and 27-21; he has also pointed out that no ELTANIN cores collected in the Southwest

Fig. 25.--Isopachs of Brunhes Sediment (After Goodell and Watkins, in press).

Fig. 26.--Locations of Paleomagnetic Stratigraphic Cross-Sections.

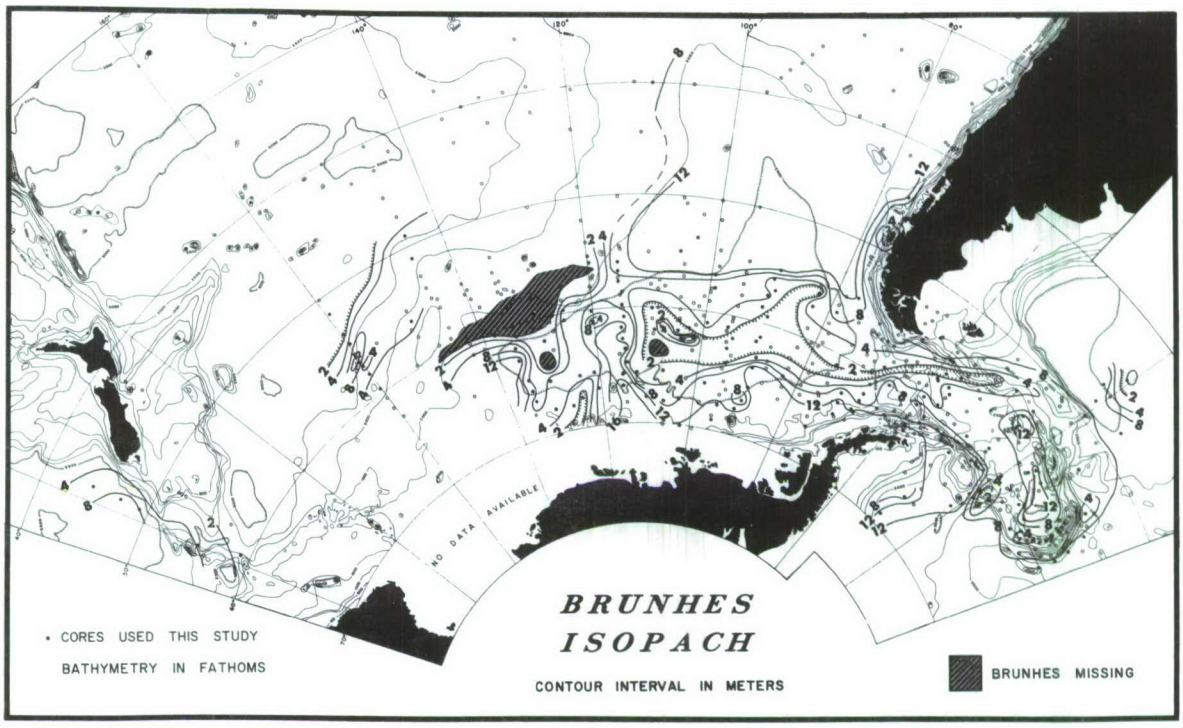
BRUNHES
ISOPACH
CONTOUR INTERVAL IN METERS
• CORES USED THIS STUDY
BATHYMETRY IN FATHOMS
BRUNHES MISSING
NO DATA AVAILABLE

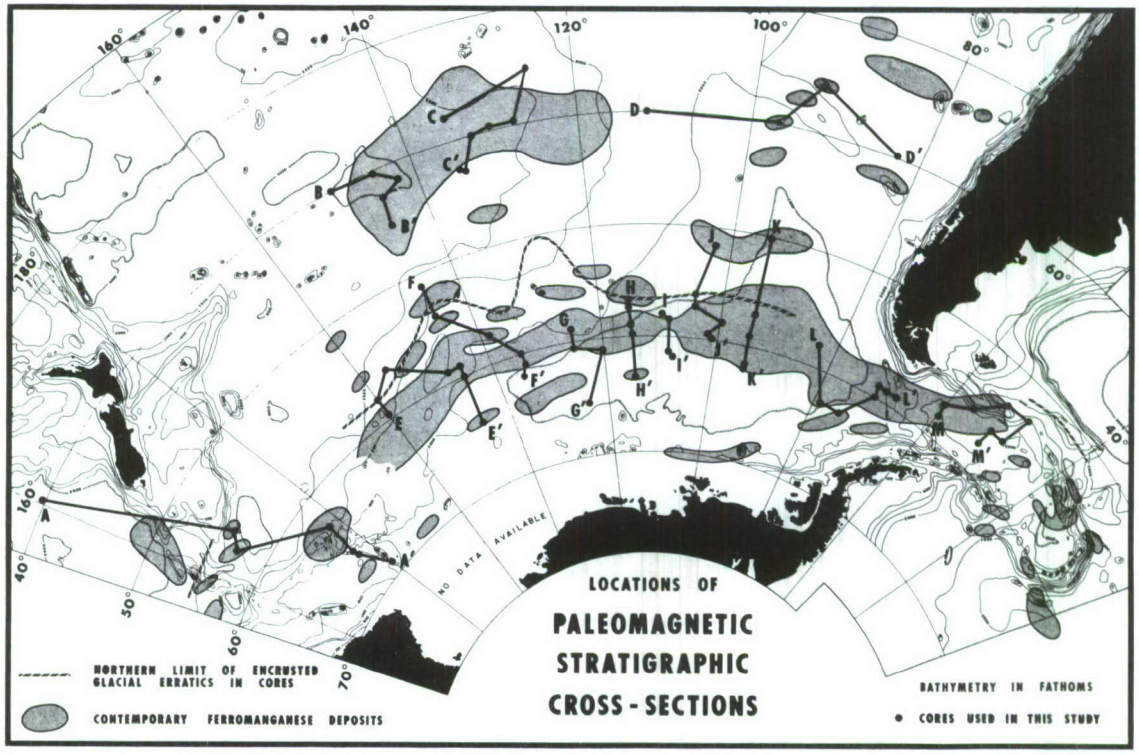
LOCATIONS OF
PALEOMAGNETIC
STRATIGRAPHIC
CROSS-SECTIONS
NORTHERN LIMIT OF ENCRUSTED GLACIAL ERRATICS IN CORES
CONTEMPORARY FERROMANGANESE DEPOSITS
BATHYMETRY IN FATHOMS
• CORES USED IN THIS STUDY
NO DATA AVAILABLE

Fig. 27.--Paleomagnetic Stratigraphic Cross-Sections AA' through DD'.

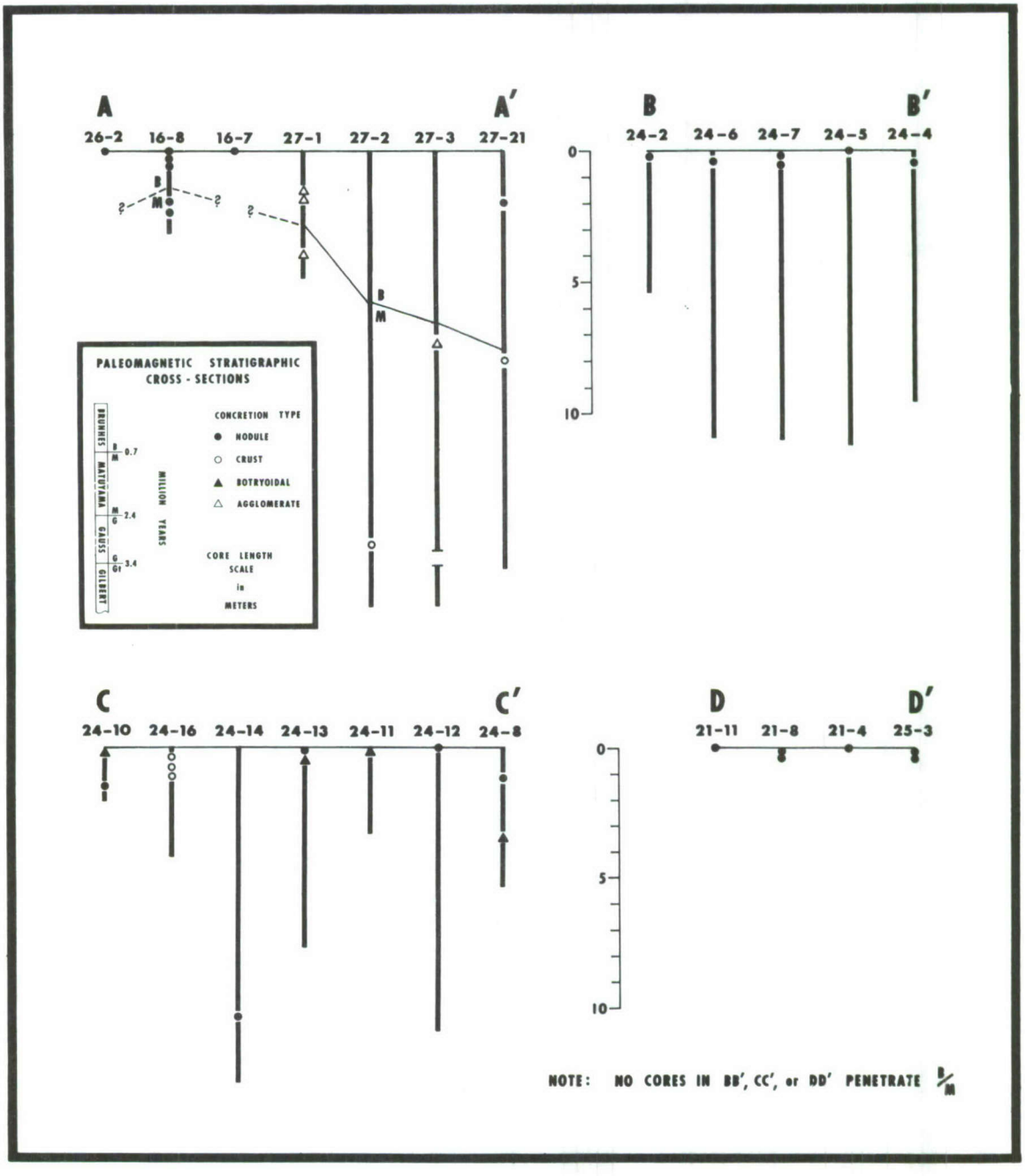
A
A′
26-2
16-8
16-7
27-1
27-2
27-3
27-21
B
M
B
B′
24-2
24-6
24-7
24-5
24-4
0
5
10
PALEOMAGNETIC STRATIGRAPHIC CROSS - SECTIONS
BRUNHES
B/M 0.7
MATUYAMA
M/G 2.4
GAUSS
G/G1 3.4
GILBERT
MILLION YEARS
CONCRETION TYPE
NODULE
CRUST
BOTRYOIDAL
AGGLOMERATE
CORE LENGTH SCALE in METERS
C
C′
24-10
24-16
24-14
24-13
24-11
24-12
24-8
D
D′
21-11
21-8
21-4
25-3
NOTE: NO CORES IN BB′, CC′, or DD′ PENETRATE B/M

Fig. 28.--Paleomagnetic Stratigraphic Cross-Sections EE' through II'.

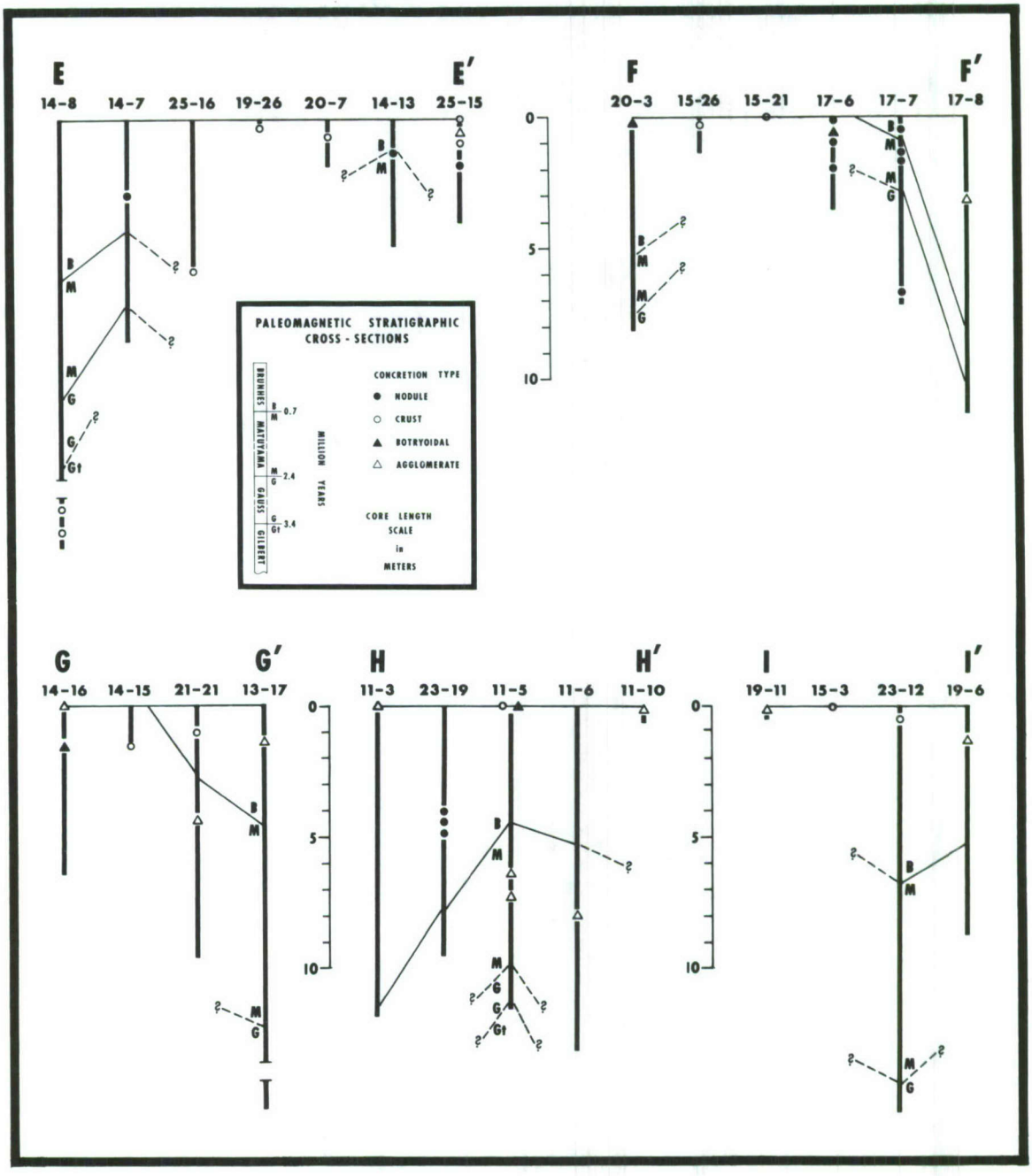
E
E′
14-8
14-7
25-16
19-26
20-7
14-13
25-15
F
F′
20-3
15-26
15-21
17-6
17-7
17-8
G
G′
14-16
14-15
21-21
13-17
H
H′
11-3
23-19
11-5
11-6
11-10
I
I′
19-11
15-3
23-12
19-6
0
5
10
PALEOMAGNETIC STRATIGRAPHIC CROSS - SECTIONS
BRUNHES
MATUYAMA
GAUSS
GILBERT
0.7
2.4
3.4
MILLION YEARS
CONCRETION TYPE
NODULE
CRUST
BOTRYOIDAL
AGGLOMERATE
CORE LENGTH SCALE in METERS

Fig. 29.--Paleomagnetic Stratigraphic Cross-Sections JJ' through MM'.

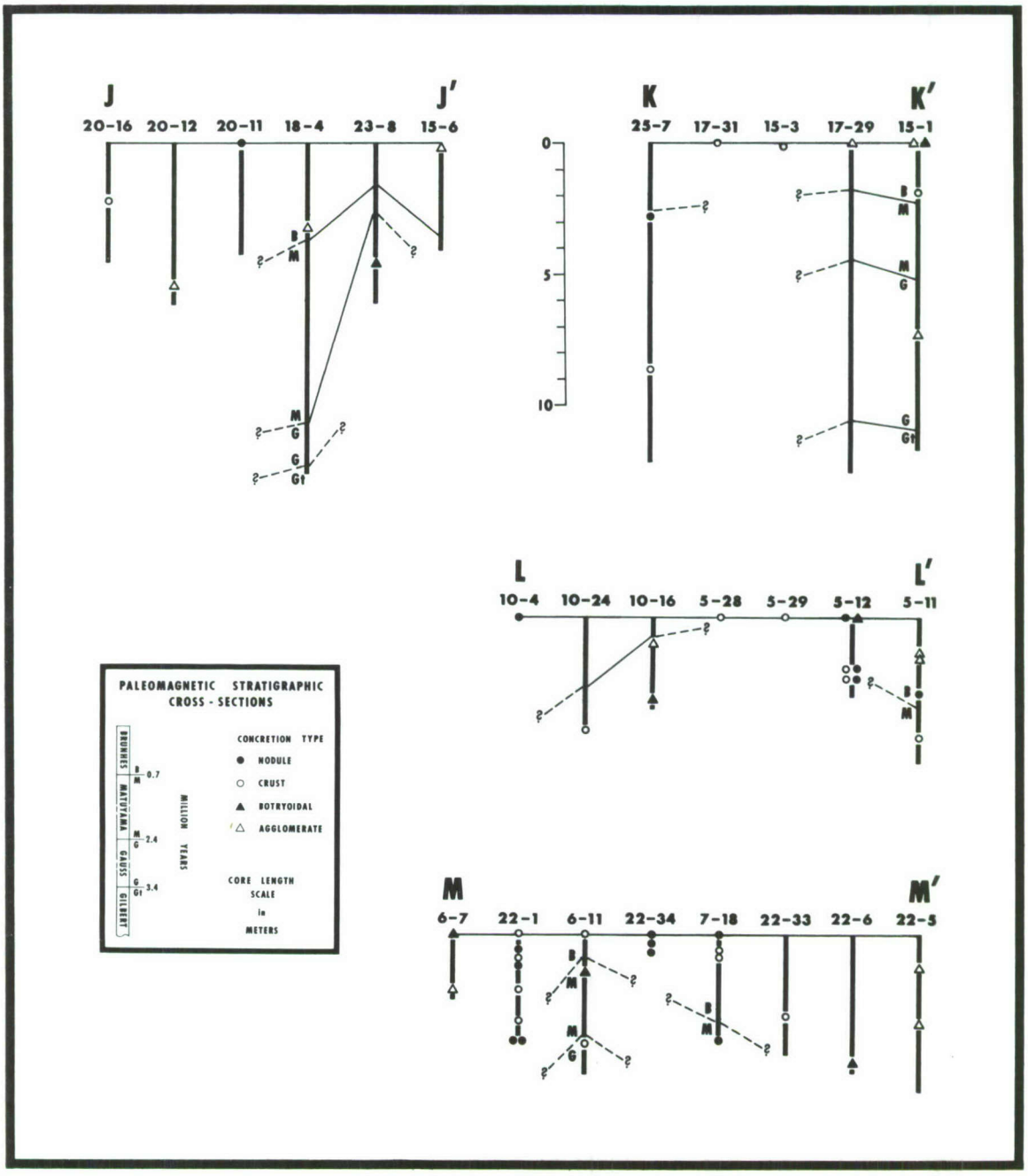
J
J'
20–16
20–12
20–11
18–4
23–8
15–6
B
M
M
G
G
Gt
K
K'
25–7
17–31
15–3
17–29
15–1
0
5
10
B
M
M
G
G
Gt
L
L'
10–4
10–24
10–16
5–28
5–29
5–12
5–11
B
M
M
M'
6–7
22–1
6–11
22–34
7–18
22–33
22–6
22–5
B
M
M
G
B
M
PALEOMAGNETIC STRATIGRAPHIC CROSS - SECTIONS
BRUNHES
MATUYAMA
GAUSS
GILBERT
B
M
0.7
M
G
2.4
G
Gt
3.4
MILLION YEARS
CONCRETION TYPE
NODULE
CRUST
BOTRYOIDAL
AGGLOMERATE
CORE LENGTH SCALE in METERS

Pacific Basin north of 50°S. Lat. reach the Brunhes-Matuyama boundary. Only the major paleomagnetic epochs are considered (Brunhes, 0.0-.07 m.y.; Matuyama, 0.7-2.35 m.y.; Gauss, 2.35-3.4 m.y.; and Gilbert, 3.4 m.y.+). The Brunhes is the most recent epoch, consisting of all sediment deposited during the last 700,000 years.

A majority of the cores do not reach the Brunhes-Matuyama boundary, hence many more nodules of Brunhes age are found in the cores. This does not necessarily mean that ferromanganese concretions are more characteristic of the last 700,000 years than the preceding millions of years. However, Table 11 may constitute some support for the idea that manganese nodules have become increasingly prevalent in the past few hundred thousand years. (The number of nodule horizons is used instead of the number of nodules themselves because some horizons consist of more than one nodule.) Table 11 shows that nodule horizons occur more frequently per given length of sediment core in the Brunhes than in older sediment. This is true even when all cores consisting only of a large nodule or nodule fragments that prevented penetration of the coring device into underlying sediment are disregarded. If sediment compaction with depth were to be taken into account, the importance of the Brunhes epoch as a time of manganese nodule formation would be magnified. To date, no massive ferromanganese deposits comparable to those accumulated around

outcropping submarine lava flows have been struck beneath more than a few centimeters of sediment.

TABLE 11.--Comparison of sediment core length per paleomagnetic epoch with number of concretion intervals per paleomagnetic epoch.

	No. of Nodule Horizons	No. of Cores Terminated by Nodules	Total Length of Sediments	Cm. of Sediment per Nodule Horizon
Brunhes	96	15	28,560 cm.	297
Matuyama	29	2	13,580 cm.	468
Gauss	4	0	4,305 cm.	1076
Gilbert	2	0	825 cm.	412

A number of factors that have thus far been neglected may cause nodules to be progressively concentrated upward in the sediment. Reducing conditions capable of causing manganese nodule dissolution, with concurrent upward migration of manganese in interstitial fluids, have been reported by Bonatti and Nayudu (1965, p. 31) and Lynn and Bonatti (1965). Calculations by Anikouchine (1967) suggested that the source of manganese found in concretions is the interstitial water of underlying sediments. But inspection of deeply buried nodules does not lead to the conclusion that already-formed nodules are dissolved, with the manganese rising in the sediment until the oxidizing environment of the sea floor is reached. Nodules more than three

million years old show only a slight surface corrosion that may be due to dissolution. And the todorokite of a Gilbert-age nodule yields as strong a diffraction pattern as any Brunhes nodule. However, it must be noted that some smaller nodules have evidently been disaggregated within the sediment, leaving only "shadows" to attest to their former presence.

Erosion of sediments by vigorous current action during the Brunhes may have had the effect of producing "desert pavements" of nodules at the sediment-water interface. However, such a mechanism is hard pressed to account for dense nodule monolayers, where discoidal concretions are arranged shoulder-to-shoulder. Lifting by burrowing organisms is an even more remote possibility.

Buried manganese nodules resemble those presently found at the surface in distribution, structure, mineralogy, and chemistry. Superimposed on the traverses of Figure 26 are the outlines of surface ferromanganese deposits visible in bottom photographs. Surficial and buried concretions do not differ in areal extent appreciably except in the Chile Rise-East Pacific Rise vicinity and the area around New Zealand. Samples from these two areas are widely scattered, and the differing distributions of surface and subsurface nodules may not be significant. Even the northerly limit of manganese-encrusted glacial erratics for buried nodules is close to that for surface concretions, as can be seen by comparing the limits shown on Figures 13 and 26.

In most places, the northern limit of glacial erratics incorporated into subsurface nodules is slightly south of the present limit, although the former boundary takes into account all nodules deposited prior to the last several thousand years.

Appendix D and Table 12 present the mineralogy and chemistry, respectively, of all cores having multiple nodule horizons for which X-ray diffraction and chemical analysis data are available. It is apparent that although the relative proportions of todorokite, quartz, and feldspar fluctuate, these fluctuations are usually minor in any one core, proving that over the past few hundred thousand years, the relative rates of detrital deposition vs. todorokite growth have not varied significantly at any one location. The relative proportions of constituent elements show a similar lack of change in nodules distributed down the length of a core. Whatever the source of the elements may be, manganese nodules from any one area have been accumulating Mn, Fe, Ni, Co, and Cu in comparable proportions during much of the Brunhes paleomagnetic epoch.

TABLE 12.--Element ratios in concretions from cores with multiple nodule horizons.

Eltanin Core No.	Depth Interval (cm)	Mn/Fe	Mn/Co	Mn/Ni	Ni/Cu
5-12	Top	0.55	37.1	65.0	1.3
	206-211	0.46	37.5	60.0	1.5
24-7	5-8	1.61	50.2	25.4	2.4
	11-15	1.64	51.2	25.6	2.5
25-3	1-3	2.04	179.2	19.3	2.6
	14-17	1.87	185.8	22.1	2.2
17-6	83-87	0.49	41.8	90.0	0.6
	193-198	0.53	45.0	105.0	0.7
22-1	0-11	0.33	34.5	58.5	1.0
	54-57	0.45	60.0	73.8	1.1
	69-72	0.38	49.4	120.0	0.6
22-34	Top	0.65	48.4	26.3	3.5
	18-22	0.59	55.8	32.1	1.4
	18-22	0.38	47.6	40.5	1.1
7-18	Top	0.24	13.8	110.0	0.1
	60	0.64	21.8	12.3	0.7

CONCLUSIONS

The purpose of this study has not been to discover the origin of manganese nodules. Such a discovery is necessarily the product of observations and experiments beyond the scope of this study. However, a number of conclusions have been reached which have genetic significance, and a number of other aspects of manganese nodules are now better understood. The principal results and conclusions follow.

(1) Ferromanganese oxide-hydroxide accumulations of the Pacific-Antarctic Ocean, Drake Passage and Scotia Sea are complex assemblages of authigenic and detrital minerals.

(2) The principal manganese oxide is todorokite, with birnessite being of secondary importance. The relative importance of δ-MnO_2 is variable; in some instances it is quantitatively as important as todorokite.

(3) X-ray amorphous $FeOOH \cdot nH_2O$ and goethite are the principal iron-bearing phases in manganese nodules.

(4) Ferromanganese accumulations incorporate a number of clastics derived from both submarine volcanism

and from continental sources. Basaltic glass, feldspar, ferromagnesian minerals, and some quartz is contributed by volcanism. Quartz and feldspar, and to a lesser extent, amphibole, illite, and chlorite are transported into the Southern Ocean via icebergs, wind, and ocean currents.

(5) Diagenetic alteration of unstable phases within the concretions produces other minerals, including montmorillonite, phillipsite, clinoptilolite, and maghemite.

(6) Manganese oxides invade fractures within nucleating objects; they may alter and replace resistant rocks and minerals, given sufficient time.

(7) The present distribution of manganese nodules in the Southern Ocean is the result of three factors--one, the action of currents that carry away debris that might mask the deposits, two, an abundance of volcanic outcrop and ejecta surfaces for the accumulation of oxides, and three, additional surfaces supplied by glacial erratic debris littering the Southern half of the study area.

(8) The amount of detrital quartz and feldspar incorporated into ferromanganese concretions approximately reflects the rate of supply of quartz and feldspar to a given area. This being the case, it must be assumed that the concretions are accumulated slowly,

the deposition of oxides being either continuous or as incremented layers.

(9) The larger Fe/Mn ratios of the Drake Passage and Scotia Sea nodules indirectly reflect an increased continental influence. Whether or not this influence has affected oxide deposition rates is not known.

(10) Nodules buried below the present sediment-water interface in the study area greatly resemble those at the surface in structure, mineralogy, and chemistry, as well as in distribution. The passage of as much as three and a half million years has apparently not altered the nature of manganese oxide minerals deposited in the Southern Ocean.

APPENDIX

APPENDIX A

LABORATORY PROCEDURE

Dredge and core samples collected during USNS ELTANIN cruises were shipped to the Florida State University, Tallahassee, for examination. Dredge samples gathered during Cruises 4-17 were utilized by Grant (1967) in his study of Antarctic Ocean manganese nodules, and those samples were re-examined for this study so that data on nodule distribution, structure, and mineralogy would be as complete as possible. Paster (written and verbal communications, 1967) inspected all ELTANIN dredge materials for evidence of ferromanganese accumulations during his search for submarine basalt samples, and his data on manganese stains and thin crusts have been utilized. For this study, Cruises 18-27 dredge nodules and Cruises 4-27 piston core nodules contributed the bulk of the data.

The types of observations made on each ferromanganese oxide accumulation are described in previous sections (Nodule Size, Shape and Surface Features; Structure and Morphogenetic Types). From each concretion population, a representative sample was chosen for chemical and X-ray diffraction analysis. Each selected concretion was scrubbed

with a plastic-bristled brush and rinsed in distilled water to remove clinging sediment. The concretions were then broken open and metallic oxide crust-subcrust portions separated by hand from nucleus sections. The iron-manganese oxide material was lightly ground in a mortar and pestle and screened through silk brocade cloth of approximately 100 mesh. Zeolite and clay nuclei were similarly ground to a powder suitable for X-ray diffraction and chemical analysis.

Chemical analysis

Sample powders were shipped in glass containers to the Materials Laboratory of Newport News Shipbuilding and Drydock Company, Newport News, Virginia. X-ray fluorescence techniques were used to determine water-free weight percents of manganese, iron, nickel, copper, cobalt, scandium, titanium, vanadium, chromium, zinc, strontium, molybdenum, silver, tin, tungsten, mercury, zirconium, and barium. Water content was also measured. In every sample, scandium, chromium, silver, tungsten, and mercury contents were less than the minimum level of sensitivity of the analytical technique.

X-ray diffraction analysis

Most of the X-ray diffractograms were made with a Norelco diffractometer utilizing a gas-proportional tube detector and a pulse height analysis unit. Powders packed into an aluminum planchet were scanned at 1 degree 2^{0} per minute with the chart speed also set at 1 degree 2^{0} per

minute. Nickel-filtered Cu-Kα radiation was generated with a tube voltage of 50 kv and a current of 30 ma. Divergent, scatter, and receiving slits were 1°, .006°, and 1°, respectively. A time constant of 8 was used for Mn-, Fe-rich samples, and a time constant of 4 was used for Mn-, Fe-poor samples. Scale factors were varied to fit the most intense peaks onto the chart paper.

D-spacings corresponding to 2θ values were measured with a transparent plastic overlay. Since quartz was present in most of the samples, it was used as an internal standard. Peak areas were calculated by multiplying the base width and peak half-height.

Some of the diffractograms were prepared using a monochromator instead of a proportional counter and pulse height analyzer. This was done to eliminate the effects of iron and manganese fluorescence so that peak area ratios and mineral identifications could be checked. Additional checks on the reliability of peak area ratios were made by both multiple runs on one powder and by scans of repacked powders.

APPENDIX B

X-RAY IDENTIFICATION

The ferromanganese accumulations of the Southern Ocean consist of an intimate mixture of several minerals. Identification of the components of such a mixture by X-ray diffractometry involves a number of problems. Variable grain size, variable crystallinity, isomorphic substitution and other chemical variations, differences in powder compactness, variable background interference (including fluorescence), perfection of pulse height analysis, voltage stability, scale factor and time constant settings, beam and aperture alignments, and, of course, variable proportions of the component minerals all influence the type of pattern (i.e., peak areas and peak height/width ratios) generated by the X-ray diffractometer. For the purposes of this study, peak area ratios such as 3.34 Å Quartz + 3.2 Å Plagioclase-Phillipsite/ 9.7 Å Todorokite of each sample have been computed. This readily allows comparison of the relative proportions of quartz, plagioclase-phillipsite, and todorokite in different samples; and the influence of fluctuations in machine performance and the differences in physical properties of the powder samples can be effectively ignored.

The three basic problems that hindered identification of diffractogram peaks during this study were (1) iron and manganese fluorescence which increased background noise, (2) the frequent masking of certain peaks because of the large number (usually 5-10) of minerals found in the ferromanganese accumulations, and (3) distinguishing the presence of minerals comprising only trace amounts of a sample. The first problem, that of fluorescence, was greatly reduced by pulse height analysis. The other two problems are basically related, and involve visual interpretation of the diffractograms. The following sections contain a discussion of the means of interpretation used in this study. Table 17 lists the sources of X-ray diffraction data used for peak identifications.

Todorokite, birnessite and δ-MnO_2

Three co-existing manganese oxide phases are probably present in most ferromanganese concretions of the Antarctic Ocean. X-ray diffractograms seldom reveal the presence of any phase other than todorokite, however. Frondel, Marvin, and Ito (1960) listed X-ray diffraction data for todorokite from a number of terrestrial manganese deposits. Manheim (1965) compared diffraction data for continental and pelagic todorokites. Other students of manganese nodule mineralogy have simply called todorokite a 10 Å-manganite on the basis of its most intense X-ray reflection.

Birnessite, a less hydrated phase than todorokite, is identified by a 7 Å basal reflection, hence this mineral is also known as a 7 Å-manganite. Jones and Milne (1956) are the original source for X-ray data on naturally-occurring birnessite. δ-MnO_2 may be thought of as a very fine-grained anhydrous phase. Its most intense X-ray reflection coincides with todorokite and birnessite peaks at about 2.4 Å. The best evidence for the presence of δ-MnO_2 is a marked increase in intensity of the broad peak at 2.4 Å relative to basal todorokite and birnessite reflections.

Table 13 is a listing of X-ray diffraction data on todorokite, birnessite and δ-MnO_2, and compares these data with those from a typical diffractogram of marine manganese minerals.

Goethite

Aside from the amorphous $FeOOH \cdot nH_2O$ phase, goethite is the most important iron-bearing material in Southern Ocean concretions. Only in a minority of samples was goethite important enough to display distinct diffraction peaks, however. The major peak at 4.18 Å usually appeared as a shoulder on the 4.26 Å quartz peak. Peaks at 2.69, 2.49, and 2.19 Å often were distinguishable.

Maghemite

Gamma-Fe_2O_3 may be a trace constituent in many manganese nodules from the study area. Only in a few samples

TABLE 13.--Comparison of X-ray diffraction data on concretion materials and manganese minerals.

East Pacific Rise Nodule (This study)		Baltic Sea Nodule (Manheim, 1965)		Pacific Ocean Nodule (Manheim, 1965)		Todorokite (Frondel, et al.,1960)		Birnessite (Jones and Milne, 1956)		δ-MnO_2 (Buser et al,,1954)	
d(Å)	I	d(Å)	I	d(Å)	I	d(Å)	I	d(Å)	I	d(Å)	I
9.7	10	9.7	100	9.7	10b	9.6	10				
7.2	2b	7.2	60b			7.15	1/4d	7.27	s		
4.85	5	4.85	24b	4.87	15b	4.80	8				
		4.56	6b			4.45	1d				
								3.60	w		
		3.58	6b			3.40	1/2d				
						3.20	1				
						3.10	1				
2.45		2.45		2.46	100b	2.46	3	2.44	m	2.43	s
thru	4b	thru	96b	2.39	10b	2.40	5				
2.38		2.34		2.34	20b	2.34	4				
		2.23	3b	2.24	10b	2.23	3				
						2.13	1/2d				
		2.06	5b								
		2.00	7			1.98	2				
						1.92	1/2				
1.50	1/2					1.78	1				
						1.74	1				
1.42	3b	1.42	21b	1.41	40b	1.53	1	1.412	m	1.42	s
		thru				1.49	3				
1.375	1/2	1.39		1.385	10b	1.42	2				
						1.39	1				

are the major diffraction peaks at 2.52 and 2.95 Å unobscured by feldspar. A tentative identification in most samples is based on the presence of minor peaks at 5.90 and 2.09 Å.

Quartz

Quartz was detected in virtually every sample. This permitted the use of quartz as an internal standard without introducing still another mineral to the already complex mineral mixtures. The 1000 peak (4.26 Å) frequently obscured the major goethite peak. The most intense quartz peak ($10\bar{1}0$ at 3.34 Å) usually obscured the plagioclase 112 peak. The 1101 quartz peak at 2.46 Å was usually superimposed on the broad manganite-δ-MnO_2 peak in this region.

Feldspar

Like quartz, feldspars were present in nearly every sample. Unlike quartz, the d-spacings and relative peak intensities were quite variable, depending upon the composition and structure of the particular feldspar or range of feldspars present. Since plagioclase feldspars, especially intermediate and calcic varieties, were predominant, subtle distinctions between the X-ray diffraction patterns of the various plagioclases were utilized to approximate the composition.

Peterson and Goldberg (1962) used X-ray diffractometry to identify the types of feldspars found in the South Pacific. Compositional distinctions in the albite-anorthite

series were based on the increasing separation of the $1\bar{3}1$ and 131 peaks with increasing calcium content, taking into account the limitations determined by previous workers. Delta 2θ of $1\bar{3}1$-131 values, in conjunction with other angular variations, has been used to identify the feldspars found in manganese nodules. These values are listed in Table 14, compiled from Peterson and Goldberg (1962).

TABLE 14.--Delta 2θ values for plagioclase $1\bar{3}1$-131 diffractogram peaks.

$\Delta 2\theta$ $1\bar{3}1$-131	Composition
>2.1	bytownite-anorthite
1.0-2.1	calcic andesine-labrodorite
1.6-1.9	oligoclase-andesine
1.1-1.6	albite-oligoclase
<1.1	albite

Alkali feldspars, probably present in most of the ferromanganese oxide-silicate mixtures, constituted such minute quantities that X-ray identification was impossible in all but a few instances. Differentiation between alkali and plagioclase feldspars was relatively easy; the most intense reflection(s) of the alkali feldspars usually results from a 3.21-3.26 Å d-spacing(s), while plagioclases are characterized by at least one intense reflection in the 3.17-3.21 Å d-spacing range. The 20$\bar{1}$ reflection of the alkali feldspars also differs from that of the plagioclases,

and it can be used to identify the particular alkali feldspar present.

Montmorillonite

Montmorillonite is another nearly invariable constituent of manganese encrustations. The identification of this mineral was based primarily on the presence of a diffraction peak at about 4.45 Å, although one or more ill-defined peaks in the 12-15 Å region were usually present. In addition, two peaks between 2.55 Å and 2.63 Å were often present, which, coupled with the 4.45 Å peak, confirmed the presence of montmorillonite. In nucleus materials comprised predominantly of montmorillonite, the twin 2.55-2.63 Å peaks were often not resolved at a scan speed of 1° 2θ per minute.

The precise composition of the montmorillonite, or more properly, montmorillonoid, was not determined. According to the criteria of Warshaw and Roy (1961), the mineral is a dioctahedral smectite. Most workers (including Arrhenius, 1963, and Bonatti, 1965) have attributed a nontronite composition to the montmorillonite formed by alteration of submarine basalts. The diffraction peaks displayed by the montmorillonite of this study do not agree well with published nontronite X-ray data, however.

Table 15 lists the spacings and intensities of peaks possessed by the montmorillonite found in Southern Ocean manganese nodules, as well as data on nontronite and continental montmorillonite.

TABLE 15.--Montmorillonite diffraction data.

Montmorillonite This Study		Montmorillonite ASTM 3-0009		Nontronite ASTM 2-0008	
d(Å)	I/I_o	d(Å)	I/I_o	d(Å)	I/I_o
15.2	10	15.3	10	13.9	10
5.12	1	5.15	8	7.1	2B
4.45	6	4.50	10	4.44	8
3.09	1	3.07	10	3.54	5
2.61	1?	2.61	10	2.79	1
2.56	4	2.55	10	2.59	2-5
2.40	1	2.41	4	2.51	2B
		2.24	2	2.27	1B
2.15	1	2.16	2		

Phillipsite

Phillipsite was detected in a majority of the manganese nodules studied. The basic criterion used for identification was a relatively sharp peak at 7.1 Å, with additional peaks at 8.2, 5.36, 2.74, and 2.68 Å. Since chlorite also possesses a 7.1 Å peak, the other peaks are necessary for an unambiguous identification. Table 16 lists the X-ray diffraction data for a nearly pure sample of phillipsite separated from the palagonite rim of a submarine basaltic volcanic bomb, which had an outer encrustation of ferromanganese oxides. Identical d-spacings and relative peak intensities were shown by a

number of phillipsite nuclei scattered throughout the study area. Phillipsite that was incorporated into or formed within accumulating ferromanganese oxides usually displayed only the most intense peaks. Of course, in most of the powder samples the most intense peak at about 3.2 Å was coincident with the major plagioclase peak, so an estimate of the relative importance of phillipsite in the sample depended on comparison of the 7.1 Å peak area with secondary plagioclase peak areas.

The peaks displayed by marine phillipsite differ noticeably from values given for continental phillipsite (e.g., by Wyart and Chatelain, 1938; and Hay, 1964). The only known set of diffraction data (Table 16) on marine phillipsite was published by Lippman (1958); his sample was apparently somewhat impure. Morgenstein (in press) has obtained data (Table 16) on a marine zeolite in scoriaceous pelagic sediments west of the Society Ridge, South Pacific, which he calls harmotome. However, the identification of the barium analogue of phillipsite is not supported by chemical analyses. Arrhenius (1963), among other workers, states that members of the harmotome-phillipsite series are common in pelagic sediments. However, no references with included diffraction data can be found.

X-ray fluorescence analysis of the nearly pure phillipsite mentioned above (Zemmels, verbal communication, 1967) demonstrated a lack of barium and the presence of

TABLE 16.--Phillipsite diffraction data.

This Study		Lippman (1958)		Morgenstein (in press)	
d(Å)	I/I_o	d(Å)	I/I_o	d(Å)	I/I_o
8.20	8	8.19	w		
7.12	57	7.14	w	7.08	80
6.38	6			6.23	60
5.36	13	5.34	w	5.30	50
5.03)	25	5.01	w	4.97	50
5.00)					
4.29	5				
4.11	3	4.13)B	w	4.08	90
		4.04)			
3.94)	1			3.91	20
3.93)					
3.76	< 1			3.65	20
3.245	28	3.26	m	3.25	50
3.185	100	3.18	s	3.21	50
3.09	< 1			3.15	100
2.95	13	2.94	w	3.12	20
2.90	< 1			2.97	30
2.84)	1				
2.83)					
2.745	13			2.73	45
2.685	24	2.67	w	2.71	10
2.56)	4			2.67	50
2.55)				2.65	10
2.52	1			2.54	20
2.46	< 1				
2.395	2				
2.33	2				
2.25	1				
2.225	< 1				
2.165	1				
2.075	< 1				
etc.					

little calcium in the phillipsite. This zeolite is probably similar to the potassium-sodium phillipsite studied by Rex (1967). If harmotome is present in any of the manganese nodules, it is either a very minor constituent, or else it may be that the presence of barium in the zeolite structure does not significantly affect the diffraction pattern. In any event, the presence or absence of harmotome in Southern Ocean manganese nodules was not delineated during this study.

Clinoptilolite

Hathaway and Sachs (1965) have published diffraction data on an authigenic marine clinoptilolite. Their data agree well with those of Mumpton (1960), among other workers. Clinoptilolite appears to be a trace constituent in many of the Southern Ocean samples studied, but because of the limited quantities present, many of the peaks were often obscured. For this reason, no single peak served as the basis for identification. Only when peaks appeared at several spacings not possessed by any other minerals was the presence of clinoptilolite deemed even probable. The most reliable peaks belong to the set 9.1-8.9, 8.0-7.9, 6.8-6.7, and 3.99-3.96 Å. The presence of several relatively intense peaks at low 2θ angles served to differentiate clinoptilolite from heulandite (Mumpton, 1960).

Analcime, mordenite, erionite, and epistilbite

Neither analcime, mordenite, erionite, nor epistilbite have been definitely reported from South Pacific pelagic sediments. The presence of these four zeolites, especially analcime, is strongly suspected in manganese nodules of the study area, but identification of these possible trace constituents is certainly not unequivocable. Many of the small but well-defined peaks that appeared on the diffractograms between 5 and 9 Å can probably be assigned to analcime, mordenite, erionite, and epistilbite, but the possibility exists that other zeolites, phyllosilicates, or unknown hydrated phases displaying the peaks attributed to the four zeolites could be present.

Reoccurrent peaks at 6.9 and 5.6 Å have been assigned to analcime. Peaks at 6.10 and 4.53 Å may belong to mordenite. The many peaks at 7.6-7.5 Å have been attributed to erionite. Epistilbite may contribute the many 8.8 Å peaks, and shares 3.85 and 2.89 Å peaks with mordenite Mordenite and erionite both have diffraction peaks at 6.6 and 5.8-5.7 Å which occur on many of the diffractograms.

Amphibole

Amphibole minerals occur in nearly every Drake Passage-Scotia Sea concretion, and in several Pacific-Antarctic Ocean samples. The basis for identification was a distinct peak at 8.45 Å. Published diffraction data show

this peak to be less intense than peaks at 3.38, 3.09, and 2.70 Å (hornblende), but work by Edwards (verbal communication, 1967) shows hornblendes with relative intensities corresponding to those of hornblendes in manganese nodules. Besides the 8.45 Å peak, only peaks at 3.10-3.05 and 2.82-2.80 Å were occasionally defined. Other amphiboles displaying peaks from 8.25 to 8.65 Å were found in several samples.

Pyroxene, olivine, magnetite, and ilmenite

These four minerals were occasionally detected in ferromanganese oxide accumulations of the Southern Ocean. The frequent small to medium 2.89-2.88 Å peaks probably belong to a pyroxene; none of the samples studied contained appreciable pyroxene. A single olivine-glass nucleus gave an excellent diffraction pattern, and many other samples showed peaks centered at 2.77 Å, which were attributed to olivine. A few samples displayed 2.98, 2.52 Å, and other peaks which are characteristic of magnetite. In feldspar-rich samples, exaggerated 2.52 Å peaks may have been due to the presence of magnetite. Well-defined, small peaks at 2.75 Å and 2.55 Å were interpreted as probable indicators of ilmenite.

Prehnite

Several nucleus samples and a few oxide crusts contained prehnite; observed d-spacings and relative intensities

matched published data very well. In a few instances, the presence of a 3.28 Å peak shouldering on the 3.2 Å plagioclase peak may have been caused by prehnite.

Minor phyllosilicates

Illite/muscovite, chlorite, and talc/pyrophyllite were incorporated into a number of the ferromanganese oxide deposits. A sharp 10 Å peak was assigned to illite/muscovite; often this peak appeared as a shoulder on the more broad, adjacent todorokite peak. Diffraction maxima at 14 and 7 Å (where evidence for phillipsite was lacking) were used as evidence for chlorite. Talc/pyrophyllite displayed 9.4-9.2 Å peaks; no attempt was made to differentiate these two related minerals.

Other contaminant minerals

Bone apatites found within manganese nodules were characterized by three peaks in the 2.82-2.70 Å region, indicating a probable fluorapatite composition. A large 3.03 Å peak was assigned to calcite. Alpha-cristobalite displayed a 4.05 Å peak that could not be attributed to a feldspar. Beta-quartz showed a single broad diffraction peak at 3.43 Å.

TABLE 17.--Sources of X-ray diffraction data.

Mineral	Reference(s)	Comments
Todorokite	Frondel, et al. (1960)	Charco Redonda, Cuba
Birnessite	Jones and Milne (1956)	Scotland, gravel pan
δ-MnO_2	Buser, et al. (1954)	Synthetic
Goethite	Rooksby (1961)	α-FeOOH
Maghemite	Rooksby (1961) Machek (1965)	See also Harrison and Peterson (1965)
Quartz	ASTM 5-0490	Internal standard
Plagioclase	ASTM 9-466	Albite
	ASTM 9-457	Oligoclase
	ASTM 10-359	Andesine
	ASTM 9-465	Labradorite
	ASTM 9-467	Bytownite
	ASTM 12-301	Anorthite
	ASTM 10-379	Anorthite
Alkali Feldspars	ASTM 13-456	Sanidine
	ASTM 9-478	Anorthoclase
	ASTM 10-479	Microcline
	ASTM 9-462	Orthoclase
Smectite	ASTM 3-0009	Montmorillonite
	ASTM 2-0008	Nontronite
	This study	Montmorillonite?
Phillipsite	Lippman (1958)	Sample impure?
	Morgenstein (1967)	Harmotome?
	This study	Sample nearly pure
Clinoptilolite	Hathaway and Sachs (1965)	Mid-Atlantic Ridge
	Mumpton (1960)	Heulandite differentiated
	This study	Approximate values
Analcime	ASTM 7-363	Zeolite, probably present
	ASTM 7-340	

TABLE 17.--Continued

Mineral	Reference(s)	Comments
Mordenite	ASTM 6-0239	Zeolite, possibly present
Erionite	ASTM 12-275	Zeolite, possibly present
Epistilbite	ASTM 11-58	Zeolite, possibly present
Amphibole	ASTM 9-434	Hornblende
Pyroxene	ASTM 3-0623	Augite
	ASTM 7-216	Enstatite
	ASTM 2-5020	Hypersthene
Olivine	ASTM 7-75	Forsterite
	ASTM 7-156	Chryolite
Magnetite	ASTM 11-614	Primary volcanic
Prehnite	ASTM 7-333	Secondary volcanic
Illite/muscovite	ASTM 9-334	Illite
	ASTM 7-42	Muscovite
Chlorite	Griffin and Goldberg (1963)	
Talc/pyrophyllite	Biscaye (1965)	Pyrophyllite
	ASTM 3-0881	Talc
Apatite	McConnell (1938)	
Calcite	ASTM 5-0586	
α-Cristobalite	ASTM 11-695	
β-Quartz	ASTM 11-252	

APPENDIX C

RELIABILITY OF THE DATA

A multitude of observations and data were collected for this study, not all of it perfectly reproducible. The types of visual observations made on the nodules have been discussed previously. Although somewhat subjective, data on morphogenetic type, oxide crust thickness, and other structural considerations were made with consistency and with no intention to produce preconceived trends. The chemical analyses are quite accurate, as runs on duplicate samples proved. The data most subject to fluctuations are those derived from X-ray diffraction.

It must be emphasized that the X-ray diffraction data are semi-quantitative. They have been used as quantitative data for the purposes of this study to show broad regional trends. Duplicate values for peak area ratios were almost always well within an order of magnitude. The fluctuations caused by machine performance, differing grain sizes, and variable packing can in no way have significantly effected the regional trends.

The method used to produce a single value for a station with multiple analyses is open to question, however.

Where more than one peak area, elemental ratio, or oxide crust thickness was obtained for a single station, the values were averaged. This was done at 17 stations of 111. For the map showing the regional variation of the todorokite proportion (Fig. 16), only two of the stations with multiple values had a single value significantly different from the average value for the station. At seven stations the individual values for feldspar are not representative of the average value. This indicates that regional feldspar trends may have little meaning, since differences within a single dredge haul can be as great as the differences used to delineate distributional trends. Multiple quartz values are more constant, and therefore probably more reliable. Only three stations show disparate quartz proportions. It must be concluded that averaging has almost no effect on regional todorokite or quartz trends.

APPENDIX D

SAMPLE DATA

Sample No.	FSU Sample	Lat. S.	Long. W.	Depth (fm)
1	RS 19-3	61-42	99-52	2765
2	RS 20-2	58-05	144-57	1654
3	RS 20-3	59-48	144-45	1766
4	RS 20-3	"	"	"
5	RS 20-3	"	"	"
6	RS 20-4	59-51	144-52	1798
7	RS 20-5	60-20	137-46	2320
8	RS 20-5	"	"	"
9	RS 20-8	52-01	99-57	2416
10	RS 20-8	"	"	"
11	RS 21-4	33-03	82-03	2122
12	RS 21-4	"	"	"
13	RS 21-6	33-02.5	83-56.5	1996
14	RS 21-6	"	"	"
15	RS 21-7	33-00	85-54	2118
16	RS 21-7	"	"	"
17	RS 21-8	32-58	88-00	1979
18	RS 21-8	"	"	"
19	RS 21-8	"	"	"
20	RS 21-9	33-04.5	89-33	2075
21	RS 21-9	"	"	"
22	RS 21-10	37-21	94-40	1875
23	RS 21-11	39-51	96-52	1990
24	RS 21-11	"	"	"
25	RS 21-12	40-08	119-35	2325
26	RS 21-12	"	"	"
27	RS 21-13	43-58	120-06	2192
28	RS 21-13	"	"	"
29	RS 21-18	56-32	119-20	2592
30	RS 21-20	61-11	120-20	2726
31	RS 22-1	57-50	56-51	2143
32	RS 22-2	57-39	52-02	2179
33	RS 23-1	62-08	95-19	2605

APPENDIX D.--Continued

Concretion Type	Concretion Fraction	Peak Area Ratios (Q + P)/T	(P + T)/Q	(T + Q)/P
AGGLOM	OC, SC	67.3	1.0	1.0
Crust	OC, SC, N	2.6	2.0	1.6
Crust	Cavity filling	15.9	--	--
Crust	OC	7.6	4.3	0.4
Crust	N	--	--	--
Crust	OC	21.3	0.3	4.1
Nodule	OC	1.7	1.7	2.8
Nodule	SC, N	23.3	--	--
Crust	N	8.3	--	--
Crust	OC	1.0	3.2	3.7
Crust	OC	2.2	7.4	0.8
Crust	N	50.0	--	--
Crust	OC	1.6	15.0	0.8
Crust	N	--	--	--
Nodule	OC	4.8	10.1	0.4
Nodule	N	50.2	--	--
Crust	OC	0.7	19.8	1.8
Crust	N	24.7	--	--
Crust	OC, SC, N	18.5	--	0.05
Nodule	OC, N	1.0	21.2	1.2
Crust	OC, N	3.4	0.9	2.9
Crust	OC, N	8.2	0.6	2.6
Crust	OC	0.2	14.0	6.5
Crust	SC, N	23.0	--	--
Nodule	OC	1.3	2.8	2.3
BOTRY	OC, N	2.4	2.4	1.4
BOTRY	OC	1.9	1.4	3.3
BOTRY	N	9.3	--	--
Nodule	OC, SC	0.3	6.0	8.3
BOTRY	OC, SC	9.0	0.6	2.6
BOTRY	OC, SC	57.2	0.7	1.6
BOTRY	OC, SC	72.0	0.7	1.5
BOTRY	OC, SC	10.5	0.8	1.7

SAMPLE DATA.--Continued

Sample No.	FSU Sample	Lat. S.	Long. W.	Depth (fm)
34	RS 23-2	61-27	94-58	2565
35	RS 23-2	"	"	"
36	RS 23-2	"	"	"
37	RS 23-3	61-24	101-14	2672
38	RS 23-5	60-24	115-01	2752
39	RS 23-5	"	"	"
40	RS 24-2	39-58	150-02	2768
41	RS 24-2	"	"	"
42	RS 24-4	45-06	145-11	2709
43	RS 24-4	"	"	"
44	RS 24-4	"	"	"
45	RS 24-4	"	"	"
46	RS 24-8	43-00	139-56	2810
47	RS 24-8	"	"	"
48	RS 24-15	35-58	134-18	2568
49	RS 24-15	"	"	"
50	RS 24-15	"	"	"
51	RS 24-15	"	"	"
52	RS 24-15	"	"	"
53	RS 24-15	"	"	"
54	RS 24-15	"	"	"
55	RS 24-15	"	"	"
56	RS 24-15	"	"	"
57	RS 24-15	"	"	"
58	RS 24-15	"	"	"
59	RS 24-15	"	"	"
60	RS 24-15	"	"	"
61	RS 24-17	42-01	130-02	2646
62	RS 24-17	"	"	"
63	RS 24-17	"	"	"
64	RS 24-18	39-38	130-13	2585
65	RS 24-19	37-04	129-58	1940
66	RS 24-19	"	"	"
67	RS 24-19	"	"	"
68	RS 24-21	41-56	124-52	2375
69	RS 24-21	"	"	"
70	RS 24-21	"	"	"
71	PC 5-9-1, Top	58-17.5	66-35	1980
72	PC 5-11-2, 135 cm.	59-19	69-17	1970

SAMPLE DATA.--Continued

Concretion Type	Concretion Fraction	Peak Area Ratios (Q + P)/T	(P + T)/Q	(T + Q)/P
BOTRY	OC, SC?	20.3	1.0	1.2
Nodule	OC, SC	14.0	0.8	1.6
Nodule	N	52.5	--	--
AGGLOM	OC, SC	66.0	0.5	2.2
BOTRY	OC, SC	4.0	1.1	2.1
Nodule	OC, SC, N	10.1	2.8	0.5
BOTRY	OC	1.3	1.2	5.9
BOTRY	OC	3.8	1.5	1.6
BOTRY	OC	2.0	1.4	2.9
BOTRY	OC, SC	2.5	0.8	4.7
BOTRY	OC	5.0	0.9	2.3
BOTRY	OC, N	16.2	0.8	1.6
Nodule	OC, SC	1.2	1.9	4.0
Nodule	SC, N	7.9	--	--
Crust	OC	2.6	3.2	1.0
Crust	N	--	--	--
Crust	Cavity Filling	--	--	--
Crust	OC, SC	1.3	2.8	2.3
Crust	N_a	74.0	--	--
Crust	N_b	--	--	--
Crust	OC	1.2	2.9	2.5
Crust	N	14.5	--	--
Crust	OC	4.3	1.0	2.4
Crust	SC, N	--	--	--
Crust	OC	0.7	5.7	2.9
Crust	N	--	--	--
Crust	OC	4.4	1.9	1.1
Crust	OC	0.9	2.8	3.9
Crust	N	111.4	--	--
Nodule	OC, SC	1.4	2.5	2.3
Nodule	OC, SC, N	1.3	3.6	1.9
Crust	OC	1.0	7.0	1.7
Crust	N_2	56.8	--	--
Crust	OC, N_b	17.1	--	--
Nodule	OC_a	3.7	1.6	1.5
Nodule	OC_b	9.7	1.9	0.8
BOTRY	OC, SC	4.3	1.5	1.4
Crustal Material		20.6	1.1	1.1
AGGLOM	OC	7.9	0.8	2.0

SAMPLE DATA.--Continued

Sample No.	FSU Sample	Lat. S.	Long. W.	Depth (fm)
73	PC 5-11-2, 157 cm.	59-01	67-30	1980
74	PC 5-11-3, 287-290 cm.	"	"	"
75	PC 5-12-1, Top	59-19	69-17	1970
76	PC 5-12-1, Top	"	"	"
77	PC 5-12-1, 206-211 cm.	"	"	"
78	PC 5-12-1, 206-211 cm.	"	"	"
79	PC 5-12-1, 216-220 cm.	"	"	"
80	PC 5-12-1, 231-235 cm.	"	"	"
81	PC 5-28-1, 0-17 cm.	60-00	70-46.5	2300
82	PC 5-29-1, 0-10 cm.	59-00	71-08	2060
83	PC 6-7-1, Top	58-13	59-44	2055
84	PC 6-7-1, 225-227 cm.	"	"	"
85	PC 6-11-1, Top	55-44	56-03	2140
86	PC 6-11-1, 136-138 cm.	"	"	"
87	PC 7-18-1, 60 cm.	53-00.5	48-53	1705
88	PC 7-18-1, 78-80 cm.	"	"	"
89	PC 7-18-3, 404-406 cm.	"	"	"
90	PC 10-4-1, Top	58-03.2	82-51	2160
91	PC 10-4-1, Top	"	"	"
92	PC 10-16-4, 320 cm.	62-52.5	74-49	2200
93	PC 10-24-2, 430 cm.	62-57	78-54.5	2518
94	PC 11-3-1, Top	56-54	115-14.5	2200
95	PC 11-5-1, Top	58-56.5	114-43	2770
96	PC 11-5-1, Top	"	"	"
97	PC 11-5-3, 725 cm.	"	"	"
98	PC 11-10-1, 7-9 cm.	63-44.5	114-40.5	2760
99	PC 14-7-3, 279-287 cm.	58-03	160-09	2275
100	PC 14-8-7,1702-1708cm.	59-40	160-17.5	2120
101	PC 14-13-1,128-130 cm.	60-02	145-17	1868
102	PC 14-15-1,159-172 cm.	60-42.5	125-12.5	2510
103	PC 14-16-1,156-160 cm.	58-59.5	125-02	2460
104	PC 15-1-1, 0-7 cm.	61-58	95-00	2620
105	PC 15-1-1, 191-194 cm.	"	"	"
106	PC 15-3-1, 14-23 cm.	59-05.5	94-57	2520
107	PC 15-13-1, 5-8 cm.	57-50	108-39	2460
108	PC 15-21-1, 0-20 cm.	57-34	138-58	1595
109	PC 15-26-1, 31-33 cm.	54-02	145-18	2000
110	PC 16-7-1, 0-8 cm.	57-16	165-32E	2712

SAMPLE DATA.--Continued

Concretion Type	Concretion Fraction	Peak Area Ratios (Q + P)/T	(P + T)/Q	(T + Q)/P
AGGLOM	OC, SC?	28.7	0.7	1.6
Nodule	OC	14.9	1.2	1.0
Nodule	OC	17.2	1.6	0.8
BOTRY	OC, N?	13.9	0.4	3.6
Crust	OC, SC, N	24.1	1.0	0.8
Nodule	OC	18.8	0.6	2.1
Nodule	OC, SC	12.1	1.1	1.3
Crust	OC, SC, N	12.8	0.6	0.6
Crust?	OC, SC	2.9	1.5	2.0
Crust	OC, SC, N?	9.0	1.3	1.2
BOTRY	OC, SC, N?	45.1	1.2	0.9
AGGLOM	OC, N?	42.5	0.8	1.4
Crust	OC	17.8	1.1	1.2
BOTRY	OC, SC	29.2	0.7	1.6
Crust?	OC, SC	7.4	0.5	3.7
Crust?	OC, N	36.6	0.7	1.5
Nodule?	OC, SC, N	3.2	1.0	2.8
Nodule?	OC	3.2	1.8	2.0
Nodule?	SC, N?	15.0	--	--
BOTRY	OC, SC, N	17.8	1.1	1.2
Crust?	OC, SC?	10.4	0.5	3.1
AGGLOM	OC, SC	15.2	0.8	1.7
Crust	OC, SC, N	4.6	1.1	1.8
BOTRY	OC, SC	4.7	1.6	1.3
AGGLOM	OC, SC	7.4	2.6	0.6
AGGLOM	OC, SC	17.7	1.4	0.5
BOTRY?	OC	4.6	0.6	3.7
Nodule?	OC	1.1	3.5	2.3
AGGLOM	OC	2.6	1.5	2.1
Crust	OC	0.3	3.6	18.5
BOTRY	OC, SC	9.9	0.7	2.1
BOTRY	OC, SC	8.4	1.0	1.5
Nodule	OC, SC, N	9.0	1.0	1.4
Crust	OC, SC, N?	9.9	1.1	1.3
BOTRY	OC	4.8	0.9	2.2
Crust?	OC, SC, N?	7.2	1.0	1.7
Crust	OC, SC, N	1.0	2.5	3.9
Crust?	OC, SC, N	9.8	--	--

SAMPLE DATA.--Continued

Sample No.	FSU Sample	Lat. S.	Long. W.	Depth (fm)
111	PC 17-6-1, 6-9 cm.	60-03	134-55	2080
112	PC 17-6-1, 22-25 cm.	60-03	134-55	2080
113	PC 17-6-1, 83-87	"	"	"
114	PC 17-6-1, 193-198 cm.	"	"	"
115	PC 17-7-2, 73-77 cm.	61-05	134-21	2425
116	PC 17-7-2, 75-78 cm.	"	"	"
117	PC 17-7-2, 75-78 cm.	"	"	"
118	PC 17-7-2, 150-152 cm.	"	"	"
119	PC 17-8-2, 320-323 cm.	62-01	135-17	2487
120	PC 17-31-1, Top	57-02	94-45	2587
121	PC 17-31-1, Top	"	"	"
122	PC 19-11-1, 7 cm.	58-05	109-47.5	2540
123	PC 20-1-1, 0-17 cm.	47-02	144-54	2645
124	PC 20-3-1, 5 cm.	51-07	145-03	2240
125	PC 20-3-1, 5 cm.	"	"	"
126	PC 20-7-3, 68-71 cm.	59-08	145-08	1725
127	PC 20-11-1, Top	57-14	104-30	2390
128	PC 20-11-1, Top	"	"	"
129	PC 20-12-4, 544-548 cm.	56-04	104-37	2320
130	PC 21-4-1, 0-10 cm.	35-44	92-42	1805
131	PC 21-8-1, 2-3 cm.	39-53.5	96-54.5	1945
132	PC 21-8-1, 31-32 cm.	"	"	"
133	PC 21-11-1, 208-218 cm.	39-58	112-00	1530
134	PC 21-21-1, 53-55 cm.	61-08	120-16	2720
135	PC 21-21-1, 53-55 cm.	"	"	"
136	PC 21-21-4, 436-439 cm.	"	"	"
137	PC 22-1-1, 0-11 cm.	57-03	60-01	1880
138	PC 22-1-1, 0-11 cm.	"	"	"
139	PC 22-1-1, 54-57 cm.	"	"	"
140	PC 22-1-1, 69-72 cm.	"	"	"
141	PC 22-1-2, 87-89 cm.	"	"	"
142	PC 22-1-2, 87-89 cm.	"	"	"
143	PC 22-6-2, 497-501 cm.	55-54	51-50	2160
144	PC 22-34-1, Top	53-23	52-54	1960
145	PC 22-34-1, 18-22 cm.	"	"	"
146	PC 22-34-1, 18-22 cm.	"	"	"
147	PC 22-34-1, 33-36 cm.	"	"	"
148	PC 24-4-1, 45 cm.	45-01	145-17	2720
149	PC 24-4-1, 77 cm.	"	"	"
150	PC 24-4-3, 623-628 cm.	"	"	"

SAMPLE DATA.--Continued

Concretion Type	Concretion Fraction	Peak Area Ratios (Q + P)/T	(P + T)/Q	(T + Q)/P
Nodule	OC, SC	4.0	1.3	1.7
BOTRY	OC, SC	6.5	1.1	1.5
Nodule	OC, SC	3.3	1.3	1.9
Nodule	OC, SC	3.7	1.8	1.3
Nodule	OC, SC, N	1.6	1.0	7.8
Nodule	OC	1.2	2.2	3.5
Nodule	N	22.1	--	--
Nodule	OC, SC	2.4	1.6	2.2
AGGLOM	OC, SC	1.5	2.4	2.0
Crust	OC, SC, N	1.9	1.9	2.2
Crust	N	4.7	--	--
AGGLOM	OC, SC	24.5	0.8	1.6
Crustal Material		9.9	1.1	1.3
BOTRY	OC	1.9	1.5	3.1
BOTRY	N	1.8	--	--
Crust	OC	3.9	2.0	1.1
Nodule	OC	4.5	1.2	1.8
Nodule	SC, N	11.1	--	--
BOTRY	OC	2.1	2.6	1.5
Nodule?	OC	1.4	13.0	1.0
Nodule	OC, SC, N	0.5	52.0	2.1
Nodule	OC, SC	1.1	52.8	1.0
Nodule?	OC	1.4	--	0.7
Crust	OC	6.9	1.1	1.5
Crust	N	--	--	--
AGGLOM	OC	9.4	0.7	1.2
Crust?	OC	8.3	0.8	2.0
Crust?	N	72.0	--	--
Nodule	OC, SC, N	11.3	0.3	5.5
Crust?	OC	8.1	0.7	2.2
Nodule	OC	21.3	0.4	3.2
Nodule	N	10.4	--	--
BOTRY	OC	16.7	0.6	1.0
Nodule	OC	7.5	0.6	2.7
Nodule	OC_a	19.9	0.5	2.8
Nodule	OC_b	8.3	0.4	4.3
Nodule	OC	9.5	0.5	3.6
Nodule?	OC	6.6	0.5	3.5
Crustal Material		2.6	1.5	2.2
Crustal Material		12.5	1.3	1.0

SAMPLE DATA.--Continued

Sample No.	FSU Sample	Lat. S.	Long. W.	Depth (fm)
151	PC 24-5-1, Top	42-34	144-57	2884
152	PC 24-5-1, Top	"	"	"
153	PC 24-5-1, Top	"	"	"
154	PC 24-6-1, 43 cm.	40-10	144-46	2887
155	PC 24-7-1, 5-8 cm.	41-33	142-20	2785
156	PC 24-7-1, 5-8 cm.	"	"	"
157	PC 24-7-1, 11-15 cm.	41-33	142-20	2785
158	PC 24-8-2, 348-350 cm.	42-53	134-39	2740
159	PC 24-10-1, 4-6 cm.	37-58	134-59	2665
160	PC 24-11-1, 12-14 cm.	40-00	132-35	2665
161	PC 24-12-1, 0-3 cm.	42-53	134-38	2720
162	PC 24-13-1, 2-3 cm.	39-37	130-11	2602
163	PC 24-13-1, 12-14 cm.	"	"	"
164	PC 24-16-1, 36-39 cm.	35-13	124-59	2150
165	PC 24-16-1, 36-39 cm.	"	"	"
166	PC 25-3-1, 1-3 cm.	39-57	82-57	2195
167	PC 25-3-1, 14-17 cm.	"	"	"
168	PC 25-7-1, 276-283 cm.	50-06	94-54	2496
169	PC 25-7-1, 276-283 cm.	"	"	"
170	PC 25-7-3, 864-870 cm.	"	"	"
171	PC 25-15-1, 0-5 cm.	64-31	145-59	2064
172	PC 25-15-1, 46-50 cm.	"	"	"
173	PC 25-15-2, 85-95 cm.	"	"	"
174	PC 25-15-2, 174-176 cm.	"	"	"
175	PC 25-16-2, 599-605 cm.	56-09	156-13	1980
176	PC 27-1-1, 157-159 cm.	63-00	177-42.5 E	1835
177	PC 27-1-2, 172-175 cm.	"	"	"
178	RS 24-17	42-01	130-02	2646
179	RS 24-17	"	"	"
180	RS 25-1	42-05	86-03	1647
181	RS 25-2	42-04	81-59	1750
182	RS 25-5	49-57	89-59	2340
183	RS 25-6	50-29	94-55	2543
184	RS 25-6	"	"	"
185	RS 25-6	"	"	"
186	RS 25-6	"	"	"
187	RS 25-7	49-59	104-53	2090
188	RS 25-7	"	"	"
189	RS 25-7	"	"	"
190	RS 27-2	63-06	177-37 E	1845

SAMPLE DATA.--Continued

Concretion Type	Concretion Fraction	Peak Area Ratios (Q + P)/T	(P + T)/Q	(T + Q)/P
Nodule	OC	0.8	2.0	7.4
Nodule	Fracture-filling	--	--	--
Nodule	SC, N	1.8	--	--
Nodule?	OC, SC, N	0.7	3.3	4.3
Nodule	OC, SC, N_a	0.9	2.9	3.9
Nodule	OC, SC, N_b	1.7	2.0	2.3
Nodule	OC, SC, N	1.2	1.7	4.4
BOTRY	OC	13.0	1.4	1.0
BOTRY	OC, SC, N	1.5	3.5	1.7
BOTRY	OC, SC	1.0	2.6	3.6
Nodule	OC, SC	1.2	3.5	2.2
Nodule	OC	1.0	3.3	1.7
BOTRY	OC, SC	1.5	3.2	1.7
Crust	N	11.2	--	--
Crust	OC	9.2	50.0	0.1
Nodule	OC, SC	0.9	8.6	1.8
Nodule	OC, SC	0.8	14.0	1.6
Nodule	N	37.7	--	--
Nodule	OC	2.0	3.4	1.3
Crust	OC, SC, N	9.1	5.4	0.3
Crust	OC	2.2	1.0	4.4
AGGLOM	OC	4.3	1.1	1.9
Crust	OC, SC, N	1.3	5.3	2.2
Nodule	OC	3.2	1.5	1.8
Crust?	OC	5.6	1.6	1.2
AGGLOM	OC	2.6	0.9	4.1
AGGLOM	OC	1.4	1.4	4.8
Crust	OC	2.3	2.6	1.3
Crust	N	27.3	--	--
Crust	OC, SC	0.7	16.5	1.7
Crust	OC	2.4	3.4	1.1
Crust	OC	2.2	3.0	1.3
AGGLOM	OC	2.3	2.2	1.7
Nodule	OC_a	1.0	6.7	1.7
Nodule	OC_b	1.4	4.0	1.7
Nodule	N	20.1	--	--
Crust	OC, SC, N	1.1	1.6	0.9
Nodule	OC	0.8	3.6	3.3
Nodule	N	21.4	--	--
AGGLOM	OC	2.1	0.9	5.0

SAMPLE DATA.--Continued

Sample No.	FSU Sample	Lat. S.	Long. W.	Depth (fm)
191	RS 27-2	63-06	177-37E	1845
192	RS 27-2	"	"	"
193	RS 27-3	63-06	177-37E	1845
194	RS 27-7	63-57	177-40E	1420
195	RS 27-7	"	"	"
196	RS 27-51	57-55	153-57.5E	1894
197	RS 27-51	"	"	"
198	RS 27-51	"	"	"
199	USC-115	58-28	60-37.5	1662
200	MT 5-1	61-09	67-50	2233
201	RD 5-4S(A)	59-02	67-18	1900
202	RD 5-4S(B)	59-02	67-18	1900
203	RD 5-4S(C)	"	"	"
204	RD 5-7	62-17.5	67-51	2075
205	RD 5-16(A)	57-59	70-52.5	2240
206	RD 5-16(C)	"	"	"
207	RD 5-17(A)	57-05	70-59	2060
208	RD 5-17(A)	"	"	"
209	RD 5-17(B)	"	"	"
210	BT 6-3	56-56	56-29	1840
211	BT 6-4	57-57	55-57	2190
212	MT 6-3	56-14	58-42	2260
213	USC 450	56-59.5	58-58	2020
214	USC 451(A)	55-54	59-03.5	2223
215	USC 451(A)	"	"	"
216	USC 451(A)	"	"	"
217	USC 451(A)	"	"	"
218	USC 451(B)	"	"	"
219	RD 6-5(A)	56-15	58-20	2165
220	RD 6-5(B & C)	"	"	"
221	RD 6-5(B & C)	"	"	"
222	RD 6-5(D)	"	"	"
223	RD 6-5(D)	"	"	"
224	RD 6-5(E)	56-15	58-20	2165
225	RD 6-5(E)	"	"	"
226	RD 6-7	58-06	59-24	2383
227	RD 6-9(B)	54-03	56-05	940
228	RD 6-9(C)	"	"	"
229	RD 6-10(B)	55-06	55-50	1570
230	RD 6-10(B)	"	"	"

SAMPLE DATA.--Continued

Concretion Type	Concretion Fraction	Peak Area Ratios (Q + P)/T	(P + T)/Q	(T + Q)/P
Crust?	N	--	--	--
Crust	OC	8.6	3.1	0.5
Crust	OC	6.1	1.0	1.7
Crust	OC	1.5	5.3	1.6
Crust	N	--	--	--
Crust	N	--	--	--
Crust	OC	7.0	1.1	1.6
Nodule?	OC	2.4	1.1	3.4
Crust	OC	14.2	1.0	1.3
AGGLOM	OC, SC	46.4	0.7	1.7
Crust	OC, SC	9.0	1.4	1.1
Nodule	OC	9.0	0.6	2.5
Nodule	OC	28.9	1.1	1.1
AGGLOM	OC, SC	30.1	0.9	1.2
Crust	OC	3.6	1.9	1.3
BOTRY	OC	6.6	0.7	2.8
Crust	OC	9.3	1.1	1.4
Crust	N	--	--	--
Crust	OC	11.4	0.5	2.7
Nodule	OC	19.5	1.0	1.2
BOTRY	OC, SC	25.5	0.9	1.2
Nodule	OC	9.8	1.0	1.5
AGGLOM	OC	25.0	0.6	1.9
Nodule	OC_a	16.0	0.9	1.2
Nodule	OC_b	12.0	1.2	1.1
Nodule	OC_c	10.8	0.9	1.6
Nodule	OC_d	5.8	1.6	1.1
AGGLOM	OC	12.4	1.1	1.2
Crust	OC	14.4	0.7	1.9
Crust	OC	7.2	1.1	1.5
Crust	N	--	--	--
Crust?	SC	107.7	--	--
Crust?	OC	28.6	1.2	0.9
Crust	OC	19.9	1.4	0.9
Crust	N	--	--	--
Crust	OC, SC	19.8	1.2	1.0
Nodule	OC	4.5	0.5	6.3
Crust?	OC	2.8	1.8	1.6
Crust?	OC	29.8	1.1	1.1
Crust?	N	--	--	--

SAMPLE DATA.--Continued

Sample No.	FSU Sample	Lat. S.	Long. W.	Depth (fm)
231	RD 6-10(C)	55-06	55-50	1570
232	RD 6-10(D)	"	"	"
233	RD 6-11(A)	55-58.5	56-05	2266
234	RD 6-11(B)	"	"	"
235	RD 6-11(B)	"	"	"
236	RD 6-12(A)	56-57	56-31	1710
237	RD 6-13(A)	57-46	55-58	2222
238	PC 7-18-1, Top	53-00	48-53	1705
239	MT 7-1	55-56	45-12.1	2045
240	BT 7-7	59-01	48-59.5	2107
241	RD 7-16	59-08.5	48-53	2105
242	RD 7-17	53-03.5	48-57	1780
243	MT 8-2	54-19	27-23	2835
244	MT 8-2	"	"	"
245	RD 10-2(A)	58-06	82-52	2170
246	RD 10-2(A)	"	"	"
247	RD 10-2(B)	58-06	82-52	2170
248	BT 10-9	62-51	74-45.5	2190
249	BT 10-11	61-02	75-04	2445
250	BT 10-13(A)	59-02	74-39	2568
251	BT 10-13(A)	"	"	"
252	BT 10-13(B)	"	"	"
253	BT 10-13(C)	"	"	"
254	BT 10-13(D)	"	"	"
255	MT 10-19	61-20	78-56	2485
256	MT 10-20	58-18	78-28	2700
257	BT 11-1	54-55	114-49	2100
258	BT 13-2	57-44	90-47	2780
259	BT 13-2	"	"	"
260	BT 13-7	65-37	123-55	2573
261	BT 13-8	63-36.5	129-54	2632
262	BT 14-1	52-01.5	159-54	2525
263	BT 14-1	"	"	"
264	BT 14-3	56-12	160-37	2390
265	MT 14-5	62-26	160-07	1600
266	RD 14-7	57-53	125-02	2120
267	BT 15-1	61-02	95-02	2730
268	MT 15-3	59-01	99-36	2680
269	BT 15-4	61-02	99-57	2700
270	BT 15-5(A)	61-06	104-58	2670

SAMPLE DATA.--Continued

Concretion Type	Concretion Fraction	Peak Area Ratios (Q + P)/T	(P + T)/Q	(T + Q)/P
Crust?	OC	20.3	0.4	2.9
Nodule?	OC	7.7	1.3	1.2
Crust	OC	16.4	0.6	2.2
Nodule	OC	10.2	1.1	1.4
Nodule	N	21.9	--	--
Nodule	OC	12.6	0.9	1.4
AGGLOM	OC, SC	16.2	1.5	0.9
Nodule	OC	3.6	0.7	4.2
Crust	OC, SC	3.4	0.9	3.0
Crust	OC	9.0	0.4	4.9
Crust	OC	14.8	0.8	1.6
Crust	OC	7.8	0.5	3.4
AGGLOM	OC, SC	8.9	1.2	1.2
AGGLOM	OC, N	27.4	--	--
Crust	OC, SC	6.9	1.5	1.1
Crust	N	0.6	--	--
Crust	OC, N	21.7	--	--
AGGLOM	OC, SC	30.5	2.6	0.5
AGGLOM	OC, SC	30.8	1.1	1.0
BOTRY	OC, SC	37.1	1.4	0.8
BOTRY	N	--	--	--
Crust	OC, SC	10.6	1.5	0.9
BOTRY	OC, SC	7.0	0.8	2.0
Crust	OC	8.6	0.9	1.8
BOTRY	OC, SC, N	5.0	1.4	1.4
AGGLOM	OC, SC	14.8	2.1	0.6
Crust?	OC	3.5	1.7	1.5
Crust	OC	11.9	1.3	1.1
Crust	SC, N	--	--	--
AGGLOM	OC, SC	12.0	1.0	1.4
AGGLOM	OC, SC	5.6	1.0	1.9
Crust	OC	1.9	1.4	3.1
Crust	N	2.3	--	--
Nodule	OC, SC	0.9	2.0	2.6
Crust	OC	17.7	0.9	1.4
AGGLOM	OC, SC	6.8	0.5	3.1
AGGLOM	OC, SC	10.0	1.1	1.2
Crust	OC	5.4	1.1	1.8
Crust	OC, SC, N	12.0	--	--
AGGLOM	OC	7.5	0.8	1.9

SAMPLE DATA.--Continued

Sample No.	FSU Sample	Lat. S.	Long. W.	Depth (fm)
271	BT 15-5(B)	61-06	104-58	2670
272	RD 15-6	59-09	104-58	2440
273	RD 15-13	55-20.5	145-03	2600
274	BT 15-14	54-02	145-18	1980
275	BT 16-7	56-22	158-28E	872
276	PC 16-8-1, 0-10 cm.	56-08	169-42E	2798
277	RD 17-1	52-10	142-09	1205
278	RD 17-1	"	"	"
279	RD 17-4(B)	64-03	135-00	2370
280	RD 17-4(A)	"	"	"
281	BT 17-5	65-04	134-53	2350
282	BT 17-101	62-12	94-46	2678
283	BT 17-12(A)	56-04	94-54	2600
284	BT 17-12(B)	"	"	"
285	BT 17-12(C)	"	"	"
286	BT 17-12(C)	"	"	"
287	BT 17-13	55-00	94-53	2424
288	BT 17-13	"	"	"
289	RS 18-2	56-04	99-20	2548

Explanation of abbreviations:

Concretion Type:
- BOTRY = Botryoidal
- AGGLOM = Agglomerate

Concretion Fraction:
- OC = Oxide crust
- SC = Subcrust
- N = Nucleus

SAMPLE DATA.--Continued

Concretion Type	Concretion Fraction	Peak Area Ratios $\frac{Q+P}{T}$	$\frac{P+T}{Q}$	$\frac{T+Q}{P}$
Crust	OC, SC	13.1	1.2	1.2
AGGLOM	OC, SC	9.3	0.9	1.7
Crust	OC	46.4	0.4	2.7
Crust	OC, N	14.0	--	--
Crust	OC	1.1	6.0	1.6
Nodule	OC	16.1	1.9	0.7
Crust	OC	0.8	9.0	1.9
Crust	OC	2.3	2.0	1.8
Nodule	OC	4.6	1.1	1.9
Nodule	OC	4.7	1.0	2.2
Nodule	OC	6.3	1.3	1.4
AGGLOM	OC, SC	3.5	2.0	1.2
Nodule	OC, N?	2.0	2.7	1.7
Crust	OC, SC, N	10.4	--	--
Nodule	OC	1.1	2.9	2.6
Nodule	N	14.3	--	--
Crust	OC, N	9.1	--	--
Crust	OC?	4.5	1.8	1.1
Crust	OC	2.2	1.3	2.9

Peak Area Ratios:

$$\frac{Q+P}{T} = \frac{3.34\ \text{Å (Quartz)} + 3.2\ \text{Å (Plagioclase-Phillipsite)}}{9.7\ \text{Å (Todorokite)}}$$

$$\frac{P+T}{Q} = \frac{3.2\ \text{Å (Plagioclase-Phillipsite)} + 9.7\ \text{Å (Todorokite)}}{3.34\ \text{Å (Quartz)}}$$

$$\frac{T+Q}{P} = \frac{9.7\ \text{Å (Todorokite)} + 3.34\ \text{Å (Quartz)}}{3.2\ \text{Å (Plagioclase-Phillipsite)}}$$

APPENDIX E

SAMPLE MINERALOGY

Sample No.	Todorokite	Quartz	Plagioclase	Montmorillonite	Phillipsite	Goethite	Maghemite	Amphibole	Birnessite	Clinoptilolite	Analcime	Olivine	Others
1	x	x	x	x	?	?	?	?			?		
2	x	x	x	x	x	?	?		?				Sd?, Md?
3	x	x	x	x	x		?	?		?	?		
4	x	x	x	x	x	?		?	x				
5	x	x	x	x	?	?	?	?		?	?		
6	x	x	x	x	?	x	?			x			
7	x	x	x	x		x	?			?		?	Md?
8	x	x	x	x	?	?	?	?		?			
9	x	x	x	x	x	?	?	x					Ba?
10	x	x	x	x	x	?		?		?		?	Md?
11	x	x	x	x	x		?		?	?			
12	x	x	x	x	?	?	?						Tc?
13	x	?	x	x	x	?	?	?	x	?			
14		?	x	x		?	?						
15	x	x	x	x	x	?	?	?		?			
16	x	x	x	x	x	?	?						
17	x	x	?	x	x	?	?		?	?			Sd-Ah?
18	x	x	x	x	?	?	?						Ma?
19	x		x	x	x	?		?	?				Tc?, Ch?
20	x	x	x	x	x	?	?	?		?			
21	x	x		x	x		?						Ap
22	?	?	?	x	x							?	Sd?
23	x	x	x	x	x	?				?			
24	x	x	x	x	x	?				x			
25	x	x	x	x	x	?		?		?	?		Im?
26	x	x	x	x	x	?				?			
27	x	x	x	x	x	?	?	?		?			
28	x	x	x	?	x	?	?			?			
29	x	x	x	x	x			?					
30	x	x	x	x	x	x	?	?		x			Py?
31	x	x	x	x	x	x	?	x		?		x	
32	x	x	x	x	x	x	?	x		?			

SAMPLE MINERALOGY--Continued

Sample No.	Todorokite	Quartz	Plagioclase	Montmorillonite	Phillipsite	Goethite	Maghemite	Amphibole	Birnessite	Clinoptilolite	Analcime	Olivine	Others
33	x	x	x	x	x		?			?			Tc?
34	?	x	x	x	x	x		x		?	?		
35	x	x	x	x	x	x	?	x		?			
36	x	x	x	x	x								
37	x	x	x	x	x	?	?						
38	x	x	x	x	x	x	?	?	x	?	?		Il?
39	x	x	x	x	x	?	?	x		?			
40	x	x	x	x	x	x	?			?			
41	x	x	x	x	x	?	?			?			Ah?
42	x	x	x	x	x	?	?	?		?	?		
43	x	x	x	x	x	?	?	?		?			
44	x	x	x	x	x	?	?	?		?			
45	x	x	x	x	x	?	?			?	?		
46	x	x	x	x	x	?	?	?		?		?	Ps?
47	x	x	x	x	x	?	?			x			
48	x	x	x	x	x	?	?		?	?			
49	x	x	x	x	x								
50		x	?		?				x				Tc?
51	x	x	x	x	?	x		?	?			?	
52	x	x	x	x	x								
53	x			x	x								Ap
54	x	x	x	x	x	x	?			?			
55	x	x	x	x	x		?						
56	x	x	x	?	x	?	x		x				Py?
57	?	x	x	x	x		?						
58	x	x	x	x	?	x			x				
59	x			x	x								
60	x	x	x	x	x	?	?						
61	x	x	x	x	?	?	?		x				
62	x	x	x	x	x								Tc
63	x	x	x	x	?	?	?			?			
64	x	x	x	x	?	?	?	?	x		?		
65	x	x	x	x	?	?	?			?	?		
66	x		x	x	x								

SAMPLE MINERALOGY--Continued

Sample No.	Todorokite	Quartz	Plagioclase	Montmorillonite	Phillipsite	Goethite	Maghemite	Amphibole	Birnessite	Clinoptilolite	Analcime	Olivine	Others
67	x	x	x	x	x	?	?			?			
68	x	x	x	x	x	?	?				?	?	
69	x	x	x	x	x	?	?						
70	x	x	x	?	x	?	?	?			?		
71	x	x	x	x	?	?	?	?	x				
72	x	x	x	x	?	?	?	x		?			Ch?
73	x	x	x	x	x	?	?	?	x	?			
74	x	x	x	x	x	?	?	x		?		?	Ch?
75	x	x	x	x	x	x	?		?	?			
76	x	x	x	x	x	x	?	x		?			Sp?
77	x	x	x	x	x		?						
78	x	x	x	x	?	?	?	x			?		
79	x	x	x	x	x	?	?	x					
80	x	x	x	x	x	?	?	x			?		Ch?
81	x	x	x	x	x	?	?	x		?			
82	x	x	x	x	x	?	?						
83	x	x	x	x	?	?		x		x		?	
84	x	x	x	x	x	?	?	x		x	?		
85	x	x	x	x	x		?	x		?			
86	x	x	x	x	x	?	?	x		?			
87	x	x	x	x	x	?	?			?	?		
88	?	x	x	x	x	?		x					Il, Ap?
89	x	x	x	x	?	?	?	?	x	?			Ap
90	x	x	x	x	?	x	?			?	?	?	
91	x		x	x	x	?	?	?			?		Ch?
92	x	x	x	x	x	?	?			?			
93	x	x	x	x	?	?	?	?					Tc?, Md?
94	x	x	x	x	x	?	?			x			Sd?
95	x	x	x	x	?	x	?			?	?		
96	x	x	x	x	x	x	?		x			?	Sd?
97	x	x	x	x	x	x	?		?	?	?		
98	x	x	x	x	x	?	?			?			
99	x	x	x	x	x	?	?	?		?		?	Sd?
100	x	x	x	x	x	?	?	x					

SAMPLE MINERALOGY--Continued

Sample No.	Todorokite	Quartz	Plagioclase	Montmorillonite	Phillipsite	Goethite	Maghemite	Amphibole	Birnessite	Clinoptilolite	Analcime	Olivine	Others
101	x	x	x	x	?	?	?	x	x	?		?	
102	x	x	x	x	?	?	?	?	x	?	?		Py?
103	x	x	x	x	?	?	?	?		?			
104	x	x	x	x	?	?	?	x	x		?	?	Sd?
105	x	x	x	x	x	?	?	x				?	
106	x	x	x	x	x	x		?				?	
107	x	x	x	x	?	x	?	x	?				
108	x	x	x	x	x	?	?	?			?	?	Sd?,Er?, Pr?
109	x	x	x	x	x	x		?		?			Tc
110	x	x	x	x	x	?		x					Il
111	x	x	x	x	?	?	?	?		?		?	
112	x	x	x	x	x	?		?					Er?
113	x	x	x	x	x	x					?		
114	x	x	x	x	?	?	?			?			Er?,Py?
115	x	x	x	x	?	?	?	x	x	?		?	
116	x	x	x	x	?	x		?	x				
117	x	x	x	x	x	?	?			?	?	?	Er?
118	x	x	x	x	x	?	?					?	
119	x	x	x	x	?	x	?			?	?		
120	x	x	x	x	?	?	?	?	?	?			Ch?
121	x	x	x	x	x		?						Ch?
122	x	x	x	x	x	x	?	x				?	Ch?
123	x	x	x	x	x	?	?						Ch?
124	x	x	x	x	?	?		?	?	?		?	Sd?
125	x		x	x	?		?	?		?		x	Gl,Py?, Pr?,Sd?
126	x	x	x	x	x	?	?			?			Ch?,Sd?, Py?
127	x	x	x	x	?	x	x				?		Py?
128	x	x	x	x	x	?							
129	x	x	x	x	?	?				?		?	
130	x	x	x	x	x	?	?			?		?	
131	x	x	x	?	x	?	?						

SAMPLE MINERALOGY--Continued

Sample No.	Todorokite	Quartz	Plagioclase	Montmorillonite	Phillipsite	Goethite	Maghemite	Amphibole	Birnessite	Clinoptilolite	Analcime	Olivine	Others
132	x	x	x	?	x	?							Ca,Ch?
133	x	x	x	x	x	?	?	x		?	?		Ca,Gl
134	x	x	x	x	?	?							
135		x		x	x		?	?					Il,Sd-Ah?
136	x	x	x	x	?	x	?	x				?	
137	x	x	x	x	x	?		x			?		
138	x	x	x	x	x	x	?	x		?			Il,Md?, Ch?
139	x	x	x	x	?	?		x		?		?	Sd?
140	x	x	x	x	x	?		x		?	?		Sd?
141	x	x	x	x	?	?	?	?		?			Sd?,Py?
142	x	x	x	x	x	?		x		?			Il
143	x	x	x	x	?	?	?	x			?		Sd?
144	x	x	x	x		?	?	x		?			Sd?
145	x	x	x	x	?	?	?	?			?	?	
146	x	x	x	x	x	x	?	?				?	Ch?
147	x	x	x	x	x	x	?	x		?		?	
148	x	x	x	x	?	?		?		?			
149	x	x	x	x	x	?	?			?	?		Ap?
150	x	x	x	x	x	?	?				?		Il?
151	x	x	x	x	?	?	?			?			
152		x	x	x	x	?	?			?	?		Il?
153	x	x	x	x	x	?	?			?	?	?	
154	x	x	x	x	x	?	?	?					
155	x	x	x	x	x	?	?	?		?	?		
156	x	x	x	x	x	?	?	?	x				
157	x	x	x	x	x		?		x				
158	x	x	x	x	x	?	?					?	
159	x	x	x	x	x	x				?			
160	x	x	x	x	x	?				?			Py?
161	x	x	x	x	x	?	?	?			?		
162	x	x	x	x	x	?	?			?		?	
163	x	x	x	x	x	?	?						
164	x	?	x	x	x	?	?			?			

SAMPLE MINERALOGY--Continued

Sample No.	Todorokite	Quartz	Plagioclase	Montmorillonite	Phillipsite	Goethite	Maghemite	Amphibole	Birnessite	Clinoptilolite	Analcime	Olivine	Others
165	x	x	x	x	x	?	?			?			Il
166	x	x	x	x	x		?		x			?	
167	x	x	x	x	x	?	?	?					Il
168	x	x	x	x	x	?	?	x		?			
169	x	x	x	x		?	?	?					Ps?
170	x	x	x	x	x	?	?	x		?	?		Tc?
171	x	x	x	x	x	x			x				
172	x	x	x	x	?	?	?			?			
173	?	x	x	x	?	?				?			Gl,Py,Sd?
174	x	x	x	x	x	x	?	?		?	?		Sd?
175	x	x	x	x	x	?	?	?					Py?Md?
176	x	x	x	x	?	?		x	x	?		?	Py?
177	x	x	x	x	?	?							Md?
178	x	x	x	x	x	?		?			?		
179	x	x	?	x	x	?	?				?		
180	x	x	x	x	x	x		x		?			Py?
181	x	x	x	x	x	?							
182	x	x	x	x	x	?	?	?				?	
183	x	x	x	x	x	?	?	?			?		
184	x	x	x	x	x	x	?			?	?	?	
185	x	x	x	x	x	?					?		Er?
186	x	x	x	x	x	?	?			?			
187	x	x	x	x	x	x						?	Md?
188	x	x	x	x	x	?						?	Er?
189	x	x	x	x	x	?	?						
190	x	x	x	x	?	x	?	?		?			
191	?	x	x	x	x	?				?			Ma,Il?
192	x	x	x	x	x	x	?	?			?	?	Er?
193	x	x	x	x	?	x		x		?			Sd?
194	x	x	x	x	?	?	?			?			Pr?
195		x	x	x	x	?	?	x					Ma,Il,Ch?
196		x	x	x	x		?			?		?	Il,Ch?
197	x	x	x	x	x	?				?			
198	x	x	x	x	x	?	?						

SAMPLE MINERALOGY--Continued

Sample No.	Todorokite	Quartz	Plagioclase	Montmorillonite	Phillipsite	Goethite	Maghemite	Amphibole	Birnessite	Clinoptilolite	Analcime	Olivine	Others
199	x	x	x	x	x	?	?	x		?			
200	x	x	x	x			x						
201	x	x	x	x	x	?		x					
202	x	x	x	x	x	?		x		?			
203	x	x	x	x		?	?	x					
204	x	x	x	x	x	?		?			?		
205	x	x	x	x	x		?	x			?		
206	x	x	x	x	x		?	x					
207	x	x	x	x	x		?	x					
208		x	x	x	x	?	?	x			?	?	Il,Sd?
209	x	x	x	x	x	?	?	x		?			Tc?
210	x	x	x	x	?	?	?	x			?		Tc?
211	x	x	x	x	x		?	x		?			
212	x	x	x	x			?	x					
213	x	x	x	x	x		?	x					
214	x	x	x	x	x		?	x			?		
215	x	x	x	x	x			x			?		
216	x	x	x	x	x			x		?			
217	x	x	x	x	x	?	?	?			?		
218	x	x	x	x		?		x					
219	x	x	x	x	x		?	x		?			
220	x	x	x	x	x	?	?	x		?			Sd?
221		x	x	x	x		?	x				?	Il,Ch?
222	?	x	x	x	x	?	?	x					Il
223	x	x	x	x	x	?	?	x					
224	x	x	x	x	x	?	?	x		?	?		
225	x	x	x	x	x	?	?	x		?			Il,Ma?, Py?,Ch?
226	x	x	x	x	x	?	?	x		?			
227	x	x	x	x	x	?	?	x		?			
228	x	x	x	x	x	?				?	?		
229	x	x	x	x	x	?	?	x		?			
230		x	x	x	x	?	?	x					Il,Pr,Ch?

SAMPLE MINERALOGY--Continued

Sample No.	Todorokite	Quartz	Plagioclase	Montmorillonite	Phillipsite	Goethite	Maghemite	Amphibole	Birnessite	Clinoptilolite	Analcime	Olivine	Others
231	x	x	x	x	x	?	?	x		?			Sd?
232	x	x	x	x	x	?	?			?			
233	x	x	x	x	x	?	?	x		?			
234	x	x	x	x	x	?	?	x		?			Ch,Pr
235	x	x	x	x	x		?			?	?		
236	x	x	x	x	x	?	?	x		?			Sd?
237	x	x	x	x	x	?	?	x		?	?		
238	x	x	x	x	x	?	?						
239	x	x	x	x	x	?	?	?		?	?		
240	x	x	x	x	x	?	?	x					
241	x	x	x	x	x	?	?	x		?			Tc?
242	x	x	x	x	x	?	?	x		?			
243	x	x	x	x	x	?	?			?			
244	?	x	x	x	?	?	?						Il,βQ, Ch?,Tc?
245	x	x	x	x	x	?	?						
246	x		x	x	x	x	?	?					Gl,Ch?,Py?
247	x	x	x	x	x	?	?			?			Pr
248	x	x	x	x	x		?	x		?			
249	x	x	x	x	x	?	?	x		?			
250	x	x	x	x	x	?		?		?			Tc?
251	x	x	x	x	x	?	?	x		?	?		Il,Py?
252	x	x	x	x	x	?	?	x		?			
253	x	x	x	x	x	?	?	x		?			
254	x	x	x	x	x	x	?	x					
255	x	x	x	x	x	x	?	x					Tc?
256	x	x	x	x	x	?	?	x					
257	x	x	x	x	?	x	?		x				
258	x	x	x	x	x	?	?	x					Tc?
259	?	x	x	x	x	?	?			?			Il?,Py?
260	x	x	x	x	x	x	?	?					
261	x	x	x	x	x	?	?						
262	x	x	x	x	x	?	?		?	?			
263	x	x	x	x	x	?	?	?		?	?	?	Gl,Pr?, Ch?,Cr?

SAMPLE MINERALOGY--Continued

Sample No.	Todorokite	Quartz	Plagioclase	Montmorillonite	Phillipsite	Goethite	Maghemite	Amphibole	Birnessite	Clinoptilolite	Analcime	Olivine	Others
264	x	x	x	x	x	?	?						
265	x	x	x	x	x	x	?	x			?		
266	x	x	x	x	x	x	?				?		
267	?	x	x	x	x	?	?	?				?	Il,Er?
268	x	x	x	x	x	?	?	?					
269	x	x	x	x	x	x	?	x		?			
270	x	x	x	x	x	?	?	x		?			Im?
271	x	x	x	x	x	?	?			?			
272	x	x	x	x	?	?	?	x		?	?		
273	x	x	x	x	?	?	?	?				?	Tc?
274	?	x	x	x			?			?			Ca,Ap
275	x	x	x	x	?	x	x	?		x			
276	x	x	x	x	x	?	?	x		?			Tc?
277	x	x	x	x	x	x	x	?	x	x			
278	x	x	x	x	x	x	?	?	x	?			
279	x	x	x	x	x	x	?	?	x	?		?	
280	x	x	x	x	?	x	?	?		?			
281	x	x	x	x	x	x	?	?	x	?			
282	x	x	x	x	?	x	?	?		?			
283	x	x	x	x	x	x	?	?				?	Py?
284	x	x	x	x	x	?		?		?			
285	x	x	x	x	x	x	?	x		?	?		Py?
286	x	x	x	x	x	?	?						
287	x	x	x	x	x	?	?	?		?			
288	x	x	x	x	x	?	?	?					
289	x	x	x	x	?	?	?		x				Py?

Key to other minerals:

Anorthoclase	= Ah	Glass	= Gl	Pyroxene	= Py
Apatite	= Ap	Illite/muscovite	= Il	β-Quartz	= βQ
Barite	= Ba	Ilmenite	= Im	Sanidine	= Sd
Calcite	= Ca	Magnetite	= Ma	Serpentine	= Sp
Chlorite	= Ch	Mordenite	= Md	Talc/ pyrophyllite	= Tc
Cristobalite	= Cr	Prehnite	= Pr		
Erionite	= Er	Psilomelane	= Ps		

APPENDIX F

MINERALS FOUND IN SOUTHERN OCEAN CONCRETIONS

Mineral	Oxide Crust		Subcrust		Nucleus		Crustal Material		Fracture Fillings	
	Def.	Poss.	Def.	Poss.	Def.	Poss.	Def.	Poss.	Def.	Poss.
Todorokite	228	7	99	5	75	8	4	0	1	0
Quartz	231	2	102	0	81	3	4	0	3	0
Plagioclase	232	2	104	0	85	2	4	0	2	1
Montmorillonite	231	2	101	3	88	2	4	0	2	0
Phillipsite	173	51	83	20	73	14	3	1	2	1
Goethite	52	161	23	72	11	60	0	4	0	1
Maghemite	4	180	0	81	0	67	0	4	0	2
Clinoptilolite	7	126	5	51	4	40	0	1	0	2
Amphibole	83	69	31	33	22	20	0	1	0	1
Olivine	1	41	1	17	1	13	0	0	0	0
Analcime	0	51	0	23	0	17	0	2	0	2
Birnessite	26	12	10	5	5	3	1	0	1	0
Sanidine-Anorthoclase	0	22	0	7	0	8	0	0	0	0
Pyroxene	1	14	1	4	1	8	0	0	0	0
Illite	5	1	3	2	14	2	0	1	0	1
Chlorite	1	8	0	5	0	13	0	1	0	0
Talc/Pyrophyllite	1	14	1	6	2	5	0	0	0	1
Apatite	3	1	1	0	4	1	0	1	0	0
Calcite	3	0	1	0	1	0	0	0	0	0
Mordenite	0	7	0	3	0	3	0	0	0	0
Erionite	0	8	0	5	0	2	0	0	0	0
Prehnite	2	2	0	1	2	3	0	0	0	0

MINERALS FOUND IN SOUTHERN OCEAN CONCRETIONS--Continued

Mineral	Oxide Crust		Subcrust		Nucleus		Crustal Material		Fracture Fillings	
	Def.	Poss.	Def.	Poss.	Def.	Poss.	Def.	Poss.	Def.	Poss.
Glass	2	0	1	0	4	0	0	0	0	0
Magnetite	0	0	0	0	2	1	0	0	0	0
Psilomelane	0	2	0	1	0	0	0	0	0	0
Ilmenite	0	2	0	0	0	0	0	0	0	0
Serpentine	0	1	0	0	0	1	0	0	0	0
Barite	0	0	0	0	0	1	0	0	0	0
Cristobalite	0	0	0	0	0	1	0	0	0	0
β-Quartz	0	0	0	0	0	1	0	0	0	0
Total Number of Samples	235		104		91		4		3	

Def. = Definitely present.

Poss.= Possibly present.

LITERATURE CITED

LITERATURE CITED

Ahrens, L. H., 1952, The use of ionization potentials, part 1: Ionic radii of the elements: Geochim. et Cosmochim. Acta, v. 2, p. 155-169.

Anikouchine, W. A., 1967, Dissolved chemical substances in compacting marine sediments: Jour. Geophys. Research, v. 72, p. 505-509.

Arrhenius, G., 1963, Pelagic sediments, p. 655-727 in Hill, M. N., Editor, The Sea, v. 3: Interscience Publ., New York, 947 p.

_____, 1967, Deep-sea sedimentation: A critical review of U.S. work: Trans. Am. Geophys. Union, v. 48, p. 604-631.

Arrhenius, G., and Bonatti, E., 1965, Neptunism and vulcanism in the sea, p. 7-22 in Sears, M., Editor, Progress in Oceanography, v. 3: Pergamon Press, Oxford, 407 p.

Arrhenius, G., Mero, J., and Korkisch, J., 1964, Origin of oceanic manganese minerals: Science, v. 144, p. 170-173.

Barnes, S. S., 1967, Minor element composition of ferromanganese nodules: Science, v. 157, p. 63-65.

Beals, H. L., 1966, Manganese-iron concretions in Nova Scotia lakes: Maritime Sediments, v. 2, p. 70-72.

Biscaye, P. E., 1965, Mineralogy and sedimentation of recent deep-sea clay in the Atlantic Ocean and adjacent seas and oceans: Geol. Soc. America Bull., v. 76, p. 803-832.

Bonatti, E., 1963, Zeolites in Pacific pelagic sediments: Trans. N. Y. Acad. Sci., v. 25, p. 938-948.

_____, 1965, Palagonite, hyaloclastites and alteration of volcanic glass in the ocean: Bull. Volcanologique, tome 28, p. 257-269.

Bonatti, E., and Joensuu, O., 1966, Deep-sea iron deposit from the South Pacific: Science, v. 154, p. 643-645.

Bonatti, E., and Nayudu, Y. R., 1965, The origin of manganese nodules on the ocean floor: Am. Jour. Sci., v. 263, p. 17-39.

Bricker, O., 1965, Some stability relations in the system $Mn-O_2-H_2O$ at 25°C and one atmosphere total pressure: Am. Mineralogist, v. 50, p. 1296-1354.

Burns, R. G., 1965, Formation of cobalt(III) in the amorphous $FeOOH \cdot nH_2O$ phase of manganese nodules: Nature, v. 205, p. 999.

Burns, R. G., and Fuerstenau, D. W., 1966, Electron-probe determination of inter-element relationships in manganese nodules: Am. Mineralogist, v. 51, p. 895-902.

Buser, W., 1959, The nature of the iron and manganese compounds in manganese nodules, p. 962-963 in Sears, M., Editor, International Oceanographic Congress, 1st, Preprints: Am. Assoc. Adv. Sci., Washington, D. C., 1022 p.

Buser, W., Graf, P., and Feitknecht, W., 1954, Beitrag zur Kenntnis der Mangan(II)-Manganite und des δ-MnO_2: Helv. Chim. Acta, v. 37, p. 2322-2333.

Buser, W., and Grütter, A., 1956, Über die Natur der Manganknollen: Schweiz. Mineral. und Petrograph. Mitt., v. 36, p. 49-62.

Chester, R., and Hughes, M. J., 1966, The distribution of manganese, iron and nickel in a North Pacific deep-sea clay core: Deep-Sea Research, v. 13, p. 627-634.

Deacon, G. E. R., 1963, The Southern Ocean, p. 281-296 in Hill, M. N., Editor, The Sea, v. 2: Interscience Publ., New York, 554 p.

Deer, W. A., Howie, R. A., and Zussman, J., 1962, Rock-forming Minerals, v. 5, Non-silicates: Wiley and Son, New York, 371 p.

Engel, A. E. J., Engel, C. G., and Havens, R. G., 1965, Chemical characteristics of oceanic basalts and the upper mantle: Geol. Soc. America Bull., v. 76, p. 719-734.

Feitknecht, W., and Marti, W., 1945, Manganite and artificial manganese dioxide: Helv. Chim. Acta, v. 28, p. 149-156.

Frondel, C., Marvin, U. B., and Ito, J., 1960, New occurrences of todorokite: Am. Mineralogist, v. 45, p. 1167-1173.

Goldberg, E. D., 1954, Marine geochemistry 1. Chemical scavengers of the sea: Jour. Geology, v. 62, p. 249-265.

_____, 1965, Minor elements in sea water, p. 163-196 in Riley, J. P., and Skirrow, G. W., Editors, Chemical Oceanography, v. 1: Academic Press, London, 712 p.

Goldberg, E. D., and Arrhenius, G. O. S., 1958, Chemistry of Pacific pelagic sediments: Geochim. et Cosmochim. Acta, v. 13, p. 153-212.

Goodell, H. G., 1964, The marine geology of the Drake Passage, Scotia Sea, and South Sandwich Trench: USNS ELTANIN, Marine Geology Cruises 1-8 (mimeographed), 263 p.

_____, 1965, The marine geology of the Southern Ocean: USNS ELTANIN, Marine Geology Cruises 9-15 (off-set), Contribution No. 11, Sedimentology Research Laboratory, Dept. of Geology, the Florida State University, Tallahassee, 196 p.

_____, 1967, Ferromanganese deposits of the Southern Ocean (Abstract): Program, 1967 Annual Meeting, Geol. Soc. America, Southeastern Section, p. 29-30.

_____, in press, The marine geology of the Southern Ocean: USNS ELTANIN, Marine Geology Cruises 16-28.

Goodell, H. G., and Watkins, N. D., in press, The paleomagnetic stratigraphy of the Southern Ocean: 20° West to 160° East Longitude: Jour. Marine Research.

Grant, J. B., 1967, A comparison of the chemistry and mineralogy with the distribution and physical aspects of marine manganese concretions of the Southern Oceans: Unpublished M.S. thesis, Dept. of Geology, the Florida State University, Tallahassee, 100 p.

Green, J., 1959, Geochemical table of the elements: Geol. Soc. America Bull., v. 70, p. 1127-1184.

Griffin, J. J., and Goldberg, E. D., 1963, Clay-mineral distributions in the Pacific Ocean, p. 728-741 in Hill, M. N., Editor, The Sea, v. 3: Interscience Publ., New York, 947 p.

Grütter, A., and Buser, W., 1957, Untersuchungen an Mangan-sedimenten: Chimia, v. 11, p. 132-133.

Hamilton, E. L., 1956, Sunken islands of the Mid-Pacific Mountains: Geol. Soc. America Memoir 64, 97 p.

Harrison, C. G. A., and Peterson, M. N. A., 1965, A magnetic mineral from the Indian Ocean: Am. Mineralogist, v. 50, p. 704-712.

Hathaway, G. C., and Sachs, P. L., 1965, Sepiolite and clinoptilolite from the Mid-Atlantic Ridge: Am. Mineralogist, v. 50, p. 852-867.

Hay, R. L., 1964, Phillipsite of saline lakes and soils: Am. Mineralogist, v. 49, p. 1366-1387.

Heezen, B. C., and Hollister, C., 1964, Deep-sea current evidence from abyssal sediments: Marine Geology, v. 1, p. 141-174.

Hem, J. D., 1964a, Chemical equilibria and rates of manganese oxidation: U. S. Geol. Survey Water-Supply Paper 1667-A, 64 p.

_____, 1964b, Deposition and solution of manganese oxides: U. S. Geol. Survey Water-Supply Paper 1667-B, 42 p.

Hewett, D. F., Fleischer, M., and Conklin, N., 1963, Deposits of the manganese oxides: Supplement: Econ. Geology, v. 58, p. 1-51.

Holmes, C. W., Goodell, H. G., and Osmond, J. K., 1967, Geochronological investigations of the southern Pacific: Contribution No. 21, Sedimentology Research Laboratory, Dept. of Geology, the Florida State University, Tallahassee, 36 p.

Hough, J. L., 1956, Sediment distribution in the Southern Oceans around Antarctica: Jour. Sed. Petrol., v. 26, p. 301-306.

Jones, L. H. P., and Milne, A. A., 1956, Birnessite, a new manganese oxide mineral from Aberdeenshire, Scotland: Mineral. Mag., v. 31, p. 283-288.

Koster, S., 1966, Recent sediments and sedimentary history across the Pacific-Antarctic Ridge: Unpublished M.S. thesis, Dept. of Geology, The Florida State University, Tallahassee, 83 p.

Krauskopf, K. B., 1956, Factors controlling the concentrations of thirteen rare metals in sea-water: Geochim. et Cosmochim. Acta, v. 9, p. 1-32.

_____, 1957, Separation of manganese from iron in sedimentary processes: Geochim. et Cosmochim. Acta, v. 12, p. 61-84.

Lippman, F., 1958, X-ray determination of phillipsite in a sediment core from the central Equatorial Pacific: Repts. Swedish Deep-Sea Expedition, v. 10, Spec. Investigations, no. 3.

Lynn, D. C., and Bonatti, E., 1965, Mobility of manganese in diagenesis of deep-sea sediments: Marine Geology, v. 3, p. 457-474.

McConnell, D., 1938, A structural investigation of the isomorphism of the apatite group: Am. Mineralogist, v. 23, p. 1-19.

McFarlin, P. F., 1967, Aragonite vein fillings in marine manganese nodules: Jour. Sed. Petrol., v. 37, p. 68-72.

Machek, A., 1965, Identification of unknown mineral from Antarctic core samples: Typewritten report, 10 p.

Maksimov, I. V., 1962, The nature of the Great East Drift: Soviet Antarctic Expedition, Information Bulletin, v. 4, p. 33-35.

Manheim, F. T., 1965, Manganese-iron accumulations in the shallow marine environment: Symposium on Marine Geochemistry, Occ. Publ. No. 3-1965, Narragansett Marine Laboratory, Univ. Rhode Island, p. 217-276.

Mason, B., 1958, Principles of Geochemistry: Wiley and Son, New York, 310 p.

Mather, T. T., 1966, The deep-sea sediments of the Drake Passage and the Scotia Sea: Unpublished M.S. thesis, Dept. of Geology, The Florida State University, Tallahassee, 100 p.

Menard, H. W., 1964, Marine Geology of the Pacific: McGraw-Hill, New York, 271 p.

_____, 1965, Sea floor relief and mantle convection, p. 315-364 in Ahrens, L. H., and others, Editors, Physics and Chemistry of the Earth, v. 6, Pergamon Press, New York, 510 p.

Menard, H. W., and Shipek, C. J., 1958, Surface concentrations of manganese nodules: Nature, v. 182, p. 1156-1158.

Mero, J. L., 1965, The Mineral Resources of the Sea: Elsevier, New York, 311 p.

Meylan, M. A., 1966, Report of the Florida State University Marine Geology Program, USNS ELTANIN, Cruise 21: Typewritten report, 5 p.

Morgenstein, M., in press, Authigenic cementation of scoriaceous deep-sea sediments west of the Society Ridge, South Pacific.

Murata, K. J., and Erd, R. C., 1964, Composition of sediments from the experimental Mohole Project (Guadalupe site): Jour. Sed. Petrol., v. 34, p. 633-655.

Murray, J., and Lee, G. V., 1909, The depth and marine deposits of the Pacific: Mem. Museum Comp. Zool., Harvard College, Cambridge, v. 38, p. 1-171.

Murray, J., and Renard, A., 1891, Manganese nodules, p. 341-378 in Thomson, C. W., Editor, Report of the Scientific Results of the Voyage of HMS CHALLENGER, v. 5, Deep-Sea Deposits: Eyre and Spottiswoode, London, 525 p.

Mumpton, F. A., 1960, Clinoptilolite redefined: Am. Mineralogist, v. 45, p. 351-369.

Peterson, M. N. A., and Goldberg, E. D., 1962, Feldspar distributions in South Pacific pelagic sediments: Jour. Geophys. Research, v. 67, p. 3477-3492.

Rankama, K., and Sahama, T. G., 1950, Geochemistry: Univ. of Chicago Press, Chicago, Ill., 912 p.

Rex, R. W., 1967, Authigenic silicates formed from basaltic glass by more than 60 million years' contact with sea water, Sylvania Guyot, Marshall Islands: Proceedings, Fifteenth Conference on Clays and Clay Minerals, p. 195-203.

Rex, R. W., and Goldberg, E. D., 1958, Quartz contents of pelagic sediments of the Pacific Ocean: Tellus, v. 10, p. 153-159.

Riley, J. P., and Sinhaseni, P., 1958, Chemical composition of three manganese nodules from the Pacific Ocean: Jour. Marine Research, v. 17, p. 466-482.

Rona, E., Hood, D. W., Muse, L., and Buglio, B., 1962, Activation analysis of manganese and zinc in sea water: Limnology and Oceanography, v. 7, p. 201-206.

Rooksby, H. P., 1961, Oxides and hydroxides of aluminum and iron, p. 354-392 in Brown, G., Editor, The X-ray Identification and Crystal Structures of Clay Minerals: Mineralogical Society, London, p. 544 p.

Skornyakova, N. S., Andrushchenko, P. F., and Fomina, L. S., 1962, Chemical composition of the Pacific Ocean's iron-manganese concretions: Okeanologiya, v. 2, p. 264-277 (English translation, Deep-Sea Research, v. 11, p. 93-104).

Skornyakova, N. S., and Zenkevitch, N., 1961, The distribution of iron-manganese nodules in surficial sediments of the Pacific Ocean: Okeanologiya. v. 1. p. 86-94.

Sorem, R. K., 1967, Manganese nodules: Nature and significance of internal structure: Econ. Geology, v. 62, p. 141-147.

Sverdrup, H. U., Johnson, M. W., and Fleming, R. H., 1942, The Oceans: Prentice-Hall, Englewood Cliffs, N. J., 1087 p.

Turekian, K. K., and Wedepohl, K. H., 1961, Distribution of the elements in some major units of the earth's crust: Geol. Soc. America Bull., v. 72, p. 175-191.

Warshaw, C. M., and Roy, R., 1961, Classification and a scheme for the identification of layer silicates: Geol. Soc. America Bull., v. 72, p. 1455-1492.

Willis, J. P., and Ahrens, L. H., 1962, Some investigations on the composition of manganese nodules, with particular reference to certain trace elements: Geochim. et Cosmochim. Acta, v. 26, p. 751-764.

Wyart, J., and Chatelain, P., 1938, Étude cristallographique de la christianite: Bull. Soc. Franç. Min., v. 61, p. 121.

Zelenov, K. K., 1964, Iron and manganese in exhalations of the submarine Banu Wuhu volcano (Indonesia): Doklady Akad. Nauk S. S. S. R., v. 155, p. 94-96 (English translation).

Zhivago, A. V., 1962, Outlines of Southern Ocean geomorphology, in Wexler, H., and others, Editors, Antarctic Research: Geophys. Monograph #7, Am. Geophys. Union, 228 p.

VITA

Maurice A. Meylan, the eldest son of Mr. and Mrs. G. J. Meylan, was born March 16, 1942, in Cortland, New York. He attended high school in Tully, New York, and graduated as valedictorian of the class of 1960. Undergraduate work was done at the University of Buffalo; he received a B.A. (cum laude) in 1964 with a major in Geology and a minor in Geography. During his senior year he served as a laboratory instructor for introductory geology in Millard Fillmore College of the University of Buffalo.

Mr. Meylan was brought to The Florida State University by a research assistantship in the Antarctic Marine Geology Program, and served as Marine Geologist aboard the USNS ELTANIN from September, 1965 to January, 1966. He is a member of the Mineralogical Society of America, the Clay Minerals Society, the American Association for the Advancement of Science, and the American Geophysical Union.

ERRATA

Corrections in the text are to be made as follows:

Page 7, Line 17 - "formaminiferal" should read "foraminiferal".

Page 67, Line 13 - "techtonically" should read "tectonically".

Page 93, Line 7 - "cocsistently" should read "consistently".